UNIVERSITÀ DI SIENA 1240

Dipartimento di Biotecnologie, Chimica e Farmacia

Dottorato di Ricerca in

Biochemistry and Molecular Biology

XXXVI Ciclo

Coordinatrice: Prof.ssa Lorenza Trabalzini

Isolation, selection, and characterization of potent human monoclonal antibodies against pandrug-resistant ST147$_{NDM-1}$ *Klebsiella pneumoniae*

Candidata
Vittoria Zucconi Galli Fonseca

Vittoria Zucconi Galli Fonseca

Firmato digitalmente da: Vittoria Zucconi Galli Fonseca

Supervisore
Prof. Rino Rappuoli

A.A. 2022/2023

Università degli Studi di Siena

Dottorato in Biochemistry and Molecular Biology

XXXVI Ciclo

Data dell'esame finale

18/04/2024

Commissione giudicatrice

Prof. Anna Maria Aloisi
Prof. Enzo Spisni
Prof. Gian Maria Rossolini
Prof. Marco Scocchi
Prof. Riccardo Manganelli

A Lula,

Abstract ***7***

Introduction ***8***

1. *Klebsiella pneumoniae* and antimicrobial resistance **8**

2. *K. pneumoniae* Virulence Factors and Pathogenicity **10**

Capsule 11

Lipopolysaccharide (LPS) and O-antigen 12

Fimbriae 14

Siderophores 14

3. *K. pneumoniae* accessory genome and its role on antibiotic resistance **15**

4. Convergence of classical and hypervirulent *K. pneumoniae* lineages **16**

5. *K. pneumoniae* in Italy **18**

6. Therapeutic approaches to fight AMR **19**

7. Therapeutic monoclonal antibodies against infectious diseases **21**

Structure and effector functions 21

Therapeutic mAbs discovery and development 25

Aims of the work ***27***

CHAPTER 1: Human monoclonal antibodies protect from bloodstream infection by pandrug-resistant Klebsiella pneumoniae ***29***

Abstract **30**

Introduction **31**

Results **34**

1. Isolation of bactericidal human mAbs against Tuscany outbreak strain $ST147_{NDM-1}$ 34

2. Kp library profiling reveals that bactericidal mAbs have different degree of cross-reactivity and antigen specificity 35

3. ST147-specific bactericidal mAbs target $ST147_{NDM-1}$ capsule and O-antigen 38

4. Functional profiling reveals that isolated mAbs have extremely potent bactericidal activity, however only anti-capsular mAbs are poly-functional 39

5. mAb poly-functionality is required for protection against fulminant $ST147_{NDM-1}$ bloodstream infection *in vivo* 42

Discussion **45**

Materials and Methods **48**

Single-cell sorting of memory B cells from convalescent donors 48
ELISA screening of mAbs binding against *Klebsiella pneumoniae* 48
Single-cell RT-PCR and nested PCR were used to amplify V_H and V_L 49
Cloning of V_H and V_L and recombinant antibody expression by TAP transfection 50
Quantification of TAP-produced mAbs by ELISA 50
Large scale expression and purification of mAbs 51
Serum Bactericidal Assay (SBA) 51
Flow cytometry analysis of mAb binding to bacterial surface 52
Antibody sequence analysis 53
Genomic analysis of Kp isolates 53
Western blot analysis of mAb binding to Kp lysates 53
Characterization of mAb binding by high-resolution and high-content confocal microscopy 54
Opsonophagocytosis assay 55
Live bacteria imaging 56
Microscopy and image analysis 56
Purification of $ST147_{NDM-1}$ capsule 57
Purification of O-antigen from Kp strains 58
ELISA on purified Kp O-antigen and capsule 59
Immunocompetent $ST147_{NDM-1}$ bacteremia model 59

Supplementary Materials 61

CHAPTER 2: Ex vivo gastrointestinal organoids as a new 3D tool for therapy development against pandrug-resistant $ST147_{NDM-1}$ Klebsiella pneumoniae 81

Introduction: 82

Results 86

1. K. pneumoniae infects the colonic epithelium at junction sites and on extrusion zones 86
2. K. pneumoniae forms bacterial clusters on apoptotic cells and promotes programmed cell death through an adhesion-independent cytotoxic effect. 89
3. 08O09 promotes colonoids survival by reducing *K. pneumoniae* bacterial adhesion and triggers enchained bacterial growth. 92

Discussion and Conclusions 93

Materials and Methods 95

Klebsiella pneumoniae strains and culture conditions: 95
Colonic epithelial organoids cultivation and growth: 95
Colonoids differentiation: 96
Colonoids polarity reversal: 96
Colonoids infection with *K. pneumoniae*: 96

Confocal microscopy: 96

Conclusions and future perspectives 98

Bibliography 100

Acknowledgements 117

Abstract

Antimicrobial resistance is a silent yet deadly threat to public health that requires immediate action at the global scale, calling for preparedness to rapidly develop novel therapeutic strategies. In this regard, in 2017 the World Health Organization (WHO) published a list of bacteria for which new antimicrobial solutions are urgently needed. Among the most critical group are the Gram-negative carbapenem-resistant enteric bacteria, including *Klebsiella pneumoniae*. In the last decades, *K. pneumoniae* acquired resistance to last-line classes of antibiotics due to the expression of carbapenemases such as the New Delhi metallo-β-lactamase 1 (NDM-1). To date, no vaccines or alternative therapies have been licensed against *K. pneumoniae*. Immunotherapy with monoclonal antibodies (mAbs) is being considered as an innovative solution for treating multidrug resistant infections, but experimental strategies for effective development have yet to be optimized for bacterial pathogens. We established an antigen-agnostic approach to efficiently screen human mAbs starting from blood of patients who recovered from *K. pneumoniae* infection, and we have successfully isolated extremely potent candidates against pandrug-resistant ST147 NDM-1-positive *K. pneumoniae* clinical isolates. These mAbs display antibacterial activity in the picomolar range in various *in vitro* assays and the selected top candidate has proved to be protective against bloodstream infections *in vivo*. Moreover, an *ex vivo* model of multidrug-resistant *K. pneumoniae* gut infection has been designed by employing human-derived intestinal organoids. The established model has been exploited on the one hand to deepen our understanding of the molecular processes that regulate host-pathogen interactions, on the other hand to further characterize bactericidal properties of the top candidate mAb. Overall, this study exemplifies a rationally designed pre-clinical approach for the development and characterization of innovative immunotherapies to target antimicrobial resistant pathogens and to address the silent pandemic caused by multidrug-resistant species.

Introduction

1. *Klebsiella pneumoniae* and antimicrobial resistance

Antimicrobial resistance (AMR) is considered one of the top ten public health threats facing humanity in the 21st century[1]. If not addressed, AMR spread could increase lethality of several pathogens, potentially leading to 10 million deaths a year by 2050[2,3]. For this reason, several international agencies are calling for preparedness

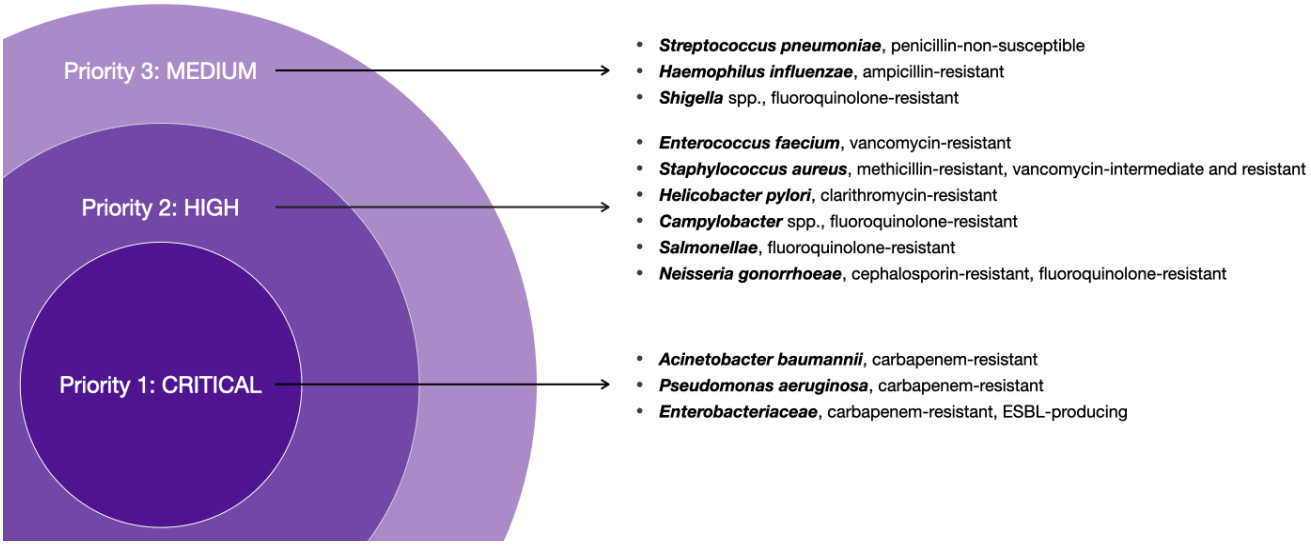

Figure 1. WHO priority list of pathogens for which new antimicrobials are urgently needed.

and coordinated action at the global scale to tackle this silent pandemic[4]. In 2017, the World Health Organization (WHO) in collaboration with the Division of Infectious Diseases at the University of Tübingen published its first list of "priority pathogens" for which new antimicrobial solutions are urgently needed[5] (**Figure 1**). Applying a multi-criteria approach to estimate the urgency of need for new therapeutic procedures, the list ranked AMR pathogens into three categories: critical, high and medium priority. Among the "Priority 1: Critical" tier are the Gram-negative pathogens of the ESKAPE (*Enterococcus faecium*, G+, *Staphylococcus aureus*, G+, *Klebsiella pneumoniae*,

G-, *Acinetobacter baumannii*, G-, *Pseudomonas aeruginosa*, G-, and *Enterobacter* species, G-) group[6]. This class of microorganisms is showing alarming multidrug resistant (MDR, resistance to three or more classes of antibiotics) characteristics, raising concerns for the increased morbidity and mortality rates associated with their infections[7]. Within the ESKAPE pathogens, *Klebsiella pneumoniae* is a global public health issue as it is one of the most widespread nosocomial bacterial opportunistic species[8].

K. pneumoniae is a Gram-negative, encapsulated, non-motile bacterium of the *Enterobacteriaceae* family that was first isolated by Carl Friedlander in the late 19th century[9]. *K. pneumoniae* can not only reside in environmental reservoirs, such as in soil, plants, and water[10], but it also naturally colonizes the mucosal surfaces of the gastrointestinal and oropharyngeal tracts of animals and humans[11]. From the gastrointestinal tract of humans, *K. pneumoniae* can access other tissues and cause a variety of infections in the human host, such as respiratory tract infections, urinary tract infections, and bloodstream infections[12]. Being an opportunistic bacterium[13], it can become extremely dangerous in nosocomial environments, where it mostly affects immunocompromised patients with concurring bacterial infections. In the last decades, *K. pneumoniae* gained genetic features that lead to community acquired infections, often in immunocompetent individuals, causing a variety of diseases (i.e., meningitis, pneumonia, pyogenic liver abscess)[14,15]. Moreover, because of its major presence in hospital settings, *K. pneumoniae* has been continually exposed to antibiotics; this translated into a constant selective pressure that endowed *K. pneumoniae* with resistance to most classes of antibiotics through the expression of drug-inactivating enzymes like extended-spectrum β-lactamases, whose encoding genes are frequently located on mobile genetic elements[16]. In this regard, the presence and frequency of carbapenemases is particularly concerning as they confer resistance to the last-resort combinations of β-lactamase inhibitors and β-lactam antibiotics[17].

2. *K. pneumoniae* Virulence Factors and Pathogenicity

K. pneumoniae pathogenicity is attributed to a set of core genes that encode for the four main virulence factors necessary for infection (**Figure 2**). The *cps* locus drives the expression of the capsular polysaccharide, or capsule, that allows evasion from the host's immune mechanisms and protection against antibacterial peptides[18]. The *rfb* locus genes are responsible for the expression of the O-antigen that can activate the host's innate immune system[19] and lead to increased lethality and bacteremia[20]. The resulting structures of capsule and O-antigens can vary and have been used to

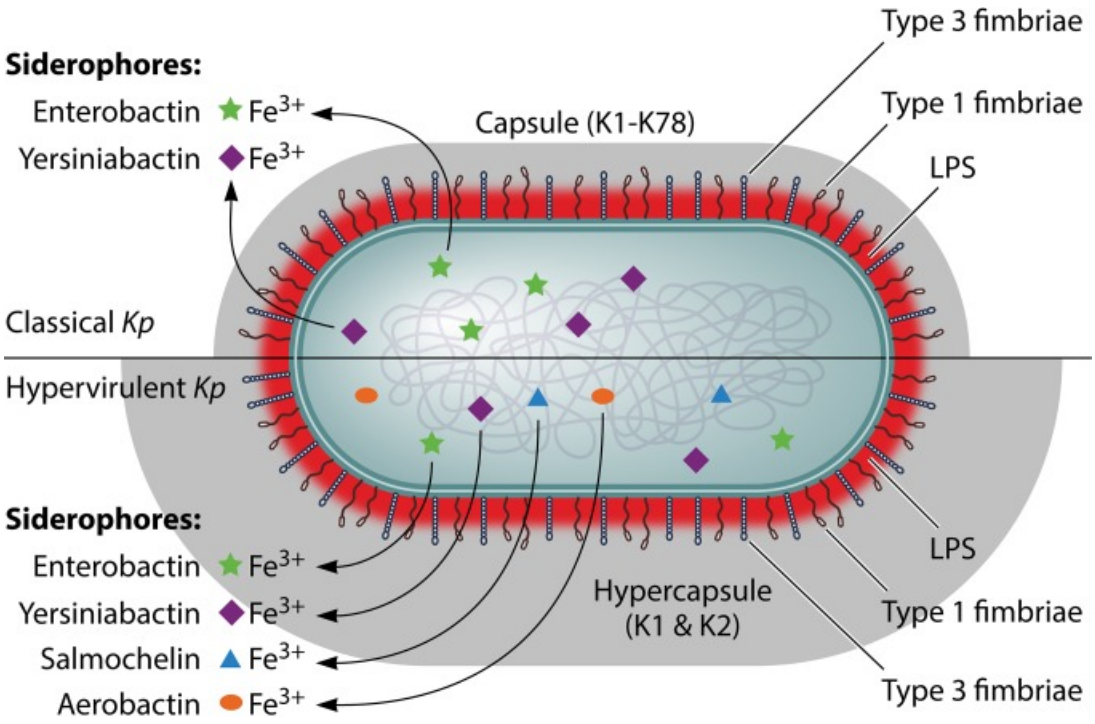

Figure 2. Virulence factors in classical and hypervirulent *K. pneumoniae* strains. The main and most characterized virulence factors for pathogenic *K. pneumoniae* are: capsule, LPS, fimbriae (type 1 and type 3), and siderophores.
Image from: Paczosa MK, Mecsas J. Klebsiella pneumoniae: Going on the Offense with a Strong Defense.

classify *K. pneumoniae* isolates into different serotypes. The *fim* and *mrk* loci are involved in the biosynthesis of type 1 and type 3 fimbriae. Fimbriae are involved in the

first steps of infection of host epithelia and in implant-associated infections[21] because of their essential role in adhesion and colonization processes, as well as in biofilm formation mechanisms[22]. Finally, siderophores, such as enterobactin, show extremely high affinity for iron[23] and can promote bacterial growth[24].

Capsule

K. pneumoniae capsular polysaccharide creates a thick mucoid layer around the bacterium that provides a shield against the environment. Moreover, the capsule protects the pathogen from the host's innate immune response. Capsule helps *K. pneumoniae* evade from complement deposition and opsonization and acts as a penetration barrier, inhibiting antimicrobial peptides activity and complement mediated lysis[25,26]. The capsule is expressed by the capsular polysaccharide synthesis (*cps*) locus and has a structure composed of repeating subunits of sugars[12]. Diversity in sugar composition and glycosidic linkages allowed identification of different types of capsule structures. Based on this and on the arrangement of *K. pneumoniae cps* locus, to date more than 79 capsular serotypes have been described[27,28]. Capsule biosynthesis follows a Wzy-dependent process[29] and the genes responsible for the process are in the *cps* locus. Its terminal regions contain genes that are related to the core capsule biosynthesis machinery, namely *gal*F, *wzi*, *wza*, *wzb*, *wzd*, *gnd*, and *ugd*[30]. The central region of the locus is variable and is linked to capsule-specific sugar synthesis as well as core assembly components Wzx and Wzy[28]. The mechanism takes place on the cytoplasmic leaflet of *K. pneumoniae* inner membrane and is initialized by either WbaP, generating a galactose-Und-PP, or by WcaJ, generating periplasmic leaflet of the inner membrane, where the Wzy polymerase can generate a high molecular weight polysaccharides. Ultimately, Wza (outer membrane translocon), Wzb (phosphatase), and Wzc (tyrosin autokinase) flip the capsule to the bacterial surface, where it stays associated to Wzi, an outer-membrane protein[22,31]. K1, K2, K5, K16, K23, K27, K28, K54, K62, and K64 capsule serotypes are among the most commonly spread and isolated worldwide (**Figure 3**), with K1, K2, and K64 being particularly worrisome as they are often associated with hypervirulent *K. pneumoniae* lineages[32–35].

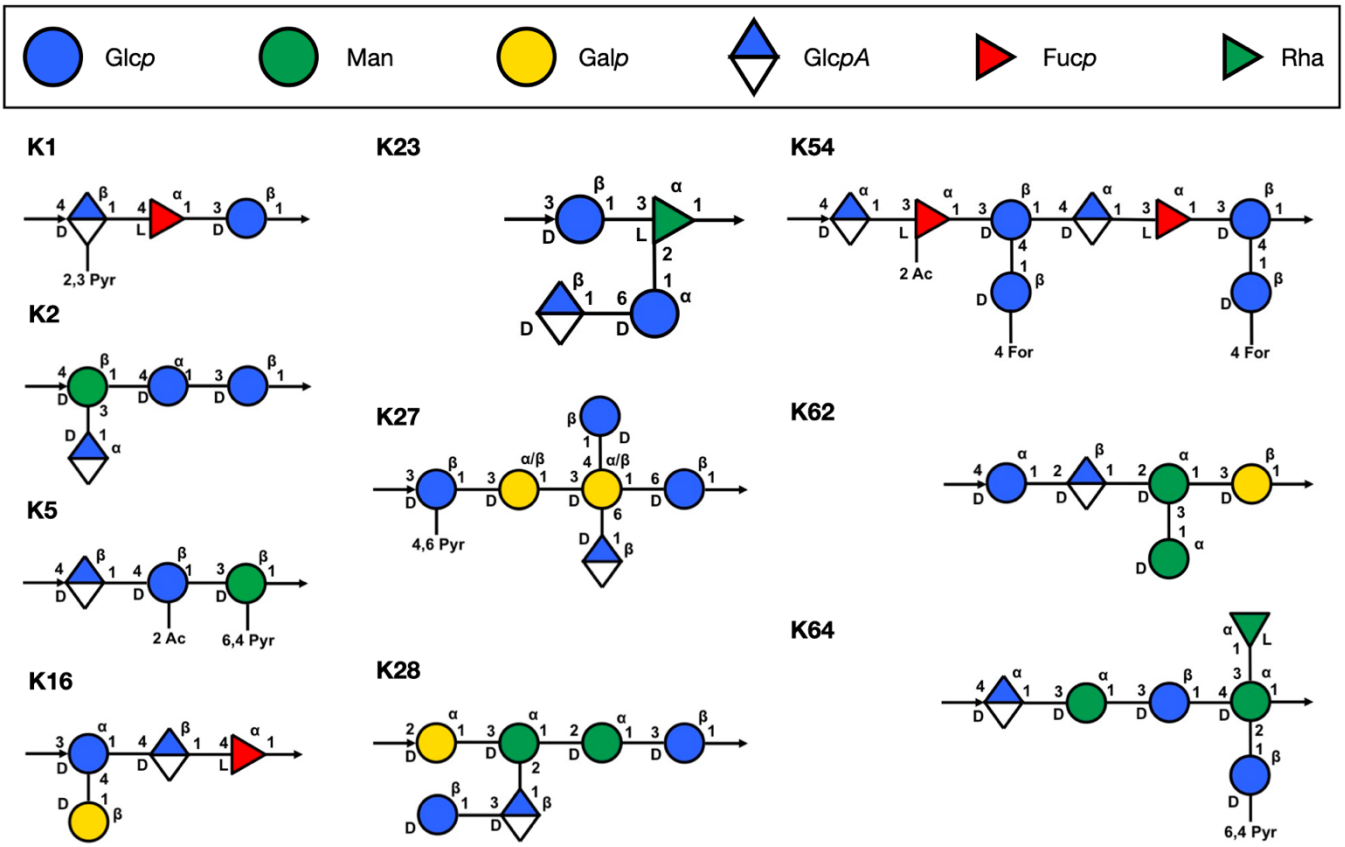

Figure 3. Capsule serotypes of the most commonly spread *K. pneumoniae* strains isolated worldwide. K1, K2, and K64 are often associated with hypervirulence.

Lipopolysaccharide (LPS) and O-antigen

LPS is a bacterial endotoxin and a major component of the outer membrane of Gram-negative bacteria. It is recognized as a bacterial virulence factor capable of causing sepsis via activation of the host response through a Toll-like receptor 4-dependent inflammatory cascade[36]. LPS molecules consist of lipid A, a core domain and the O-antigen (**Figure 4A**). LPS biosynthesis happens on the cytoplasmic leaflet of the inner membrane and O-antigen synthesis is carried out by serotype-specific glycosyltransferases. After polymerization, the Wzm/Wzt system (an ABC transporter) transfers the O-antigen products into the periplasmic leaflet of the inner membrane[31], while the lipid A-core oligosaccharide is flipped through a MsbA transporter. WaaL, a ligase, subsequently links together the polymerized O-antigen with the lipid A-core oligosaccharide and the LptA complex transfers the complete LPS to the bacterial surface. Within the LPS structure, lipid A and the core domains are more broadly

conserved among different *K. pneumoniae* clones, while 11 main serotypes are known for the *K. pneumoniae* O-antigen (**Figure 4B**). The most recent nomenclature includes O1, O2a, O2ac, O2afg, O2aeh, O3, O4, O5, O7, O8 and O12[27], but additional O-

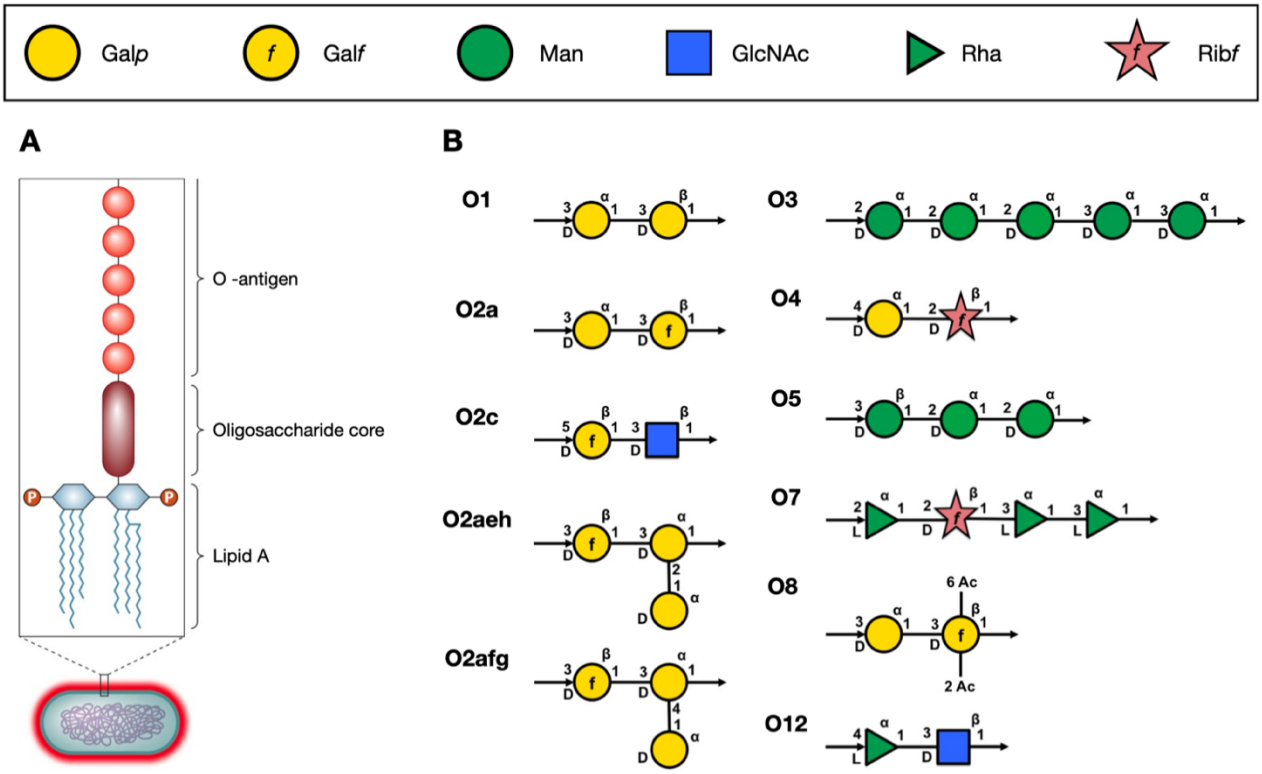

Figure 4. *K. pneumoniae* LPS and O-antigen structures. A) *K. pneumoniae* LPS is composed of broadly conserved Lipid A and core associated with repetitions of the O-Antigen. **B)** Structures of the 11 characterized O-antigen serotypes known for *K. pneumoniae*.

antigens have been identified through genomic studies of the *rfb* locus. O1, O2, and O3 types of O-antigen are associated with almost 80% of all *K. pneumoniae* infections[32,37,38]. O1, O2 and O8 share a common O2a structure, whose expression involves the *rfb* locus and the *wzm*, *wzt*, *wbbM*, *galf*, *wbbN*, and *wbbO* genes. O2afg and O2aeh modify the O2a repeating unit by side-chain addition of (α-1 → 4)- or (α-1 → 2)-Galp residues[39], while O8 serotype modifies the O2a repeating unit with a non-stoichiometric O-acetylation[40]. Rather than from a direct modification on O2a, O1 serotype is the result of the covalent attachment of the O1 antigen to the non-reducing

terminus of O2a, and it has been associated with *wbbY-wbbZ* genes[41]. O3 and O5 O-antigen structures are mannose-based and identical to the *E. coli* O9 and O8 serotypes, respectively[42,43]. O4, O7, and O12 serotypes have different repeating units of sugars compared to the other *K. pneumoniae*-specific O-antigen serotypes, with O4 and O12 structures terminating with a Kdo. The repeating units consist of a disaccharide [→4)-α-D-Galp-(1 → 2)-β-D-Ribf-(1→] (O4), a tetrasaccharide [→2)-α-L-Rhap-(1 → 2)-β-D-Ribf-(1 → 3)-α-L-Rhap-(1 →3)-α-L-Rhap-(1→] (O7), a disaccharide [→4)α-L-Rhap-(1 → 3)-β-D-GlcpNAc-(1→] (O12). In addition to this, the O4 and O12 O-antigen chains terminate with Kdo[44].

Fimbriae

In order to successfully adhere to host surfaces, *K. pneumoniae* employs fimbriae, filamentous structures that extend from the surface of bacteria. Fimbrial length is around 10 µm with a diameter that goes from 1 to 10 nm[45]. *K. pneumoniae* carries two types of fimbriae, encoded by two different genetic loci. Type 1 fimbriae, encoded by the *fim* gene cluster, promote adhesion on mucosal and epithelial surfaces and may thus boost bacterial virulence and favor colonization[46]. They consist of repeating units of the major fimbrial subunit FimA, with the FimH protein located at the distal end[47]. Type 3 fimbriae, encoded by the *mrk* locus, not only have a role in *K. pneumoniae* adhesion to surfaces, but also promote biofilm formation[48] in both biotic[49] and abiotic[50] surfaces. Type 3 fimbriae structure is made of repeating units of MrkA and present an adhesin (MrkD) on the extremity. Both types of fimbriae lead to catheter-associated urinary tract infections for their ability to colonize indwelling urinary devices[21].

Siderophores

Scavenging host iron is an effective strategy used by pathogenic bacteria to survive and establish infection within the host. Bacterial siderophores are high-affinity iron-chelating molecules that help bacteria in the iron acquisition process[51]. They can induce inflammation and bacterial dissemination during *K. pneumoniae* infections[13]. *K. pneumoniae* most common siderophore is enterobactin (Ent), encoded by the *ent* locus. Ent possesses the highest iron affinity known for any molecule[23]. The host innate immune system has developed mechanisms to bind Ent and prevent it from

binding iron[52], therefore *K. pneumoniae* strains armed themselves with multiple siderophores to overcome the obstacle. Salmochelin (Sal), yersiniabactin (Ybt), and aerobactin (Aer) are all secreted by *K. pneumoniae* as part of its accessory genome[13] and can be associated with pathogenic functions that go beyond iron acquisition[53]. For example, Ybt is the most common virulence factor associated with *K. pneumoniae* infections[14] and can promote disease in a murine model of pneumonia[54].

3. *K. pneumoniae* accessory genome and its role on antibiotic resistance

In the past decades, *K. pneumoniae* started showing worrisome characteristics of antibiotic resistance to most classes of antibiotics. Multiple antibiotic resistance genes lie in *K. pneumoniae* accessory genome, as some of them, such as extended spectrum β-lactamases (ESBL), are plasmid-borne[13]. ESBL-producing *K. pneumoniae* emerged in Europe[55] and in the United States[56] during the 1980s. ESBLs can hydrolyze third-generation cephalosporins and aztreonam and can confer resistance to other classes of antibiotics, but not to carbapenems[57]. For this reason, carbapenems have been the drug of choice to treat ESBL-producing *K. pneumoniae* infections. Treatments with carbapenems resulted in selective pressure that eventually led to the emergence of carbapenem-resistant *K. pneumoniae* lineages.

The first case of carbapenemase-expressing *K. pneumoniae* was reported in the United States (North Carolina) in 1996[58]. Several carbapenemases have been found ever since, raising concerns for the higher rates of morbidity and mortality associated with antibiotic resistant strains. Based on their molecular structures, carbapenamases can be classified following the Ambler classification system in class A, B and D. Class A and D carbapenamases display a serine residue in their active site, while class B operate through β-lactam hydrolysis and require zinc[59]. *K. pneumoniae* carbapenamases (KPC) are the most globally spread class A genes among Enterobacteriaceae and can hydrolyze all kinds of β-lactams.[60]. Moreover, presence of *bla*$_{KPC}$-bearing *K. pneumoniae* isolates has been reported across continents[61]. Among class D, oxacillinase (OXA) β-lactamases can be found in Enterobacteriaceae and confer resistance to some β-lactamase inhibitors[62]. In particular, *bla*$_{OXA-48}$ has been initially identified from a carbapenem-resistant *K.*

pneumoniae isolate and infections of OXA-48-producing strains have been reported all around the world[63]. Class B metallo β-lactamases (MBL) are able to hydrolyze all β-lactams and include the VIM (Verona integron-encoded MBL) and NDM (New Delhi MBL)[60] groups. VIM enzymes can easily spread as they are usually present on integrons, transposons or plasmids.

NDM-1 became one of the most commonly spread carbapenemases among Enterobacteriaceae[64] and it is now predominant in *K. pneumoniae* and *E. coli*[65], conferring resistance to almost all available antibiotics[66]. NDM-1 gene is located on plasmids, thus it is easily transferred among strains through horizontal gene transfer. Most NDM-1-bearing bacteria can hydrolyze all β-lactams, including carbapenems, and remain susceptible to only two antibiotics: colistin and tigecycline, both associated with toxicity to some extent[67,68]. The first case of NDM-1-expressing *K. pneumoniae* was reported in India, but to date there have been reports all across the world including China, Australia, North America, Europe, and Africa[69].In particular, $bla_{\text{NDM-1}}$ has been found in association with several *K. pneumoniae* lineages, including ST147 and ST11.

4. Convergence of classical and hypervirulent *K. pneumoniae* lineages

K. pneumoniae-associated infections have evolved into serious public health threats at the global level. Most of the strains that cause severe infection belong to two major pathotypes, namely the classical and hypervirulent ones[70]. Classical *K. pneumoniae* (cKP) is a frequent cause of opportunistic healthcare-associated infections and can easily acquire mobile genetic elements associated with antimicrobial resistance[71]. In particular, multidrug-resistant *K. pneumoniae* (MDR-cKP) strains carrying extended-spectrum β-lactamases and carbapenemases have played a major role in the global spread of AMR. Dissemination of MDR-cKP can be traced back to some successful "high-risk" clones, which are widely distributed geographically. Furthermore, carbapenem-resistant strains of *K. pneumoniae* (CR-KP) emerged in the mid-1990s and became prominent all across the world[72]. Among these, in the mid-2000s, high-risk clones ST147 and ST307 acquired carbapenemase-encoding genes such as NDM-1 and OXA-48 variants, as well as VIM[72,73]. Other clonal groups that are

associated with multidrug resistance are ST258, ST11, ST512 and many others, all globally spread[70].

The first *K. pneumoniae* strain showing characteristics of hypervirulence was reported in 1986 in Taiwan[74], with many cases identified worldwide since then. No specific marker for hypervirulent *K. pneumoniae* (hvKP) classification is known, but these strains show distinct clinical aspects and phenotypes. HvKP isolates can cause severe community-acquired infections in both immunocompromised and healthy individuals. The strong pathogenicity associated with hvKP infections can culminate in fulminant and invasive illnesses such as meningitis, liver abscesses, and endophthalmitis[75], with high mortality rates[70]. Phenotypically, HvKP isolates show characteristics of mucoviscosity and higher susceptibility to antimicrobial agents. Moreover, they carry large virulence plasmids encoding for genes related to capsule synthesis[73] and to siderophores production. In particular, *rmp* genes are regulators of the mucoid phenotype[76], while the *iut* and *iro* clusters encode for aerobactin and salmochelin siderophores[70].

Although hypervirulence and carbapenem resistance have evolved distinctly, in recent years cases of *K. pneumoniae* strains integrating both resistance genes and hypervirulence loci have been reported. Hypervirulent and carbapenem-resistant *K. pneumoniae* (CR-hvKP) lineages have emerged in the early 2010s[77] and have been reported all over the world[78]. These strains have been causing infections that are difficult, if not impossible, to treat. Interestingly, convergence of CR-KP and hv-KP can occur either when mobile genetic elements encoding for AMR genes are acquired by hv-KP strains, or when virulence genes are acquired by CR-KP, the latter case being more likely to occur. CR-KP isolates acquire and lose mobile genetic elements more readily if compared with hv-KP, as overproduction of capsule in hypervirulent strains may interfere with DNA uptake and mobile genetic elements transfer[79]. Considering the global spread of CR-KP and their acquisition of hypervirulence features[71], the need of surveillance and detailed genetic characterization to carefully monitor the global emergence of CR-hvKP isolates is undeniable. To date, CR-hvKp have been reported in Asia, Africa, Europe, as well as in South and North America, with most of the cases in China.

5. *K. pneumoniae* in Italy

In the last decade, CR-Kp became endemic in various countries, including Italy[80]. Italy faced a clonal expansion of a KPC-producing *K. pneumoniae* clone belonging to the clonal complex 258, followed by emergence of ST307 and ST11 lineages showing similar KPC-producing features. Strains carrying other types of carbapenemases remained sporadic until 2018, when a large outbreak of NDM-producing *K. pneumoniae* arose in Tuscany, mostly in the Northwest area of the region[81]. Between

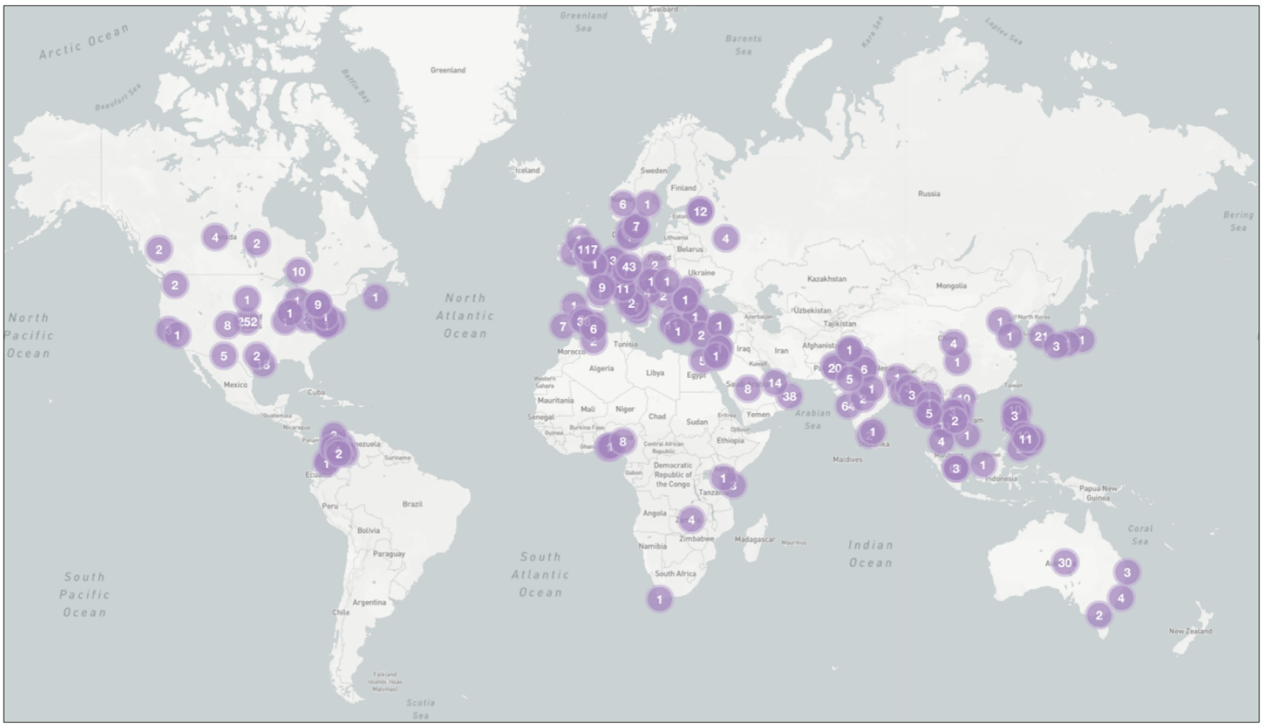

Figure 5. Global spread of ST147 *K. pneumoniae*. The map shows how ST147 *K. pneumoniae* is disseminated around the world.

2019 and 2020, *K. pneumoniae*-associated bloodstream infections spiked with an overall 30-day mortality of almost 40%[80]. Genomic analysis of strains from bloodstream infections revealed that 48 out of 54 cases (89%) were sustained by NDM-1 producing ST147 ($ST147_{NDM-1}$) *K. pneumoniae*. Analysis of the population of $ST147_{NDM-1}$ *K. pneumoniae* isolates responsible for the outbreak showed little intraclonal diversity and were mostly belonging to a subclade of ST147. The clone is named ST147-vir and bears a K64 capsular serotype, along with extensive antibiotic-

resistance genes and virulence factors, including some usually associated with hvKP strains[80]. Phylogenetic analysis of the $ST147_{NDM-1}$ lineage from the Tuscany outbreak suggested that it may be related to an endemic CR-Kp ST147 from the Middle East that acquired extra virulence and resistance plasmids[72]. Similar genetic rearrangements had been already detected in Russia (2017)[82], United Kingdom (2018-2019)[83], Egypt (2019)[84], and in the 2019 Kp outbreak in Germany[85], where different Kp STs coharboring virulence genes and blaNDM were reported. Indeed, an ancestor of the Tuscany outbreak strain[86] has been recently classified as pandrug-resistant[87,88], leaving scarce therapeutic solutions against this pathogen. Moreover, genetically related isolates and near-identical plasmids are being reported globally[73] (**Figure 5**), highlighting once more the importance of monitoring *K. pneumoniae* populations worldwide to contain the dissemination of high-risk clones.

6. Therapeutic approaches to fight AMR

> *"We owe chemotherapy the debt of reducing the high mortality rate of many bacterial infections; but in helping to solve some of the problems of infectious disease, chemotherapy has created some problems of its own. One of these problems […] has been the appearance of strains of organisms resistant to certain drugs."*
>
> S. Falkow

Over the past two centuries, living conditions of human beings steadily improved so much that life expectancy in high-income countries has increased by more than 30 years[89]. This remarkable achievement was made possible firstly by improved hygiene, but also by effective treatment of infectious diseases through vaccines and antibiotics[90] (**Figure 6**). The human immune system can be trained to recognize a specific pathogen and initiate an efficacious response through vaccines. For this reason, starting from the 20th century, vaccination on the large scale allowed the control of several major diseases, such as poliomyelitis, yellow fever and rabies, andeven led to complete eradication of the disease in the case of smallpox[91]. Global vaccine campaigns were instrumental in reducing bacterial and viral infections, especially exanthematous and other pediatric diseases[92]. Nevertheless, some diseases cannot be prevented by vaccination, which is why another significant breakthrough in the fight against infectious diseases was represented by the advent

of antibiotic treatment. Successful application of antimicrobial therapies drastically reduced mortality rates associated with infectious diseases and have revolutionized medicine and global healthcare[93].

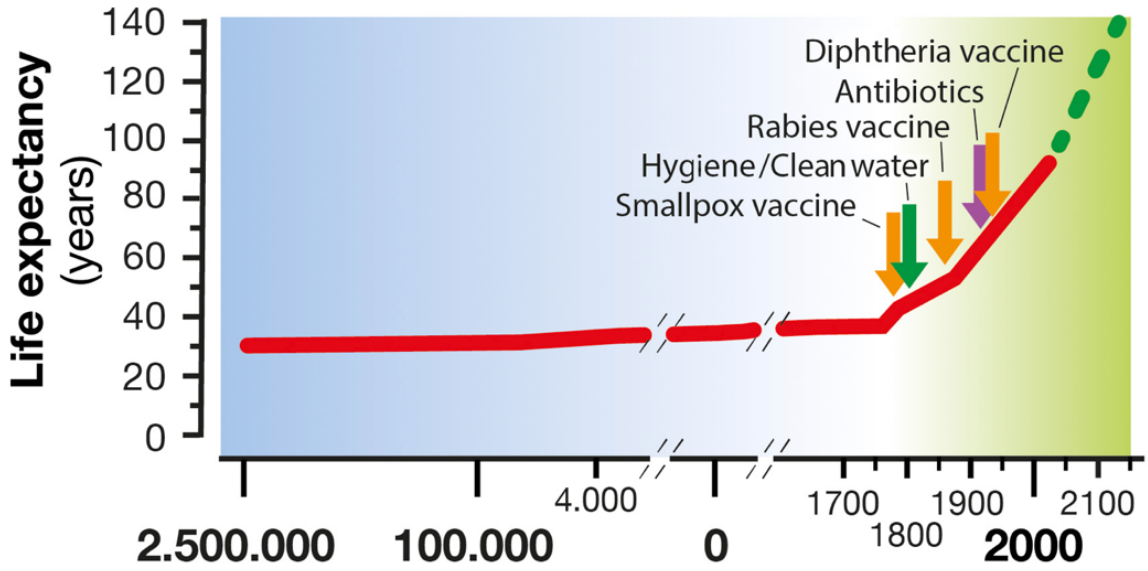

Figure 6. Life expectancy increase along human civilization. In the last century, introduction of hygiene, antibiotics and vaccines has considerably increased life expectancy. *Image from: Rosini, R., Nicchi, S., Pizza, M. & Rappuoli, R. Vaccines Against Antimicrobial*

Antimicrobial compounds can target different bacterial components, such as cell wall, macromolecular synthesis or metabolic pathways, therefore causing bacterial death or cessation of growth. Antibiotics work by targeting 5 major processes in the bacterial cell: they can damage bacterial cell wall or cell membrane integrity, interfere with DNA, RNA, and protein biosynthesis, or disrupt folic acid metabolism (**Figure 7**). All of the aforementioned characteristics are typical of bacteria and are different or nonexistent in eukaryotic cells, making antibiotics not toxic against the human host. Nevertheless, broad-spectrum antibiotics can have a negative effect on gut microbiota diversity[94], as they not only target the pathogen of concern but also beneficial bacteria[95,96]. Antibiotics are undoubtedly one of the most remarkable accomplishments in the fight against pathogens, but their use is intrinsically linked with bacterial capacity to rapidly evolve and develop resistance to antimicrobials. Indeed, the first cases of bacteria resistant to penicillin were reported in 1947[93], as early as

two years after the revolutionary antibiotic was introduced on the large scale[97]. Antimicrobial resistance is a major public health concern worldwide, with a global economic impact that may exceed one trillion US$ annually after 2030, in a low-impact scenario[98]. For these reasons, the quest for effective solutions to fight antimicrobial resistance is now essential. In this context, non-antibiotic therapies such as vaccines and therapeutic monoclonal antibodies (mAbs), monospecific antibodies that originate from a single clone of B cells as an immune response against an antigen, can prove to be essential.

Figure 7. Antibiotic targets and bacterial mechanisms of resistance. Antibiotics use different mechanisms to target and kill bacteria. Over time, bacteria developed several ways to overcome the effect of antibiotics and survive.

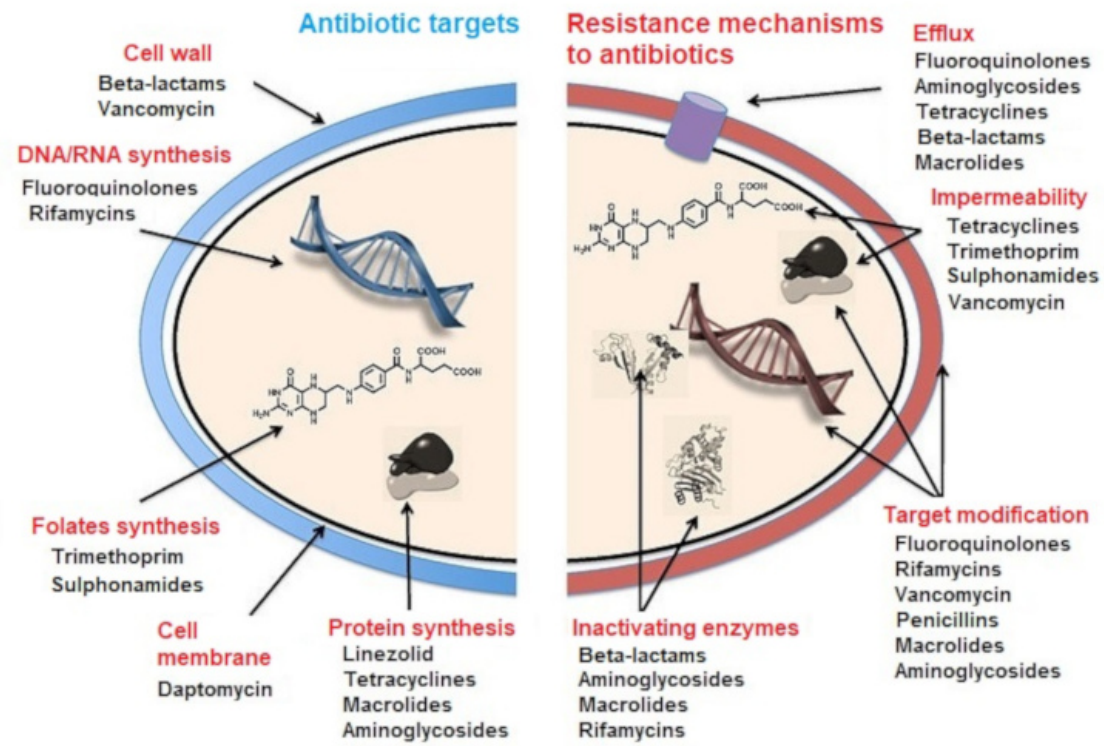

7. Therapeutic monoclonal antibodies against infectious diseases

Structure and effector functions

Human antibodies, also known as immunoglobulins (Ig), are Y-shaped heterodimeric proteins with a molecular weight of approximately 150 kDa. They are composed of two

identical light chains, which can be either κ or λ, and two identical heavy chains held together by disulfide bridges[99]. Antibodies are categorized in five different isotypes depending on their heavy chain sequences: IgA, IgD, IgE, IgG, and IgM (**Figure 8A**), each with a distinct role in the adaptive immune system[100]. Among the five isotypes, IgG is the most abundant in human serum and can be classified into four subclasses, IgG1, IgG2, IgG3, and IgG4. IgG subclasses are highly conserved but differ in their constant region, specifically in the hinge structure and in the upper CH2 domain[101]. Currently, the majority of all clinically used antibodies are IgG1 mAbs[99]. IgGs consist

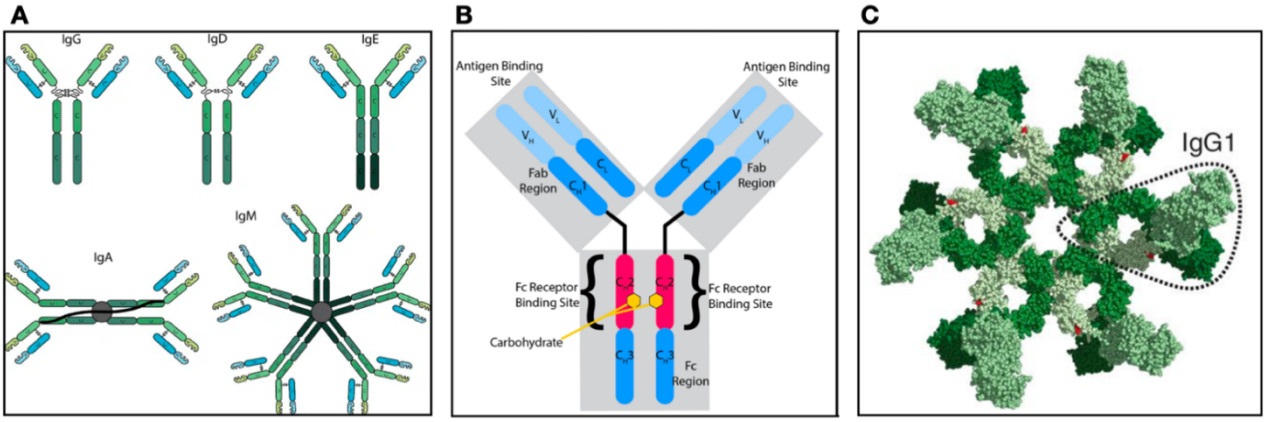

Figure 8. Human Immunoglobulins (IgG). A. Human Igs are grouped into 5 different isotypes.
B. Structure of an IgG antibody. **C.** Hexamerization of IgG1 antibodies.

of two Fragment Antigen-Binding domains (Fabs) linked to a Fragment Crystallizable (Fc) through a flexible hinge region that confers to Fabs a high degree of conformational flexibility[102]. The two Fabs comprise a variable domain composed of a pair of variable domains, one from the heavy (VH) and one from the light (VL) chain (**Figure 8B**). The complementarity determining region (CDR) of the variable chains defines the Fab antigen-binding site for the mAb to a specific epitope on the antigen[103]. On the other hand, the Fc portion of the IgG has the ability to bind Fc gamma receptors (FcγR) on the host cells[104] and determines mAbs effector functions[105].

mAbs exert their antimicrobial functions through different mechanisms of action, which can be Fab- or Fc-mediated. The ability of the Fab portion to bind bacterial

toxins, and therefore to prevent toxin binding to its target, leads to neutralization[106]. Another Fab-dependent mechanism of action is the mAb capacity of inhibiting bacterial adhesion to host cells[107], which represents the first step of a successful infection. In particular, studies on *Bordetella pertussis* have shown how mAbs targeting specific features of this pathogen could inhibit bacterial adhesion to epithelial host cells[108,109]. In addition to this, Fc-mediated effector functions can be classified in antibody-dependent cellular cytotoxicity (ADCC), antibody-dependent cellular phagocytosis (ADCP), and complement-dependent cytotoxicity (CDC)[110]. ADCC and ADCP mechanisms of action are mediated by the interaction of mAbs Fc domain with the corresponding FcγR. ADCC is mainly caused by Natural Killer (NK) cells, neutrophils and eosinophils upon activation of FcγRIIIa. ADCP, on the other hand, relies on FcγRIIa ability to activate macrophages and to increase their phagocytic effects[111]. Moreover, mAbs can facilitate phagocytosis by monocytes, macrophages, and neutrophils by coating the pathogen through a process known as opsonization. Some bacteria developed intracellular survival mechanisms to evade opsonophagocytic killing[112], nevertheless mAbs showed protective efficacy through FcR-mediated phagocytosis and neutrophil extracellular traps release against hvKP[113]. Protection against the pathogen was confirmed both *in vitro* and in three different *in vivo* models.

In addition to ADCC and ADCP, mAbs can induce activation of the complement cascade and lead to bacterial elimination through CDC. The complement system is a mechanism of the innate immune response to protect against aberrant endogenous proteins or bacterial pathogens[114]. The complement cascade can be activated via three distinct biochemical pathways: the classical pathway, the alternative complement pathway, and the lectin pathway (**Figure 9**). These three pathways are activated by different factors, but all converge at C3, eventually resulting in the formation of the activation products C3a, C3b, C5a, and the membrane attack complex (MAC)[115]. When IgGs bind to bacterial pathogens, they can recruit the C1q factor of the complement, therefore initiating the classical complement pathway[116]. The C1q molecule can fix the CH2 domain of IgG1 and triggers hexamerization of IgG (**Figure 8C**) to continue the complement cascade[117]. Upon association with IgG, C1q recruits two proteases, C1r and C1s and constitutes the C1 complex[116]. This complex has the

ability to cleave C4 and C2 proteins generating the C3 convertase, C4bC2a. The C3 convertase cleave C3 to release C3a, that can act as an opsin and can amplify complement activation, and C3b, that together with C3 convertase forms the C5 convertases. C5 convertases cleave C5 and form C5a and C5b. MAC formation is initiated when C6 and C7 bind to C5b and is completed when C8 and C9 bind to the newly formed complex. The MAC system can form pores in the cell membrane of pathogens, inducing cell lysis[115].

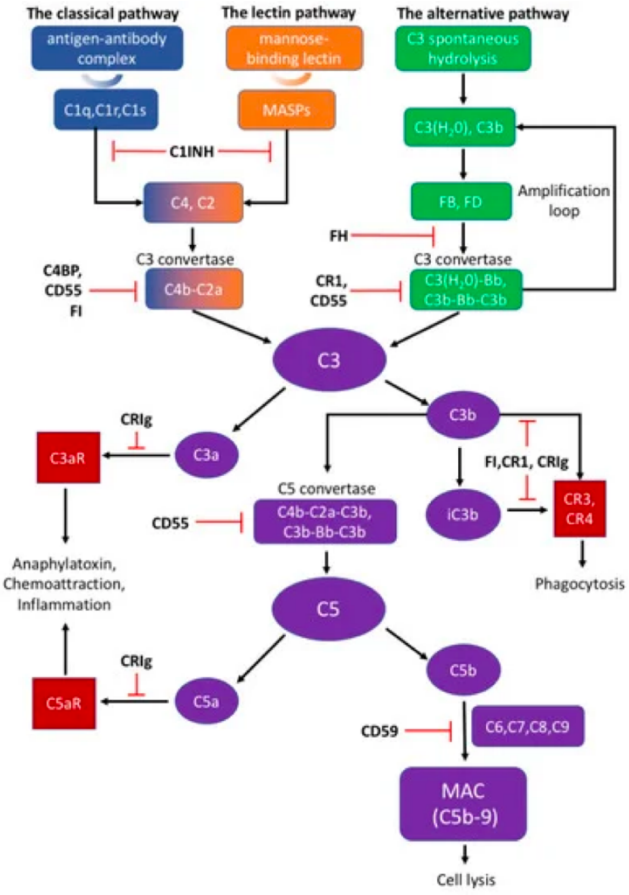

Figure 9. The complement cascade.

The classical complement pathway greatly contributes to host defense against viral pathogens, such as Influenza[118] and HIV[119], as well as against pathogenic bacteria, like *Salmonella*[120] and *Neisseria gonorrhoeae*[121]. For this reason, Fc engineering to facilitate IgG hexamerization has been exploited to enhance complement-dependent bactericidal properties of mAbs. In particular, it has been shown that by inserting specific mutations, namely E345K and E430G, in the IgG1 backbone, mAbs will form hexamers upon antigen binding. This resulted in CDC activity in an anti-CD20 mAb which was inactive prior to Fc sequence modifications[122]. Enhanced hexamerization and increased CDC was also observed upon engineering an antibacterial mAb against *N. gonorrhoeae*, where higher engagement levels of C1q and increased bactericidal activity were detected in the presence of the mutagenized mAb compared to its wild type version[123]. Notably, the mAb carrying the E430G mutation performed well *in vivo* [121].

Therapeutic mAbs discovery and development

The introduction of the hybridoma technology by Kohler and Milstein in 1975 started a new era for mAbs discovery and development[124]. Immortal clones from B cells were generated through the fusion of myeloma cell lines with lymphocytes from mice previously exposed to a given antigen. In this way, antigen-specific mAbs could then be screened and selected based on their binding affinity. The first therapeutic mAb was approved for use in humans in 1986 with the aim of preventing organ transplant rejection[102]. Nevertheless, being a fully murine antibody, its administration failed to activate human effector functions and triggered life-threatening production of human antimouse-antibodies[125]. To reduce immunogenicity, chimeric mAbs with human constant regions and murine variable regions were developed[126,127], but also further humanization of antibodies and minimization of the mouse component was achieved through CDR grafting[128]. Immunogenicity issues were further overcome with the phage display technology[129]. Phage display libraries are based on human immunoglobulin G (IgG) heavy and light chain variable region sequences obtained from immunized and infected individuals. The human variable regions can be introduced in the Gene III of filamentous bacteriophages that will express antibodies on their surface. Using the antigen of interest as a bait, selection of fully human, antigen-specific mAbs through affinity chromatography was made possible[130]. Fully human mAbs can also be produced by immunization of transgenic mice carrying the human IgG locus, therefore expressing human IgG isotypes[128].

Remarkably, advancement in human B cell sequencing and high-throughput screening as well as single cell isolation and structural characterization of antigens led in 2016 to another major breakthrough in mAbs discovery and development, the Reverse Vaccinology 2.0 approach[131]. With this method, identification of potent mAbs occurs directly from the blood of convalescent or immunized human donors and it is now widely used in the field of infectious diseases, allowing generation of immunotherapies against various viral pathogens[132–134]. The Reverse Vaccinology approach is also being used to find therapeutic mAbs against AMR bacterial strains[134]. Immunotherapies based on administration of mAbs have been considered as a valid alternative to antibiotics in the fight against AMR[135]. However, only a few antibacterial mAbs have succeeded in clinical trial and to date only three of them have obtained

approval by the FDA[112]. Raxibacumab and Obiltoxaximab, respectively a human recombinant IgG1 and a chimeric IgG1, are both directed against the toxin of *Bacillus anthracis*. Raxibacumab received approval for treatment of inhalational anthrax in combination with antibiotics[136,137], while Obiltoxaximab proved to be effective in both prophylaxis and treatment regimens of *B. anthracis* infections[138] and was approved by the FDA in 2016[139]. The last antibacterial mAb authorized by FDA is Bezlotozumab, which is directed against *Clostridium difficile* toxin B and has been employed to treat recurrent infections[140]. The main explanation for the exiguous amount of authorized antibacterial mAbs is the poor correlation between preclinical and clinical studies results; mAbs that are effective *in vivo* in animal models often show limited protection in clinical trials[141,142], highlighting a discrepancy that can be explained by the genetic and immunological differences between humans and animals. For this reason, to successfully employ mAbs as primary therapies against AMR bacteria, establishing clinically relevant *in vitro* and *in vivo* models to improve correlation between preclinical and clinical studies should be considered as a priority[142].

Aims of the work

For my PhD project I joined the *Klebsiella pneumoniae* research group of the Monoclonal Antibody Discovery Laboratory at Fondazione Toscana Life Sciences in Siena (Italy). The main focus of the study was the discovery and development of human monoclonal antibodies (mAbs) as innovative immunotherapies against a pandrug-resistant $ST147_{NDM-1}$ *K. pneumoniae* lineage that has been causing a persistent nosocomial outbreak in the Tuscany region since 2018. Moreover, I trained in Prof. Amieva's laboratory at Stanford University (Palo Alto, CA) during the third year of my PhD studies to design a novel physiologically relevant model for *K. pneumoniae* infection by exploiting *ex vivo* cultures. The purpose of the project was to unravel molecular mechanisms that drive *K. pneumoniae* host-pathogen interactions, as well as to define the protective role of the most promising mAb candidate in a human-derived model. I pursued the main objectives of my PhD research through the following aims:

- To isolate, express and select potent, fully human mAbs against pandrug-resistant *K. pneumoniae* $ST147_{NDM-1}$.
- To extensively characterize binding and protective properties of selected $ST147_{NDM-1}$-specific mAbs.
- To employ human-derived colonic organoids as host model for $ST147_{NDM-1}$ *K. pneumoniae* enteric infection.
- To evaluate mAbs efficacy in protecting against *K. pneumoniae* adhesion and proliferation on gut epithelia by interrogating the newly established organotypic model of infection.

The first chapter of my thesis describes the discovery and the characterization of human mAbs against $ST147_{NDM-1}$ *K. pneumoniae*. Those results are part of a submitted manuscript entitled "Anti-capsule human monoclonal antibodies protect against hypervirulent and pandrug-resistant *Klebsiella pneumoniae*" where my contribution consisted in:

- Amplification of variable regions of the heavy (V_H) and light (V_L) chains of mAbs through RT-PCR followed by nested PCR

- V_H and V_L cloning in expression vectors
- Large-scale expression of recombinant mAbs
- Development, application, data analysis, and figure preparation of:
  - High-throughput luminescence-based Serum Bactericidal Assay (SBA) for selection of functional mAbs
  - High-throughput fluorescence-based SBA for characterization of mAbs potency
  - Immunoblotting to evaluate mAbs binding to different *K. pneumoniae* strains
  - Purification of $ST147_{NDM-1}$ *K. pneumoniae* capsule
- Data analysis and figure preparation of:
  - ELISA screening of mAbs binding against *K. pneumoniae* from memory B cells supernatants
  - Flow cytometry of mAbs binding to the bacterial surface of different *K. pneumoniae* strains, *Klebsiella* species, and commensals

The second chapter deals with the work I carried out in Prof. Amieva's laboratory on colonic organoids and reports the data I generated upon infection of *ex vivo* models with $ST147_{NDM-1}$ *K. pneumoniae*.

CHAPTER 1:

Human monoclonal antibodies protect from bloodstream infection by pandrug-resistant *Klebsiella pneumoniae*

A patent application related to this work, where I am listed as a co-inventor, has been filed:

Antibodies against multidrug-resistant *Klebsiella pneumoniae,* 102023000000924

Abstract

Antimicrobial resistance (AMR) requires the development of innovative therapeutics to bypass the ineffectiveness of antibiotics. Despite the potential of human monoclonal antibodies (mAbs), their exploitation against AMR is still limited. Here we apply an antigen-agnostic strategy to isolate extremely potent human mAbs against the pandrug-resistant ST147 *Klebsiella pneumoniae* lineage causing a persistent nosocomial outbreak in Italy. These mAbs, targeting bacterial capsule and O-antigen, are the most potent described to date as they display *in vitro* bactericidal activity at the picomolar range. Nevertheless, only capsule-specific mAbs promoted bacterial uptake by macrophages and enchained bacterial growth in the nanomolar range of concentrations. Importantly, this *in vitro* poly-functionality translated into *in vivo* protection against ST147 bloodstream infection. Our study describes the only antimicrobial able to protect against fulminant septicemia caused by a pandrug-resistant species and expands our knowledge on effector functions of therapeutic mAbs. Our results hold universal value for AMR pandemics prevention and vaccine development.

Introduction

Antimicrobial resistance (AMR) has been enlisted by the World Health Organization, the European Medicines Agency and the United Nations as one of the top 10 global health priorities[143], due to its impact on human health and socio-economic welfare worldwide. Among pathogens with multi-drug resistance (MDR) profiles, Enterobacteriaceae causing threats in hospital settings are considered the most critical[5] and are currently dominated by *Klebsiella pneumoniae* (Kp) species[8]. Most of Kp strains that cause severe infections belong to two major pathotypes, namely the classical and hypervirulent ones[70]. Classical Kp is a frequent cause of opportunistic healthcare-associated infections and can easily acquire mobile genetic elements associated with AMR[71]. In particular, multidrug-resistant (MDR) Kp strains carrying extended-spectrum β-lactamases and carbapenemases have played a major role in the global spread of AMR. Among carbapenemases, the New Delhi Metallo-β-lactamases (NDM) are extremely alarming as they confer resistance to the most recent combinations of β-lactams and β-lactamase inhibitors (i.e., ceftazidime–avibactam, imipenem–relebactam, and meropenem–vaborbactam), which are considered the last line of defense[80,144]. NDMs are encoded by *bla*$_{NDM}$ genes located on large multi-resistance plasmids that have been spreading across high-risk MDR Kp clones throughout all continents[73,80]. Hypervirulent Kp (hvKp) isolates can cause severe community-acquired infections, such as pyogenic liver abscess, endophthalmitis, and meningitis, in both immunocompromised and healthy individuals[12,145,146]. Despite showing higher susceptibility to antimicrobial agents, hvKp strains carry large virulence plasmids encoding for genes related to capsule synthesis[73], resulting in enhanced mucoviscosity, and to siderophores production[70].

Although hypervirulence and multidrug resistance have evolved distinctly, in recent years cases of Kp strains integrating both resistance genes and hypervirulence loci have been reported[77,78]. The convergence of genetic elements conferring both MDR and hypervirulence traits in NDM-producing Kp strains is particularly alarming, as it increases the potential for widespread dissemination. Notably, NDM-1-positive sequence type ST147 clone (ST147$_{NDM-1}$) carrying both MDR and hypervirulence genes[73] has been causing a nosocomial outbreak in the Tuscany region of Italy. Between 2019 and 2020, the 30-day mortality rate associated with ST147$_{NDM-1}$

bloodstream infections in Tuscany was almost 40%[80]. Genomic surveillance data indicated that Tuscany isolates of ST147 carry a highly diversified plasmid content, along with extensive antibiotic-resistance genes and virulence factors[80]. Similar genetic rearrangements had been already observed in Russia (2017), United Kingdom (2018-2019) and Egypt (2019), where different Kp STs (ST15, ST147, ST395, and ST874) carrying hybrid plasmids coharboring virulence genes and *bla*$_{NDM}$ were reported[82–84]. The same was observed in the 2019 outbreak in Germany[85], where the hybrid element in hypermucoviscous *bla*$_{NDM\text{-}1}$/*bla*$_{OXA\text{-}48}$-carrying ST307 isolates was detected. Overall, ST147 accounts for about 5% of Kp infections worldwide[147], widely spread especially in India and South-Eastern Asiatic region. Recently, an ancestor of the Tuscany outbreak strain[73] has been recently classified as pandrug-resistant[87,88].

The convergence of genetic elements into epidemic clones represents an alarming evolutionary feature that underscores the capacity of high-risk clones to cause even larger epidemics and urges the search for alternative treatment strategies. In this context, human monoclonal antibodies (mAbs) represent a powerful tool that can rapidly progress to innovative prophylactic and therapeutic solutions against MDR Kp. Notably, mAbs are unique in having intrinsically good safety profiles and avoiding impact on the host microbiota thanks to their specificity. Several murine mAbs against Kp, primarily targeting the capsule, have shown protective efficacy in various *in vivo* mouse models against ST258[148,149]. Remarkably, one of the mAbs showed cross-functional characteristics among Kp strains bearing different capsule types, highlighting the presence of a common epitope. Nonetheless, more than 100 capsule serotypes have been described with a wide range of saccharidic compositions[32], making the task of finding a cross-reactive anti-capsule mAb extremely difficult or almost impossible. Additionally, anti-lipopolysaccharide (LPS) mAbs have demonstrated opsonophagocytic activity, but issues with specificity and efficacy have been reported[150]. In particular, an anti-O3 mAb was described not only to target the Kp LPS, but also recognized diverse LPS from intestinal microbes[151], while other studies reported several mAbs targeting different epitopes of the LPS with *in vivo* activity only against capsule-deficient strains of Kp[152]. To date, the only potential protein target identified for Kp is MrkA[153], a major component of the type III fimbrial complex, involved in biofilm formation and infection establishment. Indeed, MrkA

aminoacidic sequence is highly conserved among Kp strains[154] but, despite promising *in vitro* results of anti-MrkA mAbs, challenges remain in achieving optimal protection *in vivo*[153]. Altogether, these mAbs display characteristics which are not recommended nor reliable for therapeutic use.

Developing mAbs against AMR pathogens is withheld by two major gaps: lack of knowledge of the correlates of protection against emerging AMR strains, and lack of comprehensive screening pipelines for rational mAb isolation. In fact, while 26 mAbs against bacterial pathogens have entered clinical phases for efficacy evaluation, only a few have gained FDA approval[134], and none of them is directed against Kp. In this work, we describe a robust method for unbiased mAb selection, not bound to a particular predetermined antigen, that allowed the definition of mAb functional properties associated with protection against $ST147_{NDM-1}$ bloodstream infection. We isolated 134 Kp-specific human mAbs from patients of the 2018 nosocomial Tuscany outbreak, with 20 mAbs demonstrating potent *in vitro* bactericidal activity in the picomolar range of concentrations. Notably, one selected mAb, 08O09, targeting $ST147_{NDM-1}$ capsule type 64, was able to promote bacterial uptake in phagocytosis assays and trigger enchained bacterial growth which correlated with the ability to protect against bloodstream infection *in vivo*. Our study exemplifies how a rationally designed experimental pipeline of mAb screening allows to predict correlates of *in vivo* efficacy and thus rapidly select therapeutic anti-bacterial mAbs to target emerging pandrug-resistant Kp lineages. Therefore, our work represents the first description of a fully human mAb against the pandrug-resistant ST147 Kp strain.

Results

1. Isolation of bactericidal human mAbs against Tuscany outbreak strain $ST147_{NDM-1}$

To isolate Kp-specific mAbs representing the breadth of antibody repertoire induced by Kp infection, we used an antigen-agnostic approach. Peripheral blood mononuclear cells (PBMCs) were collected from 7 convalescent patients who recovered from $ST147_{NDM-1}$ Kp bloodstream infection of the Tuscany nosocomial outbreak. A total of 18,390 $CD19^+CD27^+IgM^-IgD^-$ memory B cells (MBCs), either IgG^+ or IgA^+-positive, was single-cell sorted and plated together with CD40L-expressing feeder cells, IL-2 and IL-21 to promote MBCs activation, proliferation and antibody secretion (**Figure 1A; Figure S1**). MBCs culture supernatants were screened by enzyme-linked immunosorbent assay (ELISA) against $ST147_{NDM-1}$ bacteria to select Kp-reactive mAbs. 214 mAbs specific for antigens displayed on the bacterial surface were identified (**Figure 1B, Table S1)**. Upon molecular cloning of their V_H and V_L variable portions, sequences of 134 Kp-reactive mAbs were recovered with successful V_H and V_L pairing. To validate the binding properties of the isolated mAbs, they were expressed on a small scale and tested by ELISA against outbreak-belonging $ST147_{NDM-1}$ Kp isolates (**Figure S2**). Further, mAbs were screened for their ability to induce complement-dependent killing of $ST147_{NDM-1}$ Kp. For this purpose, we developed a high-throughput luminescence-based serum bactericidal assay (L-SBA) that measures ATP content as a proxy of Kp viability (13, 14). Four dilutions per mAb were tested in the presence of an exogenous source of complement and those mAbs causing a reduction greater than 30% in bacterial viability were considered as positive hits. Out of the 134 Kp-binding mAbs screened, 25 candidates showing bactericidal activity against $ST147_{NDM-1}$ were selected (**Figure 1C**) and expressed on the larger scale. Upon excluding five mAbs that failed to re-confirm their activity, binding and functional properties of 20 bactericidal $ST147_{NDM-1}$-targeting mAbs were evaluated.

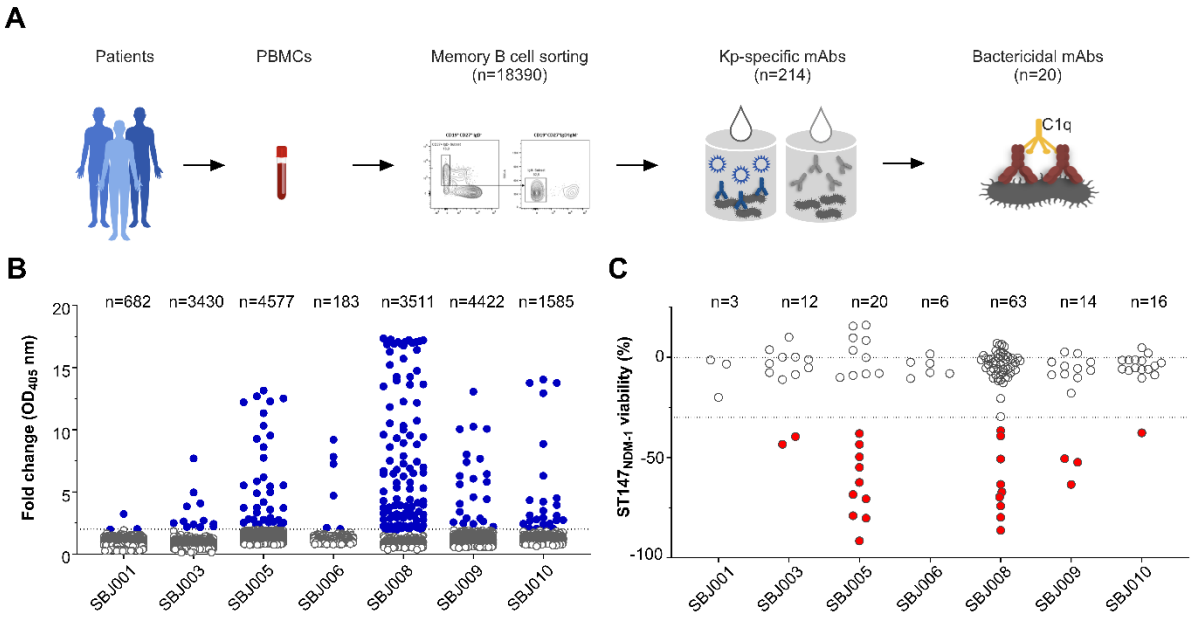

Figure 1. Isolation and selection of Kp-specific mAbs against ST147$_{NDM-1}$ Tuscany outbreak strains. A) Schematic workflow of anti-Kp antibody isolation and selection. **B)** ELISA screening of supernatants of 18,390 single cell-sorted MBCs isolated from 7 convalescent patients. The assay was performed to detect IgG/IgA against surface antigens of ST147$_{NDM-1}$ c.i.1 and ST147$_{NDM-1}$ c.i.2. 214 MBCs supernatants showed a signal at least 2-fold above the blank of OD_{405} and were thus selected for further analysis (blue dots). **C)** L-SBA on recombinant mAbs against ST147$_{NDM-1}$ c.i.1. 30% reduction in bacterial viability was used as a cut-off for selection. 25 mAbs showing bactericidal properties were identified (red dots).

2. Kp library profiling reveals that bactericidal mAbs have different degree of cross-reactivity and antigen specificity

To characterize specificity and cross-reactivity of the isolated bactericidal mAbs, flow cytometry was employed to profile their binding against a panel of bacterial strains. Pathogenic Kp belonging to different STs were included (**Table S1**), as well as other *Klebsiella* species and several commensal strains. Antibody binding to bacterial surface displayed different levels of intensity, ranging from virtually null to high, suggesting differential expression of target antigens or variable affinity of the mAbs (**Figure 2A**). Moreover, mAbs showed high specificity to pathogenic *sensu stricto* Kp strains as they did not react with other Kp phylogroups nor with commensals (**Figure S3**). Based on their binding profiles, mAbs were grouped into two main clusters

(**Figure 2A**). The first cluster (Cluster 1) encompassed mAbs with rather restricted binding characteristics, recognizing exclusively outbreak ST147 carrying either *bla*$_{NDM-1}$ or *bla*$_{NDM-9}$ genes[155]. The second group of mAbs (Cluster 2) displayed a broader binding pattern, being able to recognize up to seven different sequence types of pathogenic Kp.

Comparative whole genome sequencing analysis of Kp library allowed prediction of surface antigens targeted by mAbs. We hypothesized that Cluster 1 mAbs were likely directed against ST147$_{NDM-1}$ CPS, as they solely recognized strains bearing genes from the capsule type 64 biosynthetic locus[156] (KL64; **Table S2**) and did not cross-bind any other strain (**Figure 2A**). Regarding Cluster 2 mAbs putative target, genomic analysis of the O-antigen biosynthetic loci revealed that ST147$_{NDM-9}$ presented a single-point deletion in the *wbbO* gene, which encodes for a glycosyltransferase essential for O2a biosynthesis[157,158]. This mutation caused frameshift and premature termination of translation (**Figure S6**), hindering the production of the complete O-antigen. Indeed, HPLC and SDS-PAGE analysis of total sugar extracts from ST147$_{NDM-9}$ confirmed that ST147$_{NDM-9}$ was a natural O-antigen-deficient mutant (**Figure S7**). Considering that cluster 2 mAbs selectively reacted with ST147$_{NDM-1}$ and displayed total lack of binding to ST147$_{NDM-9}$, we assumed that these mAbs could very likely be directed against the ST147$_{NDM-1}$ O-antigen.

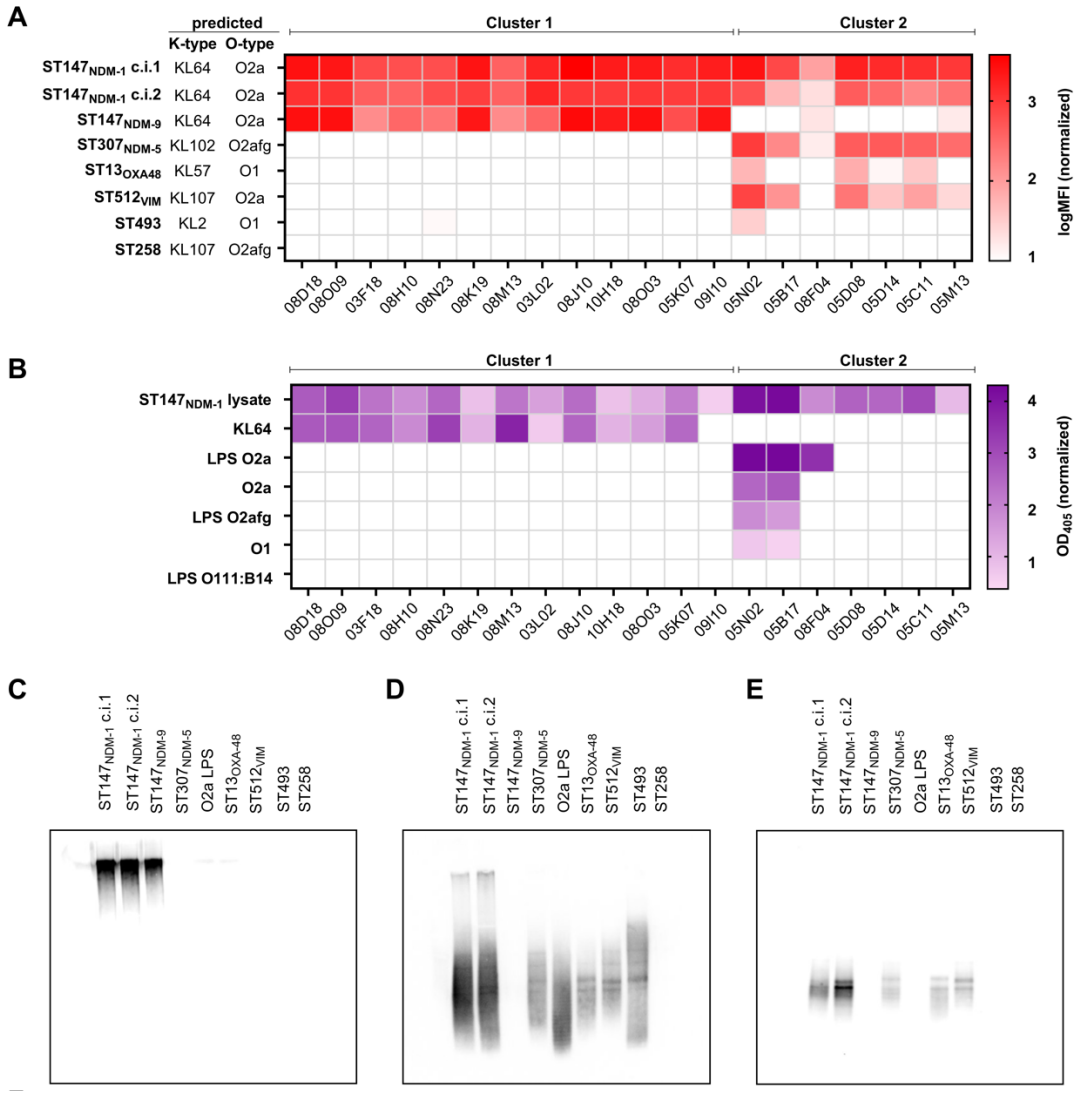

Figure 2. Binding properties of 20 bactericidal ST147$_{NDM-1}$-specific mAbs. A) Heatmap representing high-throughput flow cytometry screening of 20 functional mAbs against a panel of genetically diverse Kp strains. MFI was normalized to no mAb controls and transformed in logarithmic scale. **B)** Heatmap of ELISA results with purified CPS and O-antigens. Unrelated *E. coli* LPS O111:B4 was used as negative control and total bacterial lysate as a positive control. Values at least 3-fold above the blank of OD_{405} were considered as positive hits. **C-E)** Representative immunoblot profiles of selected anti-Kp mAbs probed against total sugar extracts of indicated strains. 08O09 (**panel C**) results show a smeared, high molecular weight band in presence of total sugar extracts of ST147 Kp species, indicating recognition of KL64 capsule. 05N02 (**panel D**) results show a wide ladder-like profile against a broad panel of Kp STs, bearing both O2- and O1-type of O-antigen. 05D08 (**panel E**) shows medium molecular weight ladder-like signal for O2 carrying-Kp strains.

3. ST147-specific bactericidal mAbs target ST147$_{NDM-1}$ capsule and O-antigen

To test these assumptions, mAb binding was assessed in ELISA against purified Kp capsule and O-antigens of various origin (**Figure S4 and S5**). KL64 capsule was recognized only by Cluster 1 mAbs (**Figure 2B**). Moreover, immunoblotting of Kp total sugar extract further confirmed that these antibodies decorated high molecular weight (MW) molecular structures of KL64-bearing Kp strains, in line with Western blot profiles of polysaccharidic capsules[159] (**Figure 2C**). Instead, ELISA against purified O-antigens revealed a more heterogeneous picture within Cluster 2 mAbs. Three mAbs bound to purified O2a O-antigen, with variable degree of cross-reactivity against O2afg and O1 O-antigens (**Figure 2B**), while immunoblotting analysis evidenced a ladder-like binding pattern, compatible with typical O-antigen immunoblotting profiles[158] (**Figure 2D**).

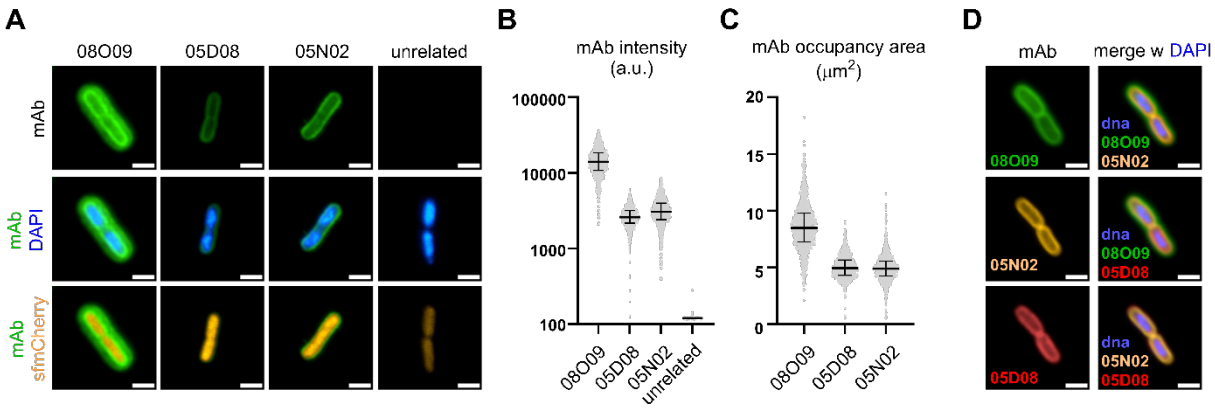

Figure 3. Microscopy characterization of anti-Kp mAb binding on ST147$_{NDM-1}$ strain.
A) Images show ST147$_{NDM-1}$ expressing sfmCherry stained with 08O09, 05D08 and 05N02 mAbs labelled with anti-human A488 conjugated secondary antibody (green). Bacterial DNA is stained with DAPI (blue). Scale bar 2 μm. **B)** Scatter plot showing quartiles range of quantification of A488 intensity at the single bacterium level (median=12289 a.u./ n=3475 for 08O09; median=2518 a.u/ n=3024 for 05D08; median=2860 a.u./ n=3269 for 05N02; median=119.1 a.u./ n=3078 for unrelated mAb). **C)** Scatter plot displaying quartiles range of the area measured on A488 spots (median=8.3μm^2/ n=3475 for 08O09; median=4.9μm^2/ n=3072 for 05D08; median=4.8μm^2/ n=3310 for 05N02). **D)** Representative images showing ST147$_{NDM-1}$ stained with 08O09-A488, 05N02-A555 and 05D08-A647 conjugated mAbs. Scale bar 2 μm.

Five other mAbs from Cluster 2 did not recognize purified O-antigens in ELISA, however they displayed a similar ladder-like binding profile in the middle MW range against total sugar extracts of Kp strains expressing O2a O-antigens (**Figure 2E**). Altogether, these analyses allowed grouping ST147$_{NDM-1}$-targeting antibodies into KL64-specific and O2a O-antigen specific mAbs, wherein some O-antigen-specific mAbs were cross-reactive against O1 type O-antigen.

High-resolution and high-content imaging of ST147$_{NDM-1}$-binding mAbs demonstrated that candidates directed against capsule and O-antigen displayed different localization patterns (**Figure 3A**). For instance, the anti-capsule mAb 08O09 displayed higher intensity binding which was distributed over a larger area with respect to the anti-O-antigen mAbs 05D08 and 05N02 (**Figure 3B, Figure 3C**, **Figure S8**). Moreover, the 08O09 signal was localized on the outermost layer of the bacteria, whereas 05D08 and 05N02 were located inside (**Figure 3D**), indicating they have non-overlapping pattern, in agreement with their molecular targets. Analysis of the germline composition of mAbs evidenced a bias in germline usage for anti-capsular mAbs, while 3 clonal pairs were detected among O-antigen-specific mAbs (**Figure S9; Table S3**).

4. Functional profiling reveals that isolated mAbs have extremely potent bactericidal activity, however only anti-capsular mAbs are poly-functional

To better assess the protective properties of anti-capsule and anti-O-antigen bactericidal mAbs, several *in vitro* assays that could predict antibody-mediated bacterial control *in vivo* were employed. Bactericidal mAbs were expressed as human IgG1 with the E430G mutation in the Fc domain, which enhances the hexamerization process that naturally occurs between Fc domains and thus potentiates antibody effector function[121,122,160]. The processivity of complement-dependent killing assays (SBA) was enhanced by optimizing a fluorescence-based SBA (F-SBA) in the 384-well format and using resazurin metabolism as a readout of bacterial viability. F-SBA profiling of mAbs against complement-sensitive pathogenic Kp strains (ST147$_{NDM-1}$, ST147$_{NDM-9}$, and ST307$_{NDM-5}$) revealed that most of the antibodies were functional in the picomolar range of concentrations, with the most potent mAb showing 0.5-6 ng/mL IC_{50} values (**Figure 4A; Figure S10**). Ability to kill different Kp strains correlated with

mAbs cross-binding properties, since anti-KL64 mAbs were effective against KL64-bearing $ST147_{NDM-1}$ and $ST147_{NDM-9}$, while anti-O-antigen mAbs displayed activity against O2 O-antigen-bearing $ST147_{NDM-1}$ and $ST307_{NDM-5}$ (**Figure 4A**). Results of F-SBA allowed ranking mAbs according to their IC_{50} and to bacterial viability reduction extent (**Figure S11**).

Since phagocytes play a crucial role in Kp clearance during infection[161,162], mAbs displaying the highest bactericidal potency were then evaluated in macrophage-mediated opsonophagocytosis assays. Super-folder (sf) mCherry-overexpressing recombinant $ST147_{NDM-1}$ was opsonized with escalating doses of mAbs prior to incubation with differentiated THP-1 cells. Then, fluorescence of internalized Kp was measured as a readout of mAb ability to promote opsonophagocytosis. Anti-KL64 mAbs were found to increase Kp uptake by THP-1 cells at doses greater than 0.6 μg/mL, except for 10H18 which showed a very mild effect (**Figure 4B**). However, no Kp uptake was detected in the presence anti-O-antigen mAbs (**Figure 4C**). On the one hand, this indicated that anti-capsular but not anti-O-antigen mAbs were able to promote bacterial engulfment. On the other hand, it showed that opsonization with anti-capsular mAbs was able to overcome inhibition of opsonophagocytosis exerted by virulence factors on Kp surface[163–166].

Finally, to analyze the impact of bactericidal mAbs on Kp over time, time-lapse imaging of $ST147_{NDM-1}$-sfmCherry incubated with increasing doses of mAbs was performed. Cluster 1 mAbs induced enchained bacterial growth in the 10 to 100 μg/mL range of concentrations (**Figure 4D**). Mechanistically, this phenotype was associated with the appearance of concatenated replicating bacteria which did not divide into sister cells. On the contrary, cluster 2 mAbs did not induce enchained growth at any tested dose (**Figure 4D**). Overall, this multi-layer analysis indicated that the isolated mAbs had an extremely potent bactericidal activity, that their functionality extended beyond opsonophagocytosis and implicated other effector mechanisms, such as enchained Kp growth. However, surprisingly, only anti-capsular mAbs were endowed with such poly-functionality.

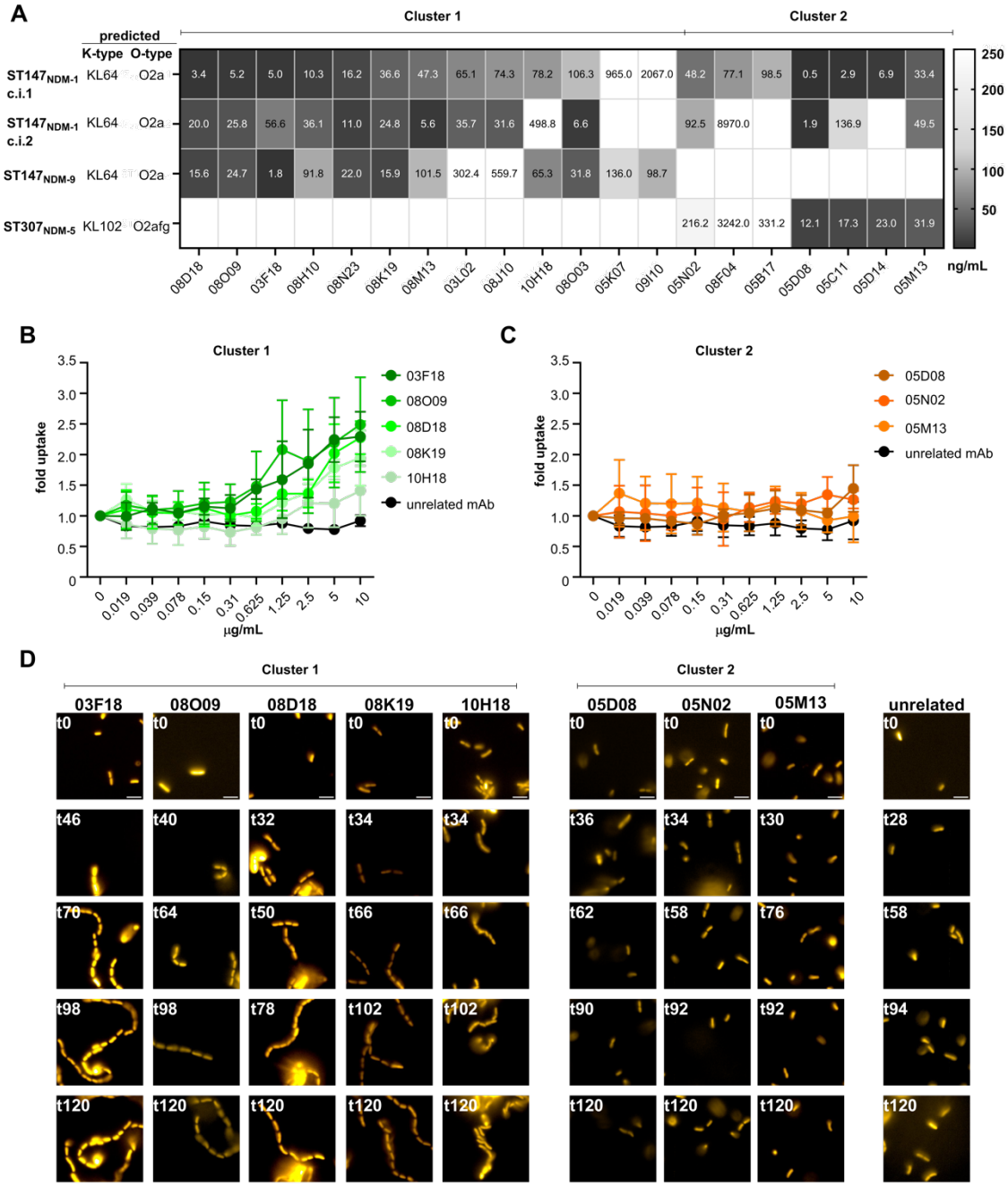

Figure 4. Functional *in vitro* characterization of 20 bactericidal ST147$_{NDM-1}$-targeting mAbs. A) Heatmap reporting IC_{50} values from F-SBA screening of 20 anti-Kp mAbs against the indicated complement-sensitive bacterial strains. **B)** Bacterial fold uptake by THP-1 macrophages measured in phagocytosis assay in the presence of anti-Kp mAbs from cluster 1. **C)** Bacterial fold uptake by THP-1 cells measured in samples treated with anti-Kp mAbs from cluster 2. **D)** Panels show still frames from time-lapse imaging of ST147$_{NDM-1}$ bacteria expressing sfmCherry grown in the presence of 100 µg/mL of indicated mAbs for 120 minutes. Scale bar 5 µm.

5. mAb poly-functionality is required for protection against fulminant $ST147_{NDM-1}$ bloodstream infection *in vivo*

To address the fundamental question of whether picomolar bactericidal activity on its own correlated with mAb efficacy *in vivo* or whether poly-functionality was required, the protective properties of the most potent mAb candidates (anti-capsular 08O09, anti-O2 O-antigen 05D08, and anti-O1/O2 O-antigen 05N02) were evaluated as prophylaxis (PRO) and treatment (THR) in an immunocompetent murine septicemia model[167]. A fulminant bloodstream infection model was selected to reflect the clinical history of donors from whom mAbs were isolated and was established to achieve 90-100% mortality within 24 hours of bacterial challenge (**Supplementary Figure S12A**).

Mice were administered uranyl nitrate 5 mg/kg three days prior to inoculation to produce a controlled degree of renal impairment. To assess the *in vivo* PRO activity against $ST147_{NDM-1}$, groups of ten mice each were administered with 1, 5, 10, and 20 mg/kg mAb dose 24 hours prior to bacterial inoculation (**Figure 5A**). Notably, 08O09 at 5 mg/kg and higher dosages extended survival significantly compared to sham control ($P < 0.05$), with 30% survival rate (**Figure 5B**). Consistent with this observation, CFU counts in the spleen showed a reduction compared with control (**Supplementary Figure S12B**). Instead, 05D08 and 05N02 mAbs did not prolong animal survival, at none of the administered doses (**Figure 5C-D**). The PRO experiment with 5 mg/kg dose of 08O09 was tested on 30 animals in total, showing consistency and reproducibility, with at least 35 h of life extension and 50% mouse survival up to 96 h (**Figure 5E**). Moreover, plasma concentration of 08O09 associated with *in vivo* efficacy was 74.3 (± 21.7) μg/mL (**Figure S13**). Next, the THR efficacy of 08O09 administered intravenously at 1, 5, 10, and 20 mg/kg one-hour post-bacterial challenge was assessed **(Figure 5F)**. In this case, moderate protection was achieved at 5 mg/kg and higher dosages (**Figure 5G**), as confirmed by lower CFU counts in the spleen (**Supplementary Figure S12C)**. Lastly, the protective properties of 08O09 in a combinatorial prophylaxis/treatment (PRO+THR) regimen were investigated. To do so, a first dose of 08O09 was administered intraperitoneally 24 hours prior to bacterial inoculation, followed by a second dose administered intravenously one hour post bacterial challenge **(Figure 5H)**. Strikingly, PRO+THR benefits were observed only for the 1 mg/kg dosage, with 30% 96 h survival. The same dose resulted otherwise

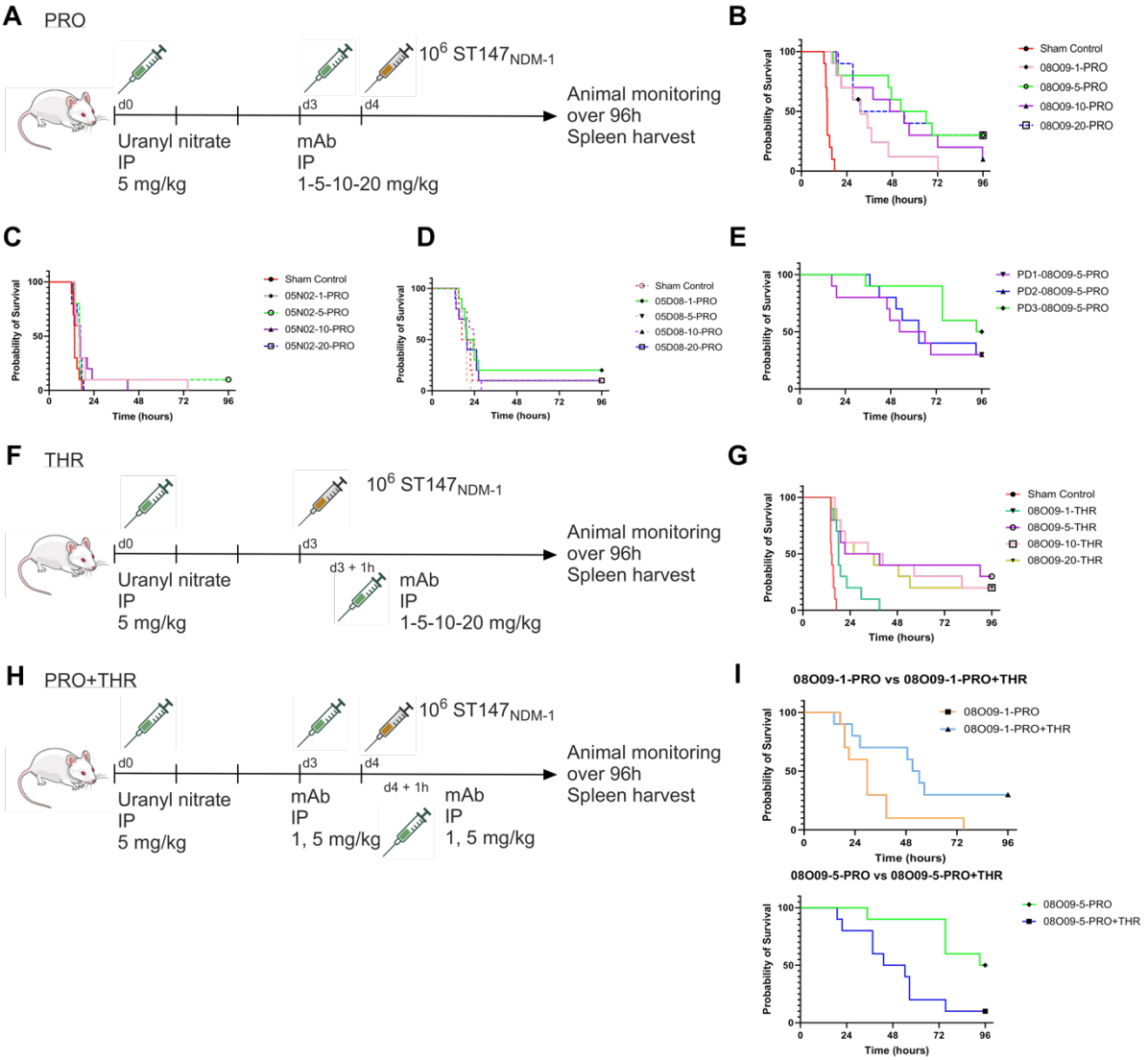

Figure 5. Evaluation of *in vivo* protective properties of 08O09, 05D08 and 05N02 mAbs in an immunocompetent ST147$_{NDM-1}$ bacteremia model. A) Scheme of prophylaxis (PRO) study. Survival analysis of 08O09 (**B**), 05N02 (**C**) and 05D08 (**D**) PRO regimens and sham control (n=10 mice per group). (**E**) Survival analysis of 08O09 PRO regimens administered as a single dose of 5 mg/kg (n=10 mice per group). (**F**) Scheme of treatment (THR) study. (**G**) Survival analysis of 08O09 THR regimens and sham control (n=10 mice per group). (**H**) Scheme of prophylaxis plus treatment (PRO+THR). (**I**) Survival analysis of 08O09 PRO regimens and PRO+THR regimens, at 1 mg/kg and 5 mg/kg single doses (n=10 mice per group).

suboptimal in monotherapy regimens (**Figure 5I and S12D**). However, when 08O09 was administered at 5 mg/kg, PRO monotherapy performed significantly better than either PRO+THR combination or THR monotherapy (**Figure 5I and S12E**).

These results suggest that, while a monotherapy suboptimal mAb dosage could be counterbalanced by the use of PRO+THR administrations, optimal mAb dosage may perform well in a PRO. Overall, these experiments highlighted for the first time the *in vivo* efficacy of a KL64-specific mAb in both prophylactic and therapeutic regimens against pandrug-resistant $ST147_{NDM-1}$ Kp bloodstream infections.

Discussion

$ST147_{NDM-1}$ Kp is highly persistent within nosocomial settings and has been causing an ongoing local outbreak in the hospitals of Pisa (Italy) from 2018. Since then, clones of the same lineage have been reported in the Tuscany area[73,80,168]. In this study, a rationally designed workflow to screen and select protective human mAbs against pandrug-resistant $ST147_{NDM-1}$ Kp has been described. The depicted antigen-agnostic methodology allowed the identification of mAbs that show correlates of *in vivo* protection, thus can be exploited as therapeutic and prophylactic agents. Through this strategy, the first fully human mAb directed against Kp capsule type KL64 has been identified and remarkably exhibited protective activity against the outbreak-causing pandrug-resistant $ST147_{NDM-1}$ Kp strain.

Taken together, the data reported here highlight the importance of developing valid predictive assays to correlate *in vitro* efficacy to successful *in vivo* experiments. Out of more than 200 $ST147_{NDM-1}$-specific mAbs isolated from convalescent donors, 20 candidates exerted bactericidal properties in the picomolar range of concentrations *in vitro*, but only those triggering phagocytosis and bacterial enchained growth proved functional in a murine model of bloodstream infection. This evidence indicates that evaluating the *in vitro* complement-dependent, mAb-mediated bactericidal activity is not enough for successful selection of mAbs for clinical use, whereas *in vitro* poly-functionality is an essential feature that protective candidates must bear. The findings of this study highlight the relevance of poly-functionality, considering that only capsule-specific mAbs that were active in multiple *in vitro* assays were able to promote mouse survival rate upon bloodstream infection. By correlating *in vitro* and *in vivo* results, anti-KL64 mAbs may improve survival rates in murine models by combining the effects of different mechanisms of protection, such as complement-dependent killing, macrophage-mediated killing, and clearance of enchained bacteria.

Kp capsule is an essential virulence factor; indeed, genetically manipulated, capsule-deficient Kp strains become avirulent in various *in vivo* models of infection[164,169,170]. For this reason, capsule-targeting mAbs could alter bacterial pathogenesis and boost bacterial uptake and lysis by macrophages. Additionally, anti-KL64 capsule mAbs may protect against bacterial spread by triggering enchained

growth. Bacterial concatenation induced by secretory IgA (sIgA) has been previously described to restrict *Salmonella typhimurium* proliferation by facilitating bacterial clearance from the intestine[171,172]. Interestingly, we observed how the same enchained phenotype could be promoted on Kp in the presence of a monomeric IgG isotype. Moreover, considering that only anti-capsular, but not anti-O-antigen, mAbs succeeded in inducing Kp enchained growth, we ought to think that targeting the most external bacterial layer, such as capsular polysaccharides, is key to promote concatenation, especially in hyper-capsulated species. At present, no information is available concerning the relative abundance of capsule and O-antigen *in vitro* and, more importantly, *in vivo*. However, studies of Kp pathogenesis[17,146,173] lead us to hypothesize that potency of 08O09 in *in vitro* and *in vivo* infection models is associated with production of a dense capsule which acts as an immunodominant antigen. Anti-O-antigen mAbs, though effective in SBA assays, may have limited access to their cognate epitopes under different experimental circumstances.

Hyper-capsulation may also explain why, despite applying an antigen-agnostic approach, we pinpointed anti-capsule and anti-O-antigen mAbs only, while no antibody against different antigens was identified. Indeed, Kp protein antigens may be masked by the thick O-antigen and capsule layers, which probably elicited most of the humoral immune response associated with the clinical isolates we have been targeting. While the work resulted in the identification of an extremely potent candidate medication against $ST147_{NDM-1}$ Kp, clinical application of 08O09 to Kp infections will be limited to the KL64 serotype. In the framework of exploiting mAbs for anti-Kp universal vaccine design, future research efforts should be directed towards the identification of functional antibodies against conserved targets, such as membrane proteins or components of fimbriae and secretion systems. To this end, implementation of targeted sorting and screening strategies will be instrumental.

The $ST147_{NDM-1}$ Kp clone responsible for the Tuscan outbreak is extensively spread worldwide, with cases reported around Europe[73,174] South-East Asia[175], and USA[176]. Additionally, genomic surveillance reports indicate that KL64, associated with enhanced virulence[177] is replacing some previously prevalent capsular loci through intraspecies clone shifting[178] and became the third emerging capsule type for hypervirulent strains after K1 and K2 serotypes[34,179]. Taken together, these data

underline the importance of selecting anti-capsular mAbs to contain and prevent KL64-bearing Kp future outbreaks. Remarkably, the top candidate mAb 08O09 isolated in this study, initially designed in the pursuit of an effective therapy against a regional outbreak of a pandrug-resistant strain, may also prove to be a broader solution against multiple Kp STs with KL64 capsular features.

Materials and Methods

Single-cell sorting of memory B cells from convalescent donors

Peripheral blood mononuclear cells (PBMCs) were isolated from heparin-treated whole blood by density gradient centrifugation (Ficoll-Paque PREMIUM, GE Healthcare). After separation, PBMC were stained with Live/Dead FSV780 (BD Horizon) in 100µL final volume diluted 1:1000 at room temperature (RT). After 20 minutes of incubation, cells were washed with phosphate-buffered saline 1X (PBS) and unspecific bindings were saturated with 100µL of 20% normal rabbit serum (Life Technologies). Following incubation at 4°C for 30 minutes, cells were washed with PBS 1X, centrifuged at 1200 rpm for 8 minutes, and stained with CD19 APC (BD cat# 561742), IgM PeCF594 (BD cat# 562539), CD27 APCR700 (BD cat# 565116), IgD PE (BD cat# 562024), CD3 PE-Cy7 (BD cat# 560910), CD14 PE-Cy7 (BD cat# 560919) and CD56 PECy7 (BD cat# 560916) in Staining Buffer (1 % Fetal Bovine Serum in PBS) at 4°C for 30 minutes. Following additional washing, cells were resuspended in Sorting Buffer (PBS/EDTA 2.5 mM). Stained memory B cells (MBCs) were single-cell sorted with a FACS Aria III Fusion BD (BD Biosciences) into 384-well plates containing 3T3-CD40L feeder cells and were incubated with IL-2 and IL-21 for 14 days[133].

ELISA screening of mAbs binding against *Klebsiella pneumoniae*

Supernatants resulting from single-cell sorting of MBCs were used as a source of IgG1 and IgA monoclonal antibodies (mAbs) to test their binding to whole bacteria in a high-throughput enzyme-linked immunosorbent assay (ELISA). Pools of $ST147_{NDM-1}$ c.i. 1 and $ST147_{NDM-1}$ c.i. 2 (**Table S2**) were grown in LB medium, pelleted at exponential phase (OD_{600}=0.5), resuspended in PBS, and plated into 384-well plastic plates (Greiner, ref. 781101). Plated bacteria were fixed at RT for 30 minutes in 0.5% of paraformaldehyde. Plates were then blocked in PBS plus 1% Fetal Bovine Serum at RT for 1h. After incubation, bacteria were incubated for 1h with MBC supernatants diluted in sample buffer (PBS – BSA 1% - Tween-20 0,05%). Next, anti-human IgG and anti-human IgA secondary antibodies conjugated with Alkaline Phosphatase (Southern Biotech) were added for 45 minutes. To detect bacteria-mAbs binding,

pNPP (p-nitrophenyl phosphate; Sigma-Aldrich) was used as soluble substrate and the final reaction was quantified at a wavelength of 405 nm by using the Varioskan Lux Reader (Thermo Fisher Scientific). After each incubation step, plates were washed three times with 100µL per well of washing buffer (PBS and 0.05% Tween-20). Sample buffer was used as a blank and we considered as positive hits those wells showing an OD_{405} value of at least 2-fold superior to blank. Cells corresponding to positive hits were lysed in 25µL of a buffer containing RNAsi Out 0,2 U/µL, ultrapure BSA 1mg/mL and H_2O DEPC (Thermo Fisher Scientific) and stored at -80^{0}C for following steps.

Single-cell RT-PCR and nested PCR were used to amplify V_H and V_L

cDNA was synthesized from 5µL of MBC lysates. Reverse transcription (RT) reaction was performed by adding 25µL per well of a mix containing 1µL of random hexamer primers (50 ng/mL),1µL of dNTPs (10 mM), 2µL 0.1 M DTT, 40 U/µL Rnase OUT, $MgCl_2$ (25 mM), 5µL of 5X buffer, 0.25µL of Superscript IV reverse transcriptase (Invitrogen) and nuclease-free water (DEPC) and RT-PCR conditions were 42°C/10 minutes, 25°C/10 minutes, 50°C/ 60 minutes and 94°C/5 minutes. After cDNA synthesis, two additional rounds of PCR were performed to obtain the variable regions of the heavy (V_H) and light (V_L) chains. Briefly, in the first round of PCR (PCR I) a total volume of 25µL containing 4µL of cDNA, 10µM of VH or 10µM VL/VK primer mix (**Table S4**), 0.5µL of dNTPs (10 mM), 1.5µL $MgCl_2$ (25 mM), 5µL of 5X Kapa Long Range Buffer, and 0.125µL of Kapa Long Range Polymerase (Sigma) was added in each well and amplified using the following conditions: 95°C/3', 5 cycles at 95°C/30'', 57°C/30'', 72°C/ 30'' and 30 cycles at 95°C/30'', 60°C/30'', 72°C/30'' and 72°C/2'. 3µL of un-purified PCR I products were used as a template for the nested PCR (PCR II) using the same cycling conditions and primers indicated in **Table S5**. PCR II products were then purified by Millipore MultiScreen PCR 96 plate according to the manufacturer's instructions. Samples were eluted in 30µL of nuclease-free water pre-warmed at 50°C and quantified by NanoDrop One (Thermo Fisher Scientific).

Cloning of V_H and V_L and recombinant antibody expression by TAP transfection

Amplified antibody sequences were ligated into human IgG1 expression vectors and used to produce transcriptionally active PCR (TAP) products. Briefly, IgG1, Igκ or Igλ expression vectors were digested with AgeI, SalI and XhoI restriction enzymes, respectively. 25 ng of linearized plasmids were ligated with 75 ng of purified V_H and V_L by Gibson Assembly (New England BioLabs). The reaction was performed in a final volume of 5µL. The ligation product was 10-fold diluted in DEPC water and used as a template for transcriptionally active PCR (TAP) reaction which allowed the direct use of linear DNA fragments for *in vitro* expression. Functional promoter (human CMV) and terminator sequences (SV40) were attached onto PCR II products directly by amplification using specific primers (**Table S6**). TAP-PCR was performed in a total volume of 25µL containing 0.25µL of Q5 polymerase (NEB), 5µL of GC Enhancer (NEB), 5µL of 5X buffer, 0.5µL dNTPs (10 mM), 0.125µL of forward/reverse primers and 3µL of ligation product, and using the following conditions: one step of 98°C/2 minutes, 35 cycles of 98°C/10 seconds, 61°C/20 seconds, 72°C/1 miunte and an extension of 72°C/5 minutes. Once purified and quantified, TAP products were transfected into Expi293F cells to allow small scale production of recombinant mAbs. Briefly, cells were transfected with both TAP amplifications in a final volume of 1mL into 96 deep well plate (Eppendorf), and after 7 days of expression mAb-containing supernatants were harvested by centrifugation.

Quantification of TAP-produced mAbs by ELISA

To quantify the concentration of mAbs in each supernatant, ELISA plates were coated with 2 μg/ml of goat anti-human IgG (Southern Biotech) at 4°C ON. Plates were washed 3 times with PBS plus Tween-20 0,05%, blocked in PBS plus BSA 1% at 37°C for 1h. Then samples were washed and incubated with TAP-produced mAbs diluted in sample buffer (PBS - BSA 1% - Tween-20 0,05%) at 37°C for 1h. Following additional washings and incubation at 37°C for 1h with AP-conjugated anti-goat IgG secondary antibody (Southern Biotech), absorbance was read by addition of PNPP. Concentrations were evaluated by linear regression analysis built by potting OD_{405} values against a standard curve generated by titration of a human IgG-unlabeled antibody (Southern Biotech).

Large scale expression and purification of mAbs

Expi293F cells (Thermo Fisher Scientific) were transiently transfected with plasmids carrying the heavy and the light chains of each antibody with a 1:2 weight/weight ratio. Cells were grown for six days at 37°C at 8% CO_2 and 125 rpm shaking, with an optimized cocktail of enhancers 1 and 2 (Thermo Fisher Scientific) added on day 1 post-transfection. Two harvests were performed on the third and sixth day by pelleting the cells at 1,100 xg for 10 minutes at RT and supernatants were pooled and clarified by centrifugation (3,000 xg for 15 minutes at 4°C), followed by 0.45 mm filtration. mAbs were purified at RT by affinity chromatography on the AKTAgo purification system (Cytiva) using the HiTrap Protein G HP column (Cytiva), which binds to the Fc domain. Specifically, the column was equilibrated in 0.02 M sodium phosphate buffer pH 7 at a flow rate of 1mL/min, which was used also for the following steps. After sample injection, the column was washed with 10 column volumes (CV), followed by mAb elution with 10 CV of 0.1 M glycine-HCl, pH 2.7. mAb pool was dialyzed in PBS pH 7.4 using Slide-A-Lyzer G2 Dialysis Cassette 3.5K (Thermo Scientific) ON at 4°C. For each purified antibody, the concentration was determined by measuring absorbance at 280 nm at Nanodrop. All purified antibodies were aliquoted and stored at -80°C.

Serum Bactericidal Assay (SBA)

Two days prior to the assay, glycerol stocks of Kp were streaked on LB-Agar plates and incubated overnight (ON) at 37°C. The following day, a single colony was inoculated in 4mL of LB and incubated ON at 37°C. Cultures were expanded to 10mL LB in a 125mL flask to obtain an OD_{600} of 0.05 and incubated at 37°C with shaking until the exponential phase (OD_{600} 0.4-0.6) was reached. Bacteria were then 1:10 diluted in PBS.

Appropriate baby rabbit complement (BRC, Cedarlane) concentrations to be used in the assay were established through complement sensitivity tests. Briefly, $2x10^6$ bacteria/ml resuspended in PBS were seeded in round bottom 96-well plates, and BRC concentrations were screened starting from 50% in 11 serial 2-fold step dilutions. After 2h incubation at 37°C, bacteria were pelleted by centrifugation. The supernatant was discarded, and bacteria were resuspended in 30 µL of PBS and transferred into

a White Optiplate (Perkin Elmer). 30 µL of BacTiter-Glo™ 1X (Promega) was added to each well and luminescence was measured by the Varioskan Lux microplate reader (Thermo Fisher Scientific) with an exposure time of 500 ms. Data were plotted and analyzed using GraphPad Prism. 12.5% BRC was established as a universal BRC concentration allowing to achieve complement-dependent antibody-mediated killing without significant toxicity.

For luminescence-based SBA (L-SBA) with TAP-expressed mAbs, $2x10^6$ bacteria/mL of $ST147_{NDM-1}$ were seeded into a 96-well U-round bottom plate in the presence of 12.5% BRC, with the addition of four serial dilutions of TAP-expressed mAbs (1:10, 1:50, 1:250, 1:1250), in a total volume of 100µL per well. Upon 2h incubation at 37°C, bacteria were pelleted by centrifugation at 4000 xg. Bacterial pellets were resuspended in 30 µL of PBS per well and transferred into a white Optiplate (Perkin Elmer). 30µL of BacTiter-Glo™ 1X (Promega) was added to each well and luminescence was measured by the Varioskan Lux microplate reader (Thermo Fisher Scientific) with 500 ms exposure. In each experiment, luminescence values obtained were used to calculate the median value for each dilution factor. Difference between the luminescence signal of each mAb and the median value of the plate was measured and plotted as percentage with a 30% cut-off.

For fluorescence-based SBA (F-SBA), $2x10^6$ bacteria/mL were seeded in 384-well black clear-bottom plate (ViewPlate®-384 F TC, PerkinElmer) in the presence of 12.5% BRC, in a final volume of 50µL per well. Purified recombinant mAbs were added in a 3-fold step serial dilution panel. After 2h incubation at 37°C, 40µL LB and 10µL of 0.025% resazurin (Sigma-Aldrich) were added to each well. Fluorescence (λ_{Ex} = 560nm and λ_{Em} = 590nm. Exposition: 250ms. Wide 12nm) was measured by the Varioskan Lux microplate reader upon 2h incubation at 37°C. GraphPad Prism was used to plot and analyze data, as well as to extrapolate IC_{50} values.

Flow cytometry analysis of mAb binding to bacterial surface

Binding of mAbs to the panel of bacterial strains (**Table S2**) was performed on bacteria in the exponential phase of growth in LB (OD_{600} 0.4-0.6). Bacteria were pelleted and resuspended in an equal volume of PBS-BSA 1%. 100µL of bacteria were plated in each well of a round bottom 96-well plates by centrifuging at 4000 xg for 5 minutes,

followed by incubation with 5 μg/ml of purified antibodies at RT for 1h. Plates were centrifuged, and pellets were washed three times with PBS-BSA 1% and incubated at RT for 30 minutes in the dark with 1:2000 diluted Alexa488-conjugated α-human IgG secondary antibody. After an additional centrifugation and washing step, bacteria were fixed with 0.5% of paraformaldehyde at RT for 30 minutes, washed again, resuspended in PBS-BSA 1% to an OD_{600} of 0.05 and read by their fluorescence. Samples were acquired on the BD FACS Canto II (BD Biosciences, USA). Data were analyzed by FlowJo software v 10 (BD Biosciences, USA).

Antibody sequence analysis

Immunoglobulin genes were identified using a custom Python script that employs NCBI IgBlast and IMGT nomenclature (in the time between 2020 and 2022). IGHV gene somatic hypermutations were counted from the start of FWR1 until the end of FWR3. Insertions or deletions were counted as one single mutation.

Genomic analysis of Kp isolates

ST147 strains were sequenced using both short- and long-reads technology. High-throughput-sequencing was performed on the MiSeq platform (Illumina; San Diego, CA, USA) with a paired-end layout of 150 bp. Paired-end short reads were quality-checked and poor-quality reads were filtered using fastp v0.20.1 (REF). The long-read library was prepared with multiplexing and sequenced according to the manufactures' guide using flow cell R9.4.1 (Nanopore). The quality of long reads was controlled by being mapped with their corresponding short reads using Filtlong v0.2.0 (https://github.com/rrwick/Filtlong) with minimum quality and length as Q8 and 2,000 bp respectively. Along with the corresponding clean reads, long reads were fed into the hybrid assembler Unicycler v0.4.8 (REF) and run under the conservative mode. ST and capsule typing prediction were performed using Kleborate v2.0.0 (REF) and Kaptive (REF).

Western blot analysis of mAb binding to Kp lysates

For sample preparation, bacteria from glycerol stocks were grown ON on LB-agar plates. Single colonies of Kp were picked from plates and grown ON with static

incubation at 37°C in LB. The following day, bacteria were grown at 37°C starting from OD 0.05 at 150 rpm in LB until they reached the exponential phase (OD 0.4-0.6). Polysaccharide extracts for immunoblotting has been prepared with lipopolysaccharide (LPS) extraction kit (Sigma). Total bacterial lysates were prepared by centrifuging the inoculum for 10 minutes at 2500 xg at 4°C, followed by filtration at 14000 xg with Nanosep 0.2 μm columns. Part of the sample was treated with proteinase K for 1h at 60^{0}C to eliminate proteins. Moreover, polysaccharide extracts were prepared by phenol extraction. Following overnight growth, bacteria were pelleted and resuspended in PBS. Upon 1 h at 100°C, an equal volume of phenol was added, and samples were incubated at 70°C for 1.5 h. Samples were centrifuged at 13000 rpm at 4°C for 30 min, then the water phase was recovered. SDS-PAGE samples were prepared by adding 1:4 loading buffer and 1:10 reducing agent and incubated for 5 minutes at 95°C. SDS-PAGE gel was transferred onto PVDF membrane using the iBlot™ Gel Transfer Device and Stacks (Thermo Fisher Scientific). Membranes were blocked for 1h at RT in TBS 1x/0.1% Tween-20/5% milk. Purified mAbs were used at 1μg/mL in TBS 1x/0.1% Tween-20/5% milk. Following ON incubation at 4°C, membranes were washed 3 times with TBS 1x/0.1% Tween-20. Incubation with secondary antibody (goat anti-human Fab) diluted 1:75000 in TBS 1x/0.1% Tween-20/5% milk was carried out for 1h at RT. Membranes were washed 3 times in TBS 1x/0.1% Tween-20 and then developed with chemiluminescence readout.

Characterization of mAb binding by high-resolution and high-content confocal microscopy

A single colony of bacteria stably expressing super-folder(sf)mCherry was picked from an LB-agar plate and grown ON in LB with 150µg/mL hygromycin. The ON culture was diluted in LB without antibiotics and grown to ODs 0.025 or 0.05. Then, 50 µL of bacteria were transferred into a 96-well Phenoplate (Perkin Elmer, 6055300) and incubated for 2 h at 37°C without CO_2 in static conditions. Subsequently, the supernatant was discarded, and the adherent bacteria were fixed in 4% paraformaldehyde (PFA)/PBS (Thermo Fisher Scientific) or Cytofix (BD) for 15 minutes at RT. For experiments aimed at staining a single anti-Kp mAb, selected

antibodies were diluted in a solution of PBS/1%BSA (Bovine Serum Albumin) at a concentration of 0.5µg/mL and incubated for 30 minutes at RT. Then, samples were washed in PBS and a mixture of goat anti-Human Alexa488 conjugated secondary antibody (diluted 1:2000) and DAPI (diluted 1:2000) in PBS/BSA1% was added for 30 minutes at RT. Finally, samples were washed in PBS and 50µL of 1% Low Melting (LM) agarose were distributed in each well. Samples were stored at 4°C and imaging was performed within the following 24 hours. For experiments in which 08O09, 05N02 and 05D08 mAbs were simultaneously stained, antibodies were conjugated with Alexa488, Alexa555 and Alexa647 fluorophores, respectively, using the Zip Alexa Fluor™ Rapid Antibody Labeling Kits (Thermo Fisher Scientific) following manufacturer instructions. After fixation in PFA, samples were first blocked in PBS/1% BSA for 30 minutes at RT and then incubated with a mixture of fluorophore-conjugated mAbs (each one at 0.5 g/mL in PBS/1% BSA) and DAPI (1:2000). Following 30 minutes incubation at RT, samples were washed in PBS and prepared for imaging by adding 50µL of 1% LM agarose. On the following day, samples were imaged.

Opsonophagocytosis assay

THP-1 cells (ATCC) were maintained in RPMI 1640 containing GlutaMax (Thermo Fisher Scientific) and complemented with 10mM Hepes (Thermo Fisher Scientific), 1mM Sodium Pyruvate (Thermo Fisher Scientific) and 10% fetal bovine serum (FBS) (Thermo Fisher Scientific). Three days before the assay, 50.000 cells per well were seeded into a 96-well black-shielded optiplate (Perkin Elmer) in the presence of 20 ng/mL phorbol-12-myristate-13-acetate (PMA) to promote monocyte differentiation into macrophages. The day after, PMA was washed out and cells were maintained in fresh medium for two additional days.

Infection of macrophage was performed using $ST147_{NDM-1}$-sfmCherry expressing Kp. Bacteria were grown ON and re-launched the following morning to reach OD_{600} 0.5. After centrifugation, bacteria were resuspended in phagocytosis media (RPMI 1640+GlutaMax, 10mM Hepes, 1mM Sodium Pyruvate) to have a 1:2 dilution of the initial culture volume. To allow bacterial opsonization, mAbs dilutions were prepared in 25µL of phagocytosis media and incubated with 25µL of bacteria for 30 minutes at 37°C in shaking conditions (500rpm). This mixture was then added to differentiated

macrophages and centrifuged for 3 minutes at RT to synchronize the infection. Following the incubation of 1hour at 37°C in the presence of 5% CO_2, samples were treated for an additional hour with 150 µg/mL streptomycin to kill not engulfed bacteria. Finally, samples were incubated for 5 minutes at RT with PBS/0.1% X100-Triton to permeabilize cells and allow the release of internalised bacteria in the supernatants. Bacterial fluorescence was read using a Varioskan Lux microplate reader as a readout of bacterial uptake.

Live bacteria imaging

$ST147_{NDM-1}$-sfmCherry was grown ON as described before and re-launched until OD_{600} 0.5. The assay was carried out in a final volume of 50µL containing exponential Kp diluted 1:100, 12.5% BRC and escalating doses of anti-Kp mAbs in PBS. Samples were prepared in 96-well Phenoplate (Perkin Elmer, 6055300) and briefly centrifuged at 1000 rpm to keep bacteria closer to the bottom of the well. Acquisition started immediately after centrifugation and was carried out at 37°C by acquiring frames every 2 minutes for 2 hours.

Microscopy and image analysis

Imaging was performed using the Opera Phenix platform (Perkin Elmer) and all samples were acquired using a 63X N.A. 1.15 water objective.

For mAb binding experiments carried out in fixed conditions, 20 fields of view (FOV)/well were selected. For each FOV, five z-stacks separated by a z-step of 0.5µm were acquired. Imaging was performed in the confocal mode by exciting the samples with lasers at 425 nm, 488 nm and 561 nm and collecting the emitted light using bandpass filters 435-480 nm, 500-550 nm and 570-630nm, respectively.

For bacterial live imaging experiments, 3 FOV/well were acquired and three z-stacks separated by a z-step of 0.5µm were imaged. Imaging was performed in the widefield mode by exciting the samples with lasers at 561nm and collecting the light using the bandpass emission filter 570-630 nm.

Images were analyzed with Harmony (v4.9), provided by Perkin Elmer, by using custom-made image analysis pipeline described in supplementary materials. Individual bacteria were detected using the DAPI channel and filtered according to

their morphology based on data available in literature. To measure mAb intensity levels, the mean intensity of the A488 signal was measured within a ROI drawn around each bacterium. To measure mAb occupancy area, A488 spots were detected, and their morphology features were measured. A488 spots displaying an area smaller than 0.5 m^2 were discarded from the analysis because they were not representative of the distribution of the mAb signals around the bacteria.

Purification of $ST147_{NDM-1}$ capsule

For capsule extraction, $ST147_{NDM-1}$ Kp from glycerol stocks was grown at 37°C ON in LB in the presence of meropenem. 200 µL of liquid culture were plated on carbohydrate-rich Worfel-Ferguson agar plates to increase Kp capsule production[180]. The Worfel-Ferguson agar plates contain 0.2% yeast extract, 0.2% sodium chloride, 0.1% potassium sulphate, 0.025% magnesium sulphate, 2% sucrose, and 1.5% Agar. Upon ON incubation at 37°C, bacteria were mechanically collected from the plates and resuspended in LB. The samples were centrifuged for 8 minutes at 4000 rpm, pellets were collected and resuspended in H_2O. After a 6h incubation at 99°C, samples were centrifuged for 8 minutes at 4000 rpm. Supernatants were collected and filtered with 0.22 μM filters. To allow DNA precipitation, 1% CTAB, 5mM Na_2SO_4 and 0.24 mM NaCl were added to the solution. Samples were vortexed and incubated at 100°C with 550 rpm for 4 h, then centrifuged for 15 minutes at 14000 rpm. Supernatants were collected, diluted 1:10 with 5mM Na_2SO_4, and incubated at 37°C for 1h. Upon 15 minutes of centrifugation at 4000 xg, the pellet was resuspended in 4mL of 1M $CaCl_2$. To remove impurities, 25% of EtOH was added to the sample and left on a tilting plane for 30 minutes at RT. The sample was centrifuged for 15 minutes at 4000 xg and the supernatant was collected. To allow capsule precipitation, 80% of EtOH was added to the collected supernatant and left for 1h at RT on a tilting plane. Incubation was followed by centrifugation for 15 minutes at 4000 xg. The obtained pellet was resuspended in 1mL of 1M NaCl and purified with Amicon 10K filters with at least 10 washing steps in MilliQ H_2O to remove protein contaminants and other impurities. Sugar content was evaluated by phenol-H_2SO_4 assay, protein content was estimated by microBCA (Thermo Fisher Scientific) and DNA presence was measured using the Qubit kit (REF). Protein and DNA contaminants were <1% compared to the sugar

concentration, quality of the estimated molecular size distribution was done by SEC-HPLC, with a Tosoh TSK gel PWXL guard - G3000 PWXL columns connected in series (4.0 cm x 6.0 mm; cod. 808033, and 30 cm x 7.8 mm; cod. 808021, respectively), as a running buffer, 0.1 M NaCl, 0.1 M NaH_2PO_4, pH 7.2

Purification of O-antigen from Kp strains

O-antigen was extracted following a published protocol[181], with slight modifications. In brief, 300mL of LB supplemented with 0.4 % glucose were inoculated with Kp. After reaching the logarithmic phase of growth bacteria were pelleted at 4,000 rpm for 15 minutes. The obtained pellet was resuspended in 15mL of 3% acetic acid for at least 4h at 90°C shaking at 500 rpm. Upon incubation, the supernatant was collected and pH was neutralized with 100mM NaOH. Samples were desalted using Disposable PD10 columns (Cytiva). 100 mM of citrate buffer pH 2.7 was added with continuous stirring to achieve the final citrate concentration of 20mM. The sample was then incubated at RT for 30 minutes, followed by centrifugation at 12,000 rpm at 15°C for 30 minutes. The supernatant was collected, and a Sartobind MA75 column (Sartorius) was used for cation-exchange purification. After neutralization followed by a second desalting step, anion exchange was performed with HiTrap Q FF (Cytiva) by AKTAgo purification system. The column was previously equilibrated with 5 CV of Buffer A (10 mM Tris-HCl pH 8). The sample was diluted to 100mL loaded with the sample pump. The column was washed with 5 CV of Buffer A, and elution was performed with 10 CV of Buffer B (10 mM TRIS pH8 + 200 mM NaCl). The flow rate for all steps was 5mL/min. The O-antigen-containing sample was eluted in the flow-through and the concentration was increased by using Amicon 10K columns. Total sugar quantification was measured by phenol-sulfuric assay and quality of the estimated molecular size distribution was done by SEC-HPLC, with a Tosoh TSK gel PWXL guard - G3000 PWXL columns connected in series (4.0 cm x 6.0 mm; cod. 808033, and 30 cm x 7.8 mm; cod. 808021, respectively). 0.1 M NaCl, 0.1 M NaH_2PO_4, pH 7.2. was used as running buffer. Detection was performed with a UV and a refraction index detector. Protein impurities were measured by microBCA.

ELISA on purified Kp O-antigen and capsule

To perform the ELISA, purified O2a-LPS and O2afg -LPS were kindly provided by Chris Whitfield's group[158]. In addition, in-house purified KL64 capsule and O2a and O1 O-antigens were used to coat high-binding 384-well plates (Greiner ref. 781061) and incubated at 4°C ON. The next day, plates were blocked in PBS-BSA 1% at 37°C for 1h. After blocking, plates were incubated with each mAb as primary antibody at a final concentration of 10 μg/ml for 2h at RT, in the presence of PBS, 1% BSA, and 0.05% Tween-20. Next, anti-human IgG secondary antibody conjugated with Alkaline Phosphatase (Southern Biotech) was added for 1h at 37°C. To detect antigen-mAbs binding, pNPP (p-nitrophenyl phosphate; Sigma-Aldrich) was used as a soluble substrate, and the final reaction was quantified at a wavelength of 405 nm using the Varioskan Lux Reader. After each incubation step, plates were washed three times with 100 µL per well of washing buffer (PBS plus 0.05% Tween-20). Sample buffer and an unrelated mAb were used respectively as blank and negative control, and we considered positive hits those wells showing an OD_{405} value 3-fold higher than the blank. As a positive control, a 1:100 dilution of a mix of plasma from different patients was used.

Immunocompetent ST147$_{NDM-1}$ bacteremia model

In vivo studies were performed in the laboratory of Dr. David P. Nicolau and Dr. Kamilia Abdelraouf, at the Center for Anti-infective Research and Development in Hartford Hospital (USA). 08O09, 05N02 and 05D08 were resuspended in PBS to the concentrations required to deliver 1, 5, 10, and 20 mg/kg doses based on the mean weight of the study mice population. For prophylaxis (PRO) studies, single dose mAb at examined doses was administered through intraperitoneal (IP) route 24 h prior to bacterial inoculation. For treatment (THR) studies, single dose mAb at examined doses was administered through intravenous (IV) route 1 h post bacterial inoculation. For prophylaxis plus treatment (PRO+THR) studies, one dose of mAb was administered IP 24 h prior to bacterial inoculation, and a second dose of the same mAb at the same dose was administered IV 1 h post bacterial inoculation. All dosing solutions were kept on ice while filled syringes with dosing solutions were refrigerated

until use. PBS solution with a pH of 7.4 was utilized as the vehicle for dosing control animals throughout the study.

Specific pathogen-free, female ICR mice weighing 20-22 grams were obtained from Charles River Laboratories, Inc., (Wilmington, MA). The animals were allowed to acclimate for a minimum of 48 h before commencement of experimentation and were provided food and water *ad libitum*. The protocol was reviewed and approved by the Institutional Animal Care and Use Committee at Hartford Hospital. Mice were administered uranyl nitrate 5 mg/kg three days prior to inoculation to produce a controlled degree of renal impairment. In total, 322 mice were used. $ST147_{NDM-1}$ was previously frozen at - 80°C in skim milk (BD BioSciences, Sparks, MD). Prior to mice inoculation, two transfers of the organisms were performed onto Trypticase Soy Agar plates with 5% sheep blood (TSA II™; Becton, Dickinson & Co.; Sparks, MD) and incubated at 37°C for approximately 24 h. After 18-24 h of incubation of the second transfer, a bacterial suspension of approximating the target number of CFU/mL in 5% hog gastric mucin was made for inoculation. Final inoculum concentrations were confirmed by serial dilution and plating techniques. Septicemia was produced by IP injection of 0.5 ml of the inoculum.

Supplementary Materials

Supplementary Figure 1. Gating strategy for single cell sorting of total memory B cells. Flow cytometry plots reporting gating strategy to identify as follows: live cells, lymphocyte population, single cells, CD19-positive cells (B cells), $CD19^{+}$ $CD27^{+}$ IgD^{-} cells (memory B cells), $CD19^{+}$ $CD27^{+}$ $IgD^{-}IgM^{-}$ B cells (memory B cells expressing IgG, IgA or IgE).

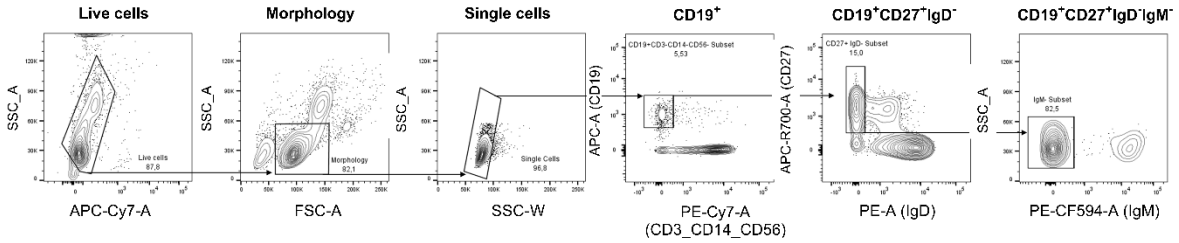

Supplementary Figure 2. Heatmap of ELISA results of 134 recombinant mAbs against ST147$_{NDM-1}$ clinical isolates. ELISA against two different ST147$_{NDM-1}$ clinical isolates was performed to confirm mAb binding to Kp surface. Values at least 3-fold times above the OD_{405} blank were considered as positive hits.

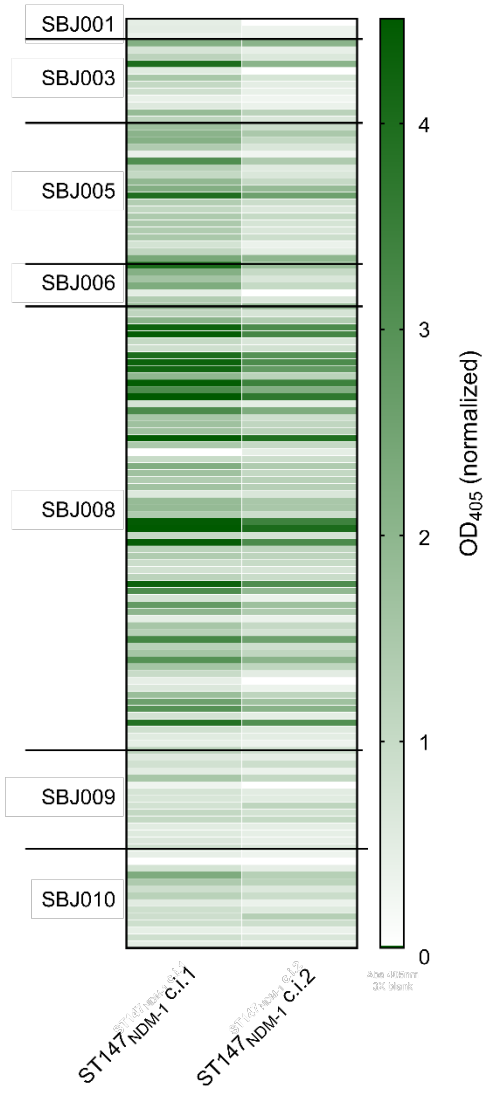

Supplementary Figure 3. Flow cytometry analysis of 20 anti-Kp mAbs binding properties against other *Klebsiella* species and commensals. Heatmap representing the summary of high-throughput flow cytometry screening of 20 functional anti-Kp mAbs against *Klebsiella oxytoca* and *Klebsiella variicola*, isolates, as well as against commensals. MFI values were normalized on no mAb controls and transformed in logarithmic scale.

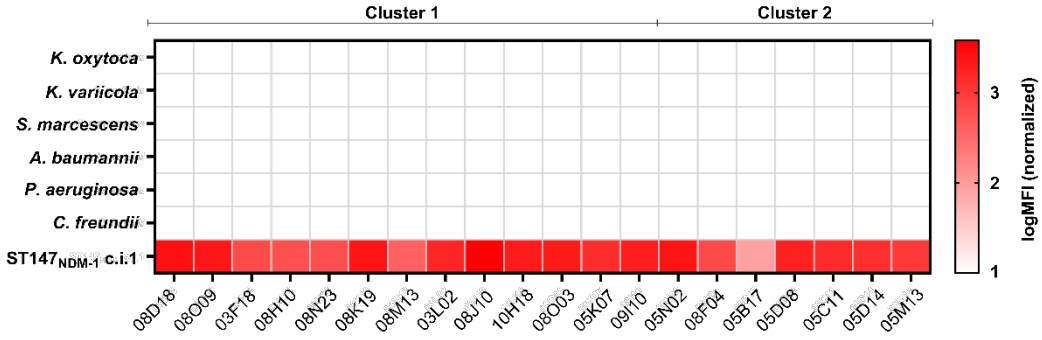

Supplementary Figure 4. Purification of capsule type KL64 from ST147$_{NDM-1}$ Kp. **A)** SEC-HPLC emission (λ=280nm) and RIU normalized profiles of purified KL64 capsule from ST147$_{NDM-1}$. The three arrows indicate molecular weight standards of 410, 80 and 12 kDa. ST147$_{NDM-1}$ capsular polysaccharide was purified following the protocol reported in Materials and Methods. **B)** Theoretical structure of capsule type 64 as described in literature[156].

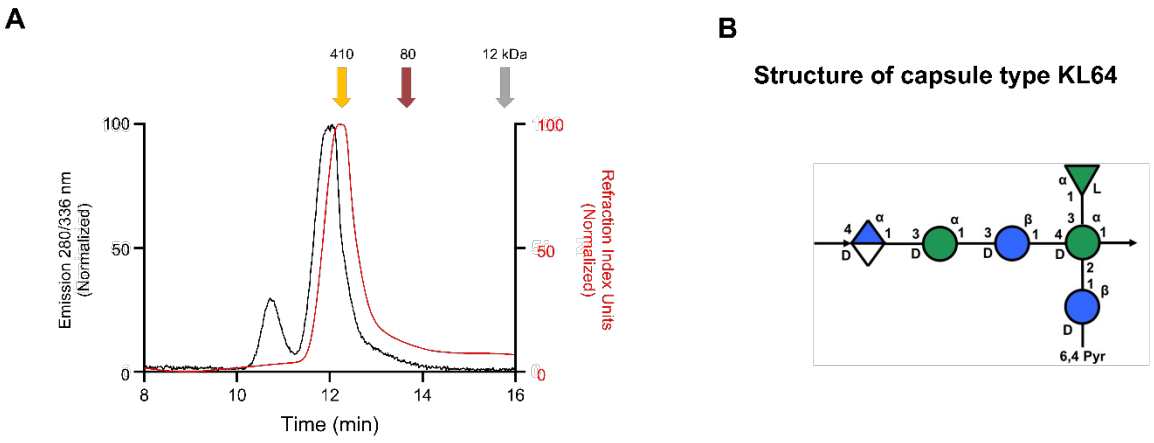

Supplementary Figure 5. Purification of different O-antigen subtypes. SEC-HPLC profiles of purified O-antigens, **(A)** O2a purified from ST147$_{NDM-1}$ and **(B)** O1v2 purified from ST13$_{OXA-48}$. The three arrows indicate molecular weight standards of 410, 80 and 12 kDa. **C)** Molecular structures of O1, O2a, and O2afg O-antigen types as reported in literature[158].

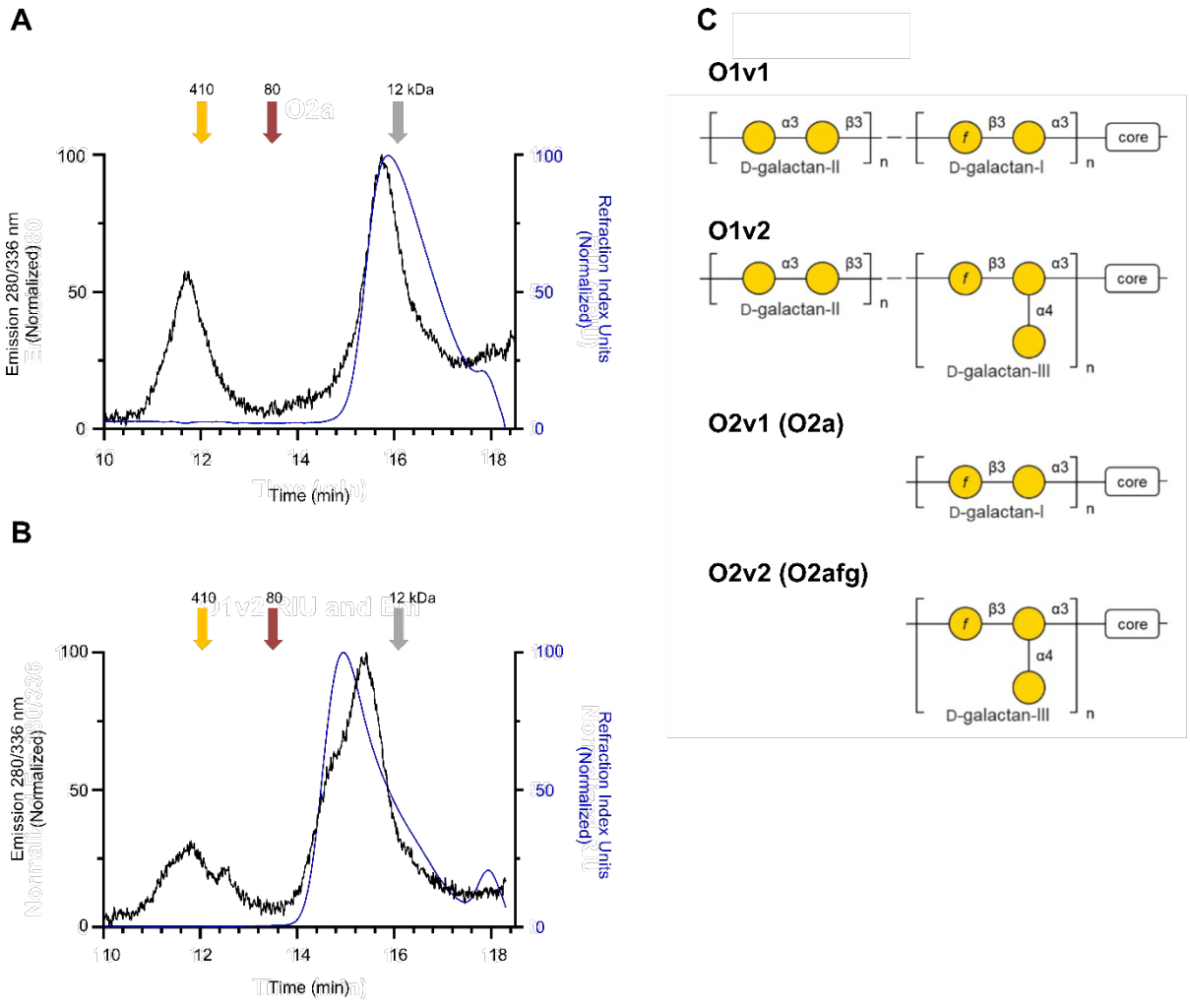

Supplementary Figure 6. Annotation of K and O locus on selected strains. For each sequence, the presence of K-locus (blue) and O-locus (red) genes is presented; genes with premature stop codons are visualized as shades.

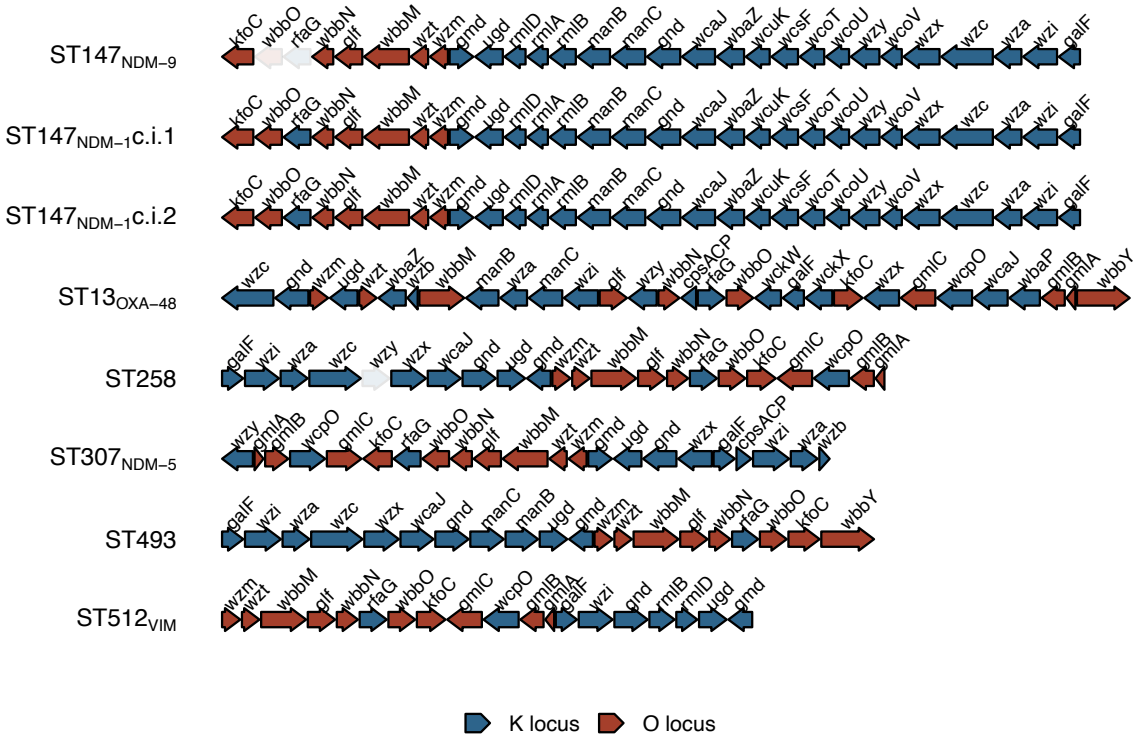

Supplementary Figure 7. Polysaccharide characterization of O-antigen deficient strain ST147$_{NDM-9}$. A) SEC-HPLC analysis of total sugar content after hydrolysis with acetic acid. The three peaks correspond to capsule, O-antigen, and the core. The three arrows indicate molecular weight standards of 410, 80, and 12 kDa. **B)** Silver staining analysis of total sugar extract from ST147$_{NDM-1}$ and ST147$_{NDM-9}$ Kp strains. ST147$_{NDM-9}$ lacks LPS ladder-like signal in the 25-50 kDa range, which is present in the ST147$_{NDM-1}$ loaded sample.

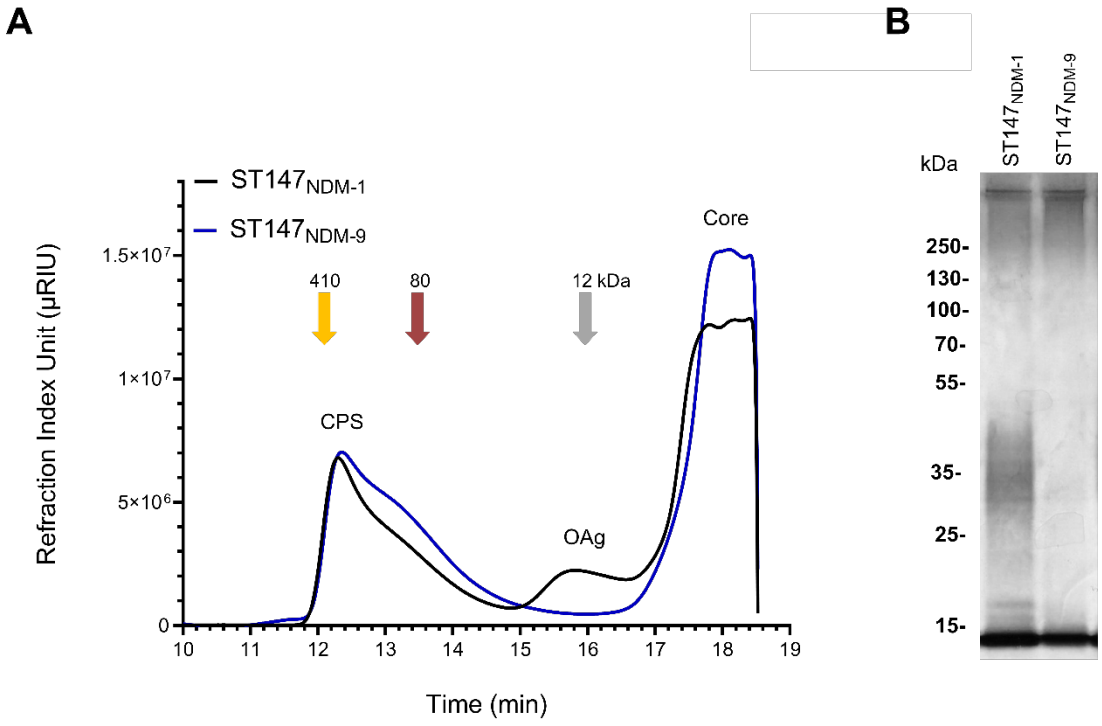

Supplementary Figure 8. ROI definition and spot detection for mAb binding characterization. Images show the binding pattern of A488-labelled anti-Kp mAbs on $ST147_{NDM-1}$ Kp (left), the ROI where A488 signal was detected (middle), and the morphology of A488 spot (right). Scale bar 2 μm.

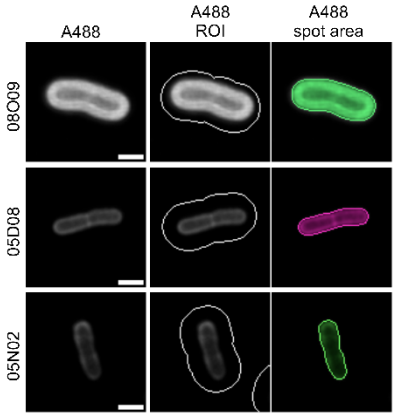

Supplementary Figure 9. Sequence analysis of 20 selected mAbs. **A)** Frequency of IGHV (top left) and IGHJ (top right) genes usage, IGKV (bottom left) and IGKJ (bottom right) genes usage. **B)** IGHV and IGHJ genes pairing heatmap (left), IGKV and IGKJ genes pairing heatmap (right). **C)** Percentage of variable chain identity with respect to the inferred germline. Antibodies similarity was analyzed by calculating a distance matrix using CLUSTAL Omega for the heavy (red) and light (green) chains separately. **D)** CDR3 length distribution, heavy chains (left, red) and light chains (right, green).

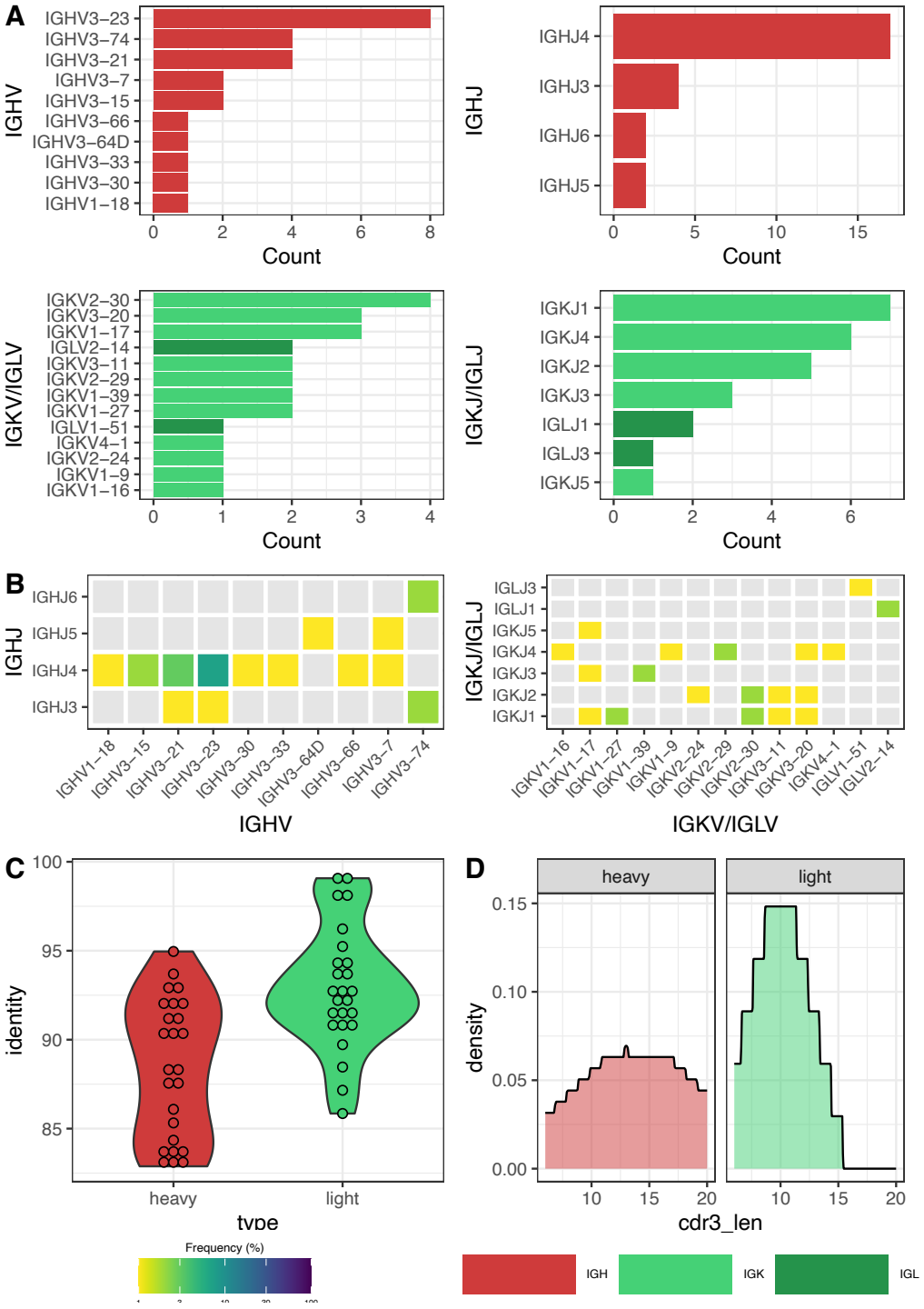

Supplementary Figure 10. F-SBA profiling of 20 functional mAbs against four complement-sensitive pathogenic Kp strains. F-SBA curves of 20 bactericidal anti-Kp mAbs against $ST147_{NDM-1}$ c.i.1 **(A)**, $ST147_{NDM-1}$ c.i.2 **(B)**, $ST147_{NDM-9}$ **(C)**, and $ST307_{NDM-5}$ **(D)**. Single experiments were normalized to no mAb controls. For each mAb, the bactericidal curve and the associated IC_{50} value were obtained using the [Inhibitor] vs. normalized response, variable slope analysis on GraphPad Prism. IC_{50} values are reported in Figure 4A.

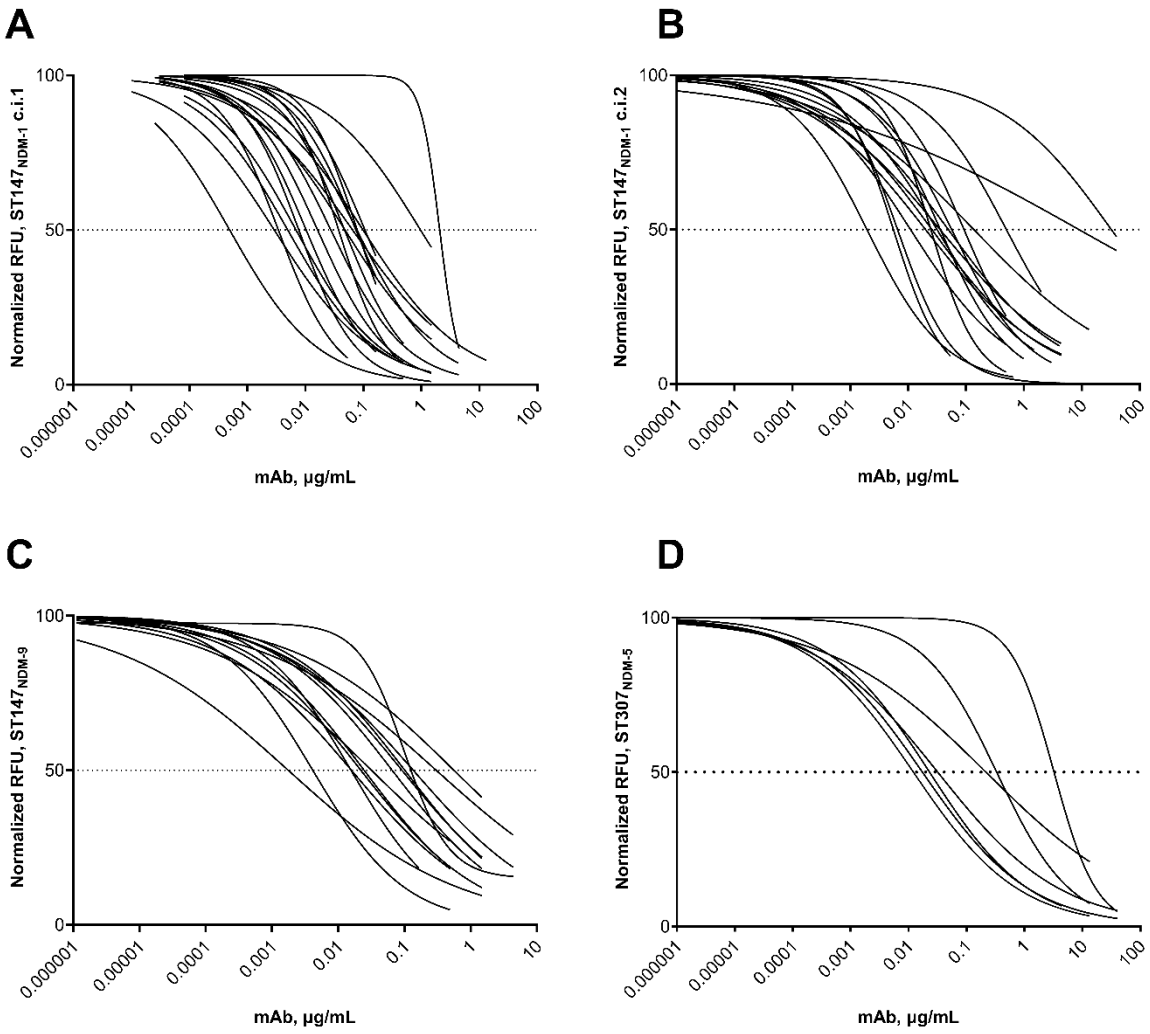

Supplementary Figure 11. Complement-dependent killing efficacy of 20 functional mAbs against four complement-sensitive pathogenic Kp strains. Heatmap displays the percentage of reduction in resazurin fluorescence as a readout of bacterial viability, normalized to no mAb controls. Results were extrapolated from F-SBA experiments with single mAbs.

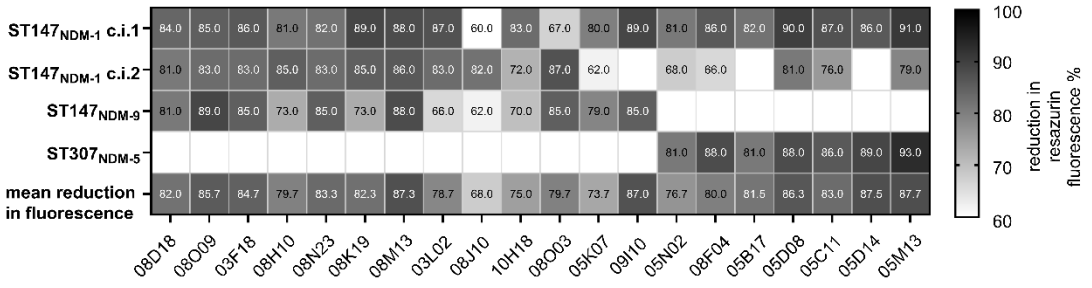

Supplementary Figure 12. Evaluation of *in vivo* protective properties of 08O09, 05D08 and 05N02 mAbs in immunocompetent ST147$_{NDM-1}$ bacteremia model. (A) Survival analysis for groups of mice infected with ST147$_{NDM-1}$ *K. pneumoniae* at four tested inoculums (in log_{10} CFU/mL). **(B)** 08O09 prophylaxis (PRO) regimens log_{10} CFU/spleen at endpoint compared with controls. **(C)** 08O09 treatment (THR) regimens log_{10} CFU/spleen at endpoint compared with controls. **(D)** Dose response comparison of survival time over 96 h in mice infected and receiving mAb 08O09 treatment (THR) and prophylaxis plus treatment (PRO+THR) at 1 mg/kg **(E)** and 5 mg/kg single doses. 10 animals per group were tested.

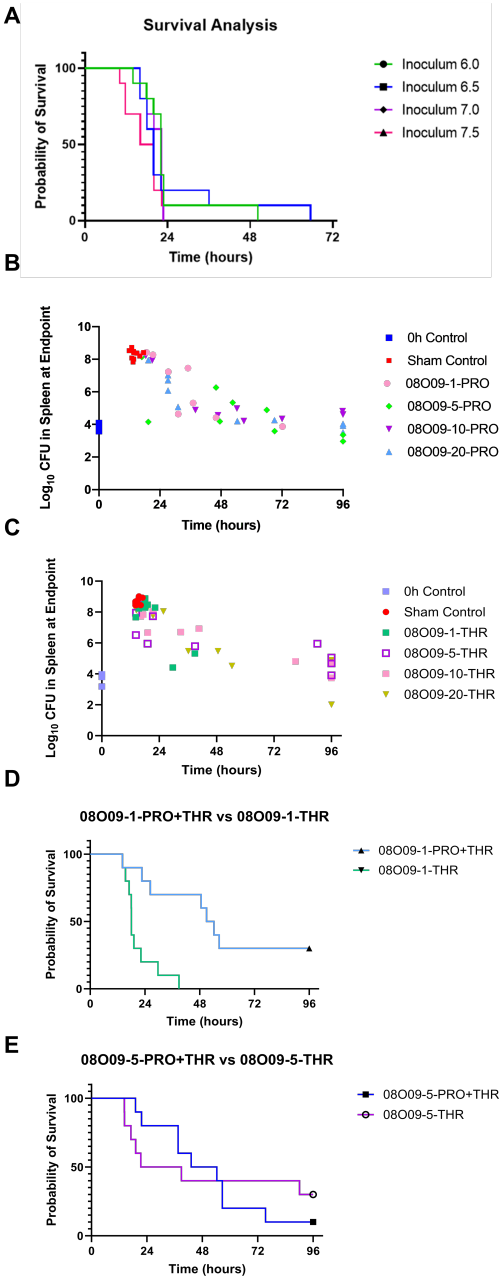

Supplementary Figure 13. Single-Time-Point Concentration Study.

The concentration of human mAb 08O09 in mouse plasma was measured by quantitative ELISA 24 h post administration of a single dose at 5 mg/kg by IP injection. Values were obtained by measuring absorbance at 405 nm and by interpolating a sigmoidal curve obtained with mouse plasma. The graph was made in GraphPad Prism.

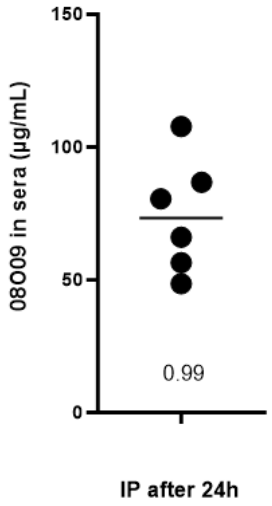

Supplementary Tables

Table S1. Information about patients from the Tuscany outbreak enrolled in the study.

Patient ID	Age	Date of Bacteremia	Collection Date	Months after infection	Kp strain
SBJ001	67	21/08/19	21/03/20	7	$ST147_{NDM-1}$
SBJ003	69	16/02/20	07/10/20	8	$ST147_{NDM-1}$
SBJ005	74	02/11/19	12/11/20	12	$ST147_{NDM-1}$
SBJ006	77	05/11/20	04/12/20	1	$ST147_{NDM-1}$
SBJ008	43	27/08/20	07/01/21	5	$ST147_{NDM-1}$
SBJ009	61	11/04/20	08/01/21	8	$ST147_{NDM-1}$
SBJ0010	74	20/04/20	25/01/21	8	$ST147_{NDM-1}$

Table S2. Kp isolates used in the manuscript. ST, K locus, O locus and presence of carbapenemase gene information were predicted from genomic analysis.

Strain name	Origin	ST	K locus	O locus	O type	Carbapenemase gene
$ST147_{NDM-1}$ c.i.1	Bacteremia	147	KL64	O2v1	O2a	bla_{NDM-1}
$ST147_{NDM-1}$ c.i.2	Bacteremia	147	KL64	O2v1	O2a	bla_{NDM-1}
$ST147_{NDM-9}$	Bacteremia	147	KL64	O2v1	O2a	bla_{NDM-9}
$ST307_{NDM-5}$	Abdominal drainage	307	KL102	O2v2	O2afg	bla_{NDM-5}
ST258	Urinary infection	258	KL107	O2v2	O2afg	-
$ST512_{VIM}$	n/a	512	KL107	O2v2	O2a	bla_{VIM}
$ST13_{OXA-48}$	Rectal swab	13	KL57	O1v2	O1	bla_{OXA-48}
ST493	ATCC43816	493	KL2	O1v1	O1	-

Table S3. Sequence analysis of 20 functional mAbs.

Sample	Type	V_usage	D_usage	J_usage	Variable region germline identity, %	CDR3 AA length
SBJ03-F18	light	IGKV1-9*01		IGKJ4*01	93,706	9
SBJ03-F18	heavy	IGHV3-21*01	IGHJ3*01	IGHJ4*02	95,222	13
SBJ03-L02	light	IGKV1-27*01		IGKJ1*01	95,088	9
SBJ03-L02	heavy	IGHV3-30*18	IGHJ2*01	IGHJ4*02	95,578	14
SBJ05-B17	heavy	IGHV3-74*01	IGHJ1*01	IGHJ6*02	90,203	20
SBJ05-B17	light	IGKV1-39*01		IGKJ3*01	89,895	9
SBJ05-C11	heavy	IGHV1-18*01	IGHJ1*01	IGHJ4*02	89,384	13
SBJ05-C11	light	IGLV1-51*01		IGLJ3*02	93,515	11
SBJ05-D08	heavy	IGHV3-15*01	IGHJ5*01	IGHJ4*02	95,286	10
SBJ05-D08	light	IGLV2-14*03		IGLJ1*01	95,578	10
SBJ05-D14	light	IGLV2-14*01		IGLJ1*01	93,75	10
SBJ05-D14	heavy	IGHV3-15*01	IGHJ5*01	IGHJ4*02	92,256	10
SBJ05-K07	heavy	IGHV3-23*04	IGHJ5*01	IGHJ4*02	96,259	18
SBJ05-K07	light	IGKV1-27*01		IGKJ1*01	98,592	9
SBJ05-M13	light	IGKV2-24*01		IGKJ2*01	95,695	10
SBJ05-M13	heavy	IGHV3-64D*06	IGHJ4*01	IGHJ5*02	90,753	6
SBJ05-N02	heavy	IGHV3-74*01	IGHJ1*01	IGHJ6*02	92,905	20
SBJ05-N02	light	IGKV1-39*01		IGKJ3*01	95,819	9
SBJ08-D18	heavy	IGHV3-23*04	IGHJ5*01	IGHJ4*02	93,493	12
SBJ08-D18	light	IGKV1-17*01		IGKJ3*01	97,535	9
SBJ08-F04	heavy	IGHV3-33*01	IGHJ6*01	IGHJ4*02	97,635	16
SBJ08-F04	light	IGKV3-11*01		IGKJ1*01	99,301	9
SBJ08-H10	heavy	IGHV3-23*04	IGHJ4*01	IGHJ4*02	91,186	12
SBJ08-H10	light	IGKV3-20*01		IGKJ1*01	94,81	9
SBJ08-J10	heavy	IGHV3-23*04	IGHJ1*01	IGHJ4*02	90,785	11
SBJ08-J10	light	IGKV2-30*01		IGKJ2*03	96,321	9
SBJ08-K19	heavy	IGHV3-21*01	IGHJ2*01	IGHJ3*02	96,918	14
SBJ08-K19	light	IGKV3-11*01		IGKJ2*03	99,303	10
SBJ08-M13	heavy	IGHV3-23*04	IGHJ6*03	IGHJ4*02	93,836	15
SBJ08-M13	light	IGKV1-16*02		IGKJ4*01	98,592	9
SBJ08-N23	heavy	IGHV3-66*01	IGHJ6*01	IGHJ4*02	92,15	14
SBJ08-N23	light	IGKV2-30*02		IGKJ1*01	96,296	8
SBJ08-O03	heavy	IGHV3-23*04	IGHJ3*01	IGHJ4*02	93,878	13

SBJ08-O03	light	IGKV3-20*01		IGKJ4*01	97,544	12
SBJ08-O09	light	IGKV3-20*01		IGKJ2*03	96,194	10
SBJ08-O09	heavy	IGHV3-23*04	IGHJ2*01	IGHJ3*01	94,218	12
SBJ09-I10	heavy	IGHV3-23*04	IGHJ1*01	IGHJ4*02	89,492	14
SBJ09-I10	light	IGKV1-17*01		IGKJ5*01	97,183	9
SBJ10-H18	heavy	IGHV3-21*01	IGHJ6*01	IGHJ4*02	95,254	12
SBJ10-H18	light	IGKV2-30*01		IGKJ1*01	97,674	9

Table S4. List of primers mix used for PCR I.

PRIMER NAME	SEQUENCE
Heavy chain primers	
L-VH1_VH7 fw	CACTCCCAGGTGCAGCTGGTGCAG
L-VH2 fw	TGGGTCTTRTCCCAGGTCACCTTG
L-VH 3fw	AAGGTGTCCAGTGTSAGGTGCAG
L-VH4_6 fw	GTCCTGTCCCAGGTGCAGCTGCAG
L-VH5 fw	GAGTCTGTTCCGAGGTGCAGCTGG
IgG CH rev	GTGCCAGGGGGAAGACCGATG
IgA CH rev	GCMGAGGCTCAGCGGGAAGAC
IgM CH rev	GAGACGAGGGGGAAAAGGGTTG
Kappa chain primers	
L-VK1 fw	CAGGTGCCAGATGTGHCATCCAG
L-VK2 fw	CTGGATCCAGTGSGGATATTGTGATG
L-VK3 fw	CCCAGATACCACCGGAGAAATTGTG
L-VK4 fw	CTCTGGTGCCTACGGGGACATCGTG
L-VK5 fw	CTGATACCAGGGCAGAAACGACAC
CK rev 1st	GAACACTCTCCCCTGTTGAAGCTCTTTG
Lambda chain primers	
L-VL1 fw	GGTCCTGGGCCCAGTCTGTGCTG
L-VL2 fw	GGTCCTGGGCCCAGTCTGCCCTG
L-VL3 fw	TCTGTGRCCTCCTATGAGCTGAC
L-VL4_VL5_VL9 fw	CTCTCGCAGCCTGTGCTGACTCA
L-VL6 fw	GTTCTTGGGCCAATTTTATGCTG
L-VL7 fw	GGTCCAATTCTCAGGCTGTGGTG
L-VL8 fw	GAGTGGATTCTCAGACTGTGGTG
L-VL10 fw	GTCAGTGGTCCAGGCAGGGCTGAC
CL rev 1st	GTGCTCCCTTCATGCGTGACC

Table S5. List of primers mix used for PCR II.

PRIMER NAME	SEQUENCE
Heavy chain primers	
HIFI*_C134_VH1_5_7	GT ATC ATC CTT TTT CTA GTA GCA ACT GCA ACC GGT GTACATTCC CAG GTG CAG CTG GTG CAG TCT G
HIFI*_C134_VH2	GT ATC ATC CTT TTT CTA GTA GCA ACT GCA ACC GGT GTACATTCC CAG GTC ACC TTG AAG GAG TCT GGT C
HIFI*_C134_VH3	GT ATC ATC CTT TTT CTA GTA GCA ACT GCA ACC GGT GTACATTCC GAG GTG CAG CTG GTG GAG TCT GGG GGA G
HIFI*_C134_VH4_6_a	GT ATC ATC CTT TTT CTA GTA GCA ACT GCA ACC GGT GTACATTCC CAG GTG CAG CTG CAG GAG TCG GG
HIFI*_C134_VH4_6_b	GT ATC ATC CTT TTT CTA GTA GCA ACT GCA ACC GGT GTACATTCC CAG GTG CAG CTG CAG CAG TGG GG
HIFI*_IgG CH rev	CTT GGA GGA GGG TGC CAG GGG GAA GAC CGA TGG GCC CTT GGT GGA RGC
HIFI*_IgA CH rev	CTT GGA GGA GGG TGC CAG GGG GAA GAC CGA CTT GGG GCT GGT CGG GGA
HIFI*_IgM CH rev	CTT GGA GGA GGG TGC CAG GGG GAA GAC CGA TGG GGC GGA TGC ACT CCC
Kappa chain primers	
HIFI*_C135_VK1	GT ATC ATC CTT TTT CTA GTA GCA ACT GCA ACC GGT GTACATTCC GCC ATC CAG ATG ACC CAG TCT CCA TC
HIFI*_C135_VK2_a	GT ATC ATC CTT TTT CTA GTA GCA ACT GCA ACC GGT GTACATTCC GAT ATT GTG ATG ACC CAG ACT CCA CTC TC
HIFI*_C135_VK2_b	GT ATC ATC CTT TTT CTA GTA GCA ACT GCA ACC GGT GTACATTCC GAT ATT GTG ATG ACT CAG TCT CCA CTC TC
HIFI*_C135_VK3_a	GT ATC ATC CTT TTT CTA GTA GCA ACT GCA ACC GGT GTACATTCC GAA ATT GTG TTG ACA CAG TCT CCA G
HIFI*_C135_VK3_b	GT ATC ATC CTT TTT CTA GTA GCA ACT GCA ACC GGT GTACATTCC GAA ATT GTG ATG ACG CAG TCT CCA G
HIFI*_C135_VK4	GT ATC ATC CTT TTT CTA GTA GCA ACT GCA ACC GGT GTACATTCC GAC ATC GTG ATG ACC CAG TCT CCA G
HIFI*_C135_VK5	GT ATC ATC CTT TTT CTA GTA GCA ACT GCA ACC GGT GTACATTCC GAA ACG ACA CTC ACG CAG TCT CCA G
HIFI*_C080_VK_Rev	GA TTT CAA CTG CTC ATC AGA TGG CGG GAA GAT GAA GAC AGA TGG TGC AGC CAC AGT TC

Lambda chain primers	
HIFI*_C080_VL1	GT ATC ATC CTT TTT CTA GTA GCA ACT GCA ACC GGT TCCTGGGCC CAG TCT GTG CTG ACT CAG CCG CCC TCA G
HIFI*_C080_VL2	GT ATC ATC CTT TTT CTA GTA GCA ACT GCA ACC GGT TCCTGGGCC CAG TCT GCC CTG ACT CAG CCT GCC TCC G
HIFI*_C080_VL3_a	GT ATC ATC CTT TTT CTA GTA GCA ACT GCA ACC GGT TCCTGGGCC TCC TAT GAG CTG ACA CAG CCA C
HIFI*_C080_VL3_b	GT ATC ATC CTT TTT CTA GTA GCA ACT GCA ACC GGT TCCTGGGCC TCC TAT GAG CTG ACT CAG GAC C
HIFI*_C080_VL4	GT ATC ATC CTT TTT CTA GTA GCA ACT GCA ACC GGT TCCTGGGCC CAG CCT GTG CTG ACT CAA TCG TCC TCT G
HIFI*_C080_VL5-9	GT ATC ATC CTT TTT CTA GTA GCA ACT GCA ACC GGT TCCTGGGCC CAG CCT GTG CTG ACT CAG CCR ACT TC
HIFI*_C080_VL6	GT ATC ATC CTT TTT CTA GTA GCA ACT GCA ACC GGT TCCTGGGCC AAT TTT ATG CTG ACT CAG CCC CAC TC
HIFI*_C080_VL7	GT ATC ATC CTT TTT CTA GTA GCA ACT GCA ACC GGT TCCTGGGCC CAG GCT GTG GTG ACT CAG GAG CCC TC
HIFI*_C080_VL8	GT ATC ATC CTT TTT CTA GTA GCA ACT GCA ACC GGT TCCTGGGCC CAG ACT GTG GTG ACC CAG GAG CCA TC
HIFI*_C080_VL10	GT ATC ATC CTT TTT CTA GTA GCA ACT GCA ACC GGT TCCTGGGCC CAG GCA GGG CTG ACT CAG CCA CCC TCG G
HIFI*_CL_generic	G TGT GGC CTT GTT GGC TTG AAG CTC CTC ACT CGA GGG YGG GAA CAG AGT G

Table S6. List of primers used for producing transcriptionally active PCR (TAP) products.

NAME	SEQUENCE
CMV_TAP_FW	TTAGGCACCCCAGGCTTTAC
polyA_TAP_Rev	AGATGGTTCTTTCCGCCTCA

CHAPTER 2:

Ex vivo gastrointestinal organoids as a new 3D tool for therapy development against pandrug-resistant $ST147_{NDM-1}$ Klebsiella pneumoniae

Introduction:

The human intestinal tract is populated by a plethora of microorganisms that all together are essential for human health. This community of bacteria, archaea, fungi, protists, and viruses is referred to as the gut microbiota and its interaction with the host plays a key role in preventing dysbiosis and maintaining intestinal health as well as in causing disease[182]. Most gut microbiota microorganisms have a symbiotic relationship with the host[183], however bacterial pathogens can disrupt this equilibrium and cause not only acute infections, but also inflammatory and autoimmune diseases, as well as metabolic syndromes and cancer[182,184,185]. Moreover, reckless use of antibiotics resulted in reduction of microbiota diversity[186] and in the selection of MDR opportunistic bacteria already inhabiting the intestinal tract[6,187]. These opportunistic pathogens may then translocate across the intestinal barrier and cause disease.

The intestinal barrier separates the gut external environment, the lumen, from the internal one, the interstitial environment, through the intestinal epithelium[186]. Gut epithelium consists mainly of enterocytes, but it also includes other types of specialized cells such as Goblet cells, which secrete mucins to support epithelial integrity and protection from microorganisms[188], as well as M cells and Paneth cells, involved in antimicrobial defense mechanisms[189] (**Figure 1**). The intestinal barrier fulfills two apparently contradictory, but equally essential tasks. On the one hand it regulates the permeability of fluids and uptake of nutrients through an intercellular barrier made of tight and adherens junctions[190,191]. On the other hand, the intestinal epithelia are continuously undergoing cell death and shedding as well as quick cell renewal which generates a new epithelial monolayer every 3 to 6 days[192]. Constant tissue replenishment is sustained by dividing stem cells that are present at the bottom of colonic crypts[193]. Rapid turnover threatens the integrity of the epithelial barrier, which needs to be maintained in order to restrict invasion of potentially harmful microbes[190]. In this regard, several bacterial and viral pathogens have developed mechanisms to penetrate the intestinal barrier through paracellular or transcellular pathways. Through paracellular pathways pathogens can break the tight and adherens junctions between enterocytes, therefore compromising epithelial integrity[194,195]. In this way, they can infiltrate between neighboring cells and cross the epithelial barrier[196]. Alternatively,

pathogens can penetrate inside the cells through intracellular pathways, apically invading enterocytes or M cells and subsequently exiting through basolateral exocytosis[186,196].

To investigate the mechanisms underlying development and progression of infectious diseases, as well as to design new and effective therapeutic solutions, *in vitro* and *in vivo*

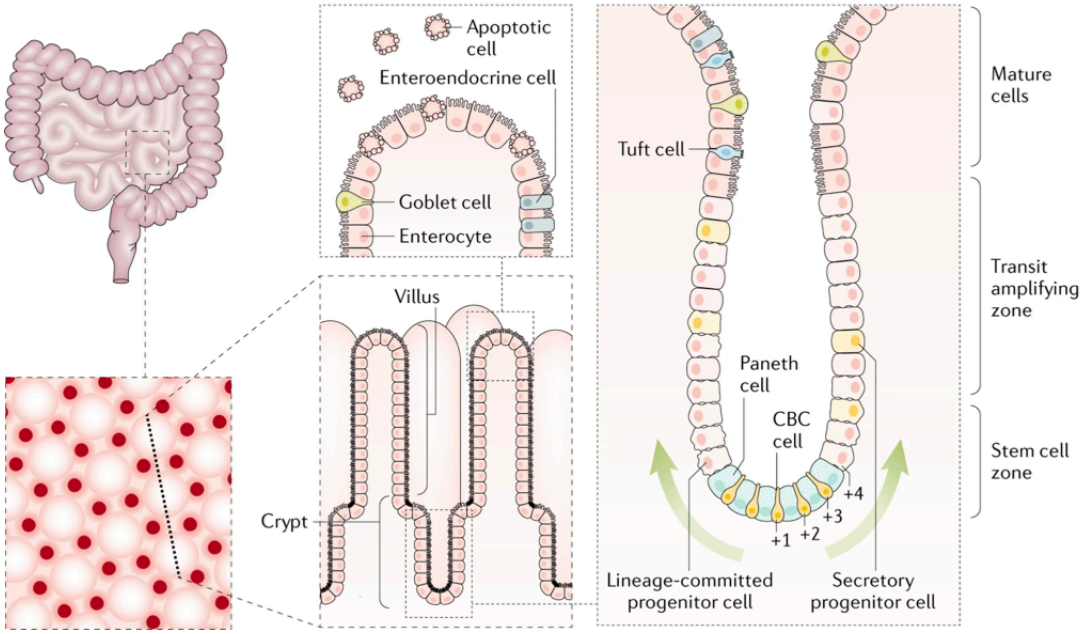

Figure 1. Intestinal structure.
Image from: Tales from the crypt: new insights into intestinal stem cells.

models have been extensively used. 2D monolayer cultures of human immortalized cell lines have been employed as the main *in vitro* tool to study pathogenesis and virulence of bacterial infections. In addition to being used to shed light on molecular mechanisms of infection, application of *in vitro* models can help screening antimicrobial compounds in a convenient and high-throughput way[197]. Nevertheless, *in vitro* systems can result simplistic as they cannot recapitulate the diversity of cell types nor the complexity of host-pathogen interactions[198]. Mouse models are the gold standard for studying interactions between host and microbes but can lack experimental control and scalability[199]. Moreover, some pathogens cause strictly human-specific infection, therefore *in vivo* models may not recapitulate biologically relevant human host responses[200]. Hence, in recent years *in vivo* and *in vitro* systems have been complemented by *in vitro* and *ex vivo* physiologically relevant models[201] that can be used to interrogate the driving principles of bacterial pathogenesis and the host response to microbial insults. These novel approaches derive from human

tissues or human stem cells and aim to close the gap between transformed cell cultures and animal models. In fact, human-derived organoids[202] and organs-on-chips[203] allow clonal expansion, genetic manipulation, and study of tissue-specific dynamics[204–207]. Among *ex vivo* models, human tissue stem cell-derived organoids can be developed from mature organs[201] (**Figure 2**). Pluripotent stem cells can establish *in vitro* organoids cultures within a week and have unlimited proliferative capacity. Even though tissue-derived organoids lack the mesenchymal component, they are essential to unravel the interplay between human tissues and infectious agents.

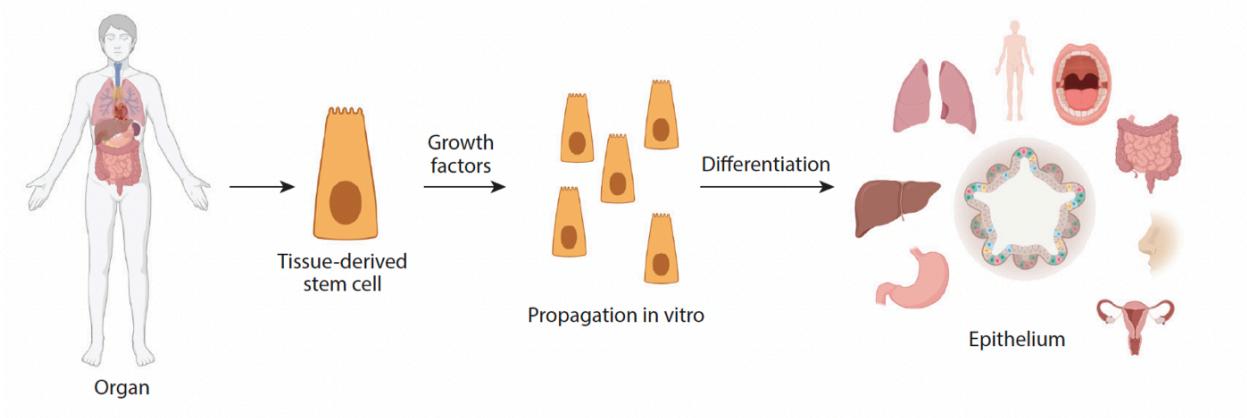

Figure 2. Establishment of tissue stem cell–derived organoids. Tissue stem cell–derived organoids originate from mature organs stem cells. These stem cells can divide and differentiate into organoids that recapitulate the epithelial layer of the tissue of origin.
Image from: Organoid Models for Infectious Disease.

Epithelial organoid models are great tools to investigate tissue-specific responses to bacterial infections[186,208,209]. Organoids are grown in extracellular matrix hydrogels[210], such as Matrigel, and self-assemble into 3D cultures that can be maintained and frozen similarly to routine culture cell lines. Moreover, the use of growth factors in culture media can induce differentiation of organoids to recapitulate the diversity of cell types and mimic functional epithelium[211,212]. The apical surface of organoids, where most pathogens usually attack, grows facing the interior luminal compartment. To access the apical surface of basolateral-out organoids, different techniques such as microinjections[213], disruption of spheroids[214] and dissociation of 3D organoids to generate two-dimensional monolayers[215,216] have been employed, each with its own advantages and drawbacks[217].

Recently, methodologies for inverting organoids topology have been described[217,218] (**Figure 3**). By reversing the polarity of basolateral-out organoids, the apical surface of gastrointestinal epithelia can be directly presented to enteric pathogens without disrupting the epithelial integrity[218]. The easy access to the apical surface in apical-out organoids is an

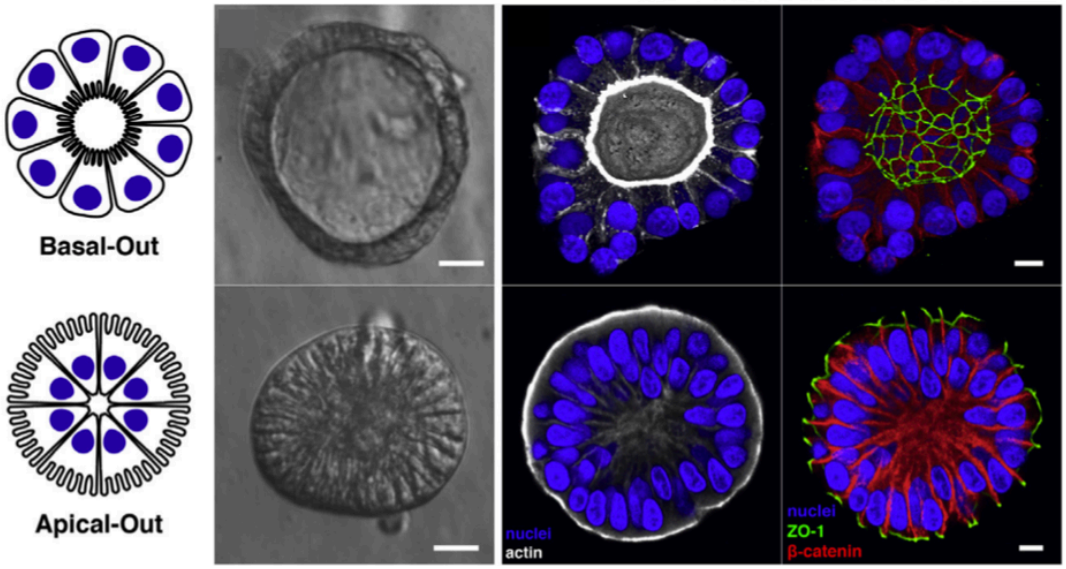

Figure 3. Organoids polarity reversal. Basal-out and apical-out organoids illustrated schematically, imaged by modulation contrast microscopy, and by confocal microscopy. Nuclei are depicted in blue, actin in white, ZO-1 in green, and β-catenin in red. Scale bars are 10 mm.
Image from: Controlling Epithelial Polarity: A Human Enteroid Model for Host-Pathogen Interactions.

extremely powerful tool to further investigate the molecular mechanisms underlying bacterial pathogenesis as well as host-pathogen interactions. In this regard, identifying cellular and bacterial factors involved in microbial adhesion and invasion, with particular emphasis on detecting specific elements essential for host infection, can prove crucial for the development of innovative antimicrobial therapies and novel protective vaccines. Moreover, the possibility of deriving organoids from specific patients could also pave the way to the development of personalized medicine approaches.

Here, apical-out organoids, generated from reversing the polarity of human tissue stem cell-derived organoids, have been employed to unravel *Klebsiella pneumoniae* mechanisms of infection at the host epithelial surface. In addition to this, the most promising mAb candidate (08O09) isolated in the MAD-Lab has been tested in this infection model

with the aim of evaluating its efficacy in protecting against *K. pneumoniae* dissemination in a physiologically relevant model of infection.

Results

***1. K. pneumoniae* infects the colonic epithelium at junction sites and on extrusion zones.** To explore the first steps of *K. pneumoniae* pathogenesis, bacterial capacity to adhere to colonic epithelia was evaluated. In addition to this, to investigate whether *K. pneumoniae* may preferentially bind to cells that can be found at the bottom of colonic crypts

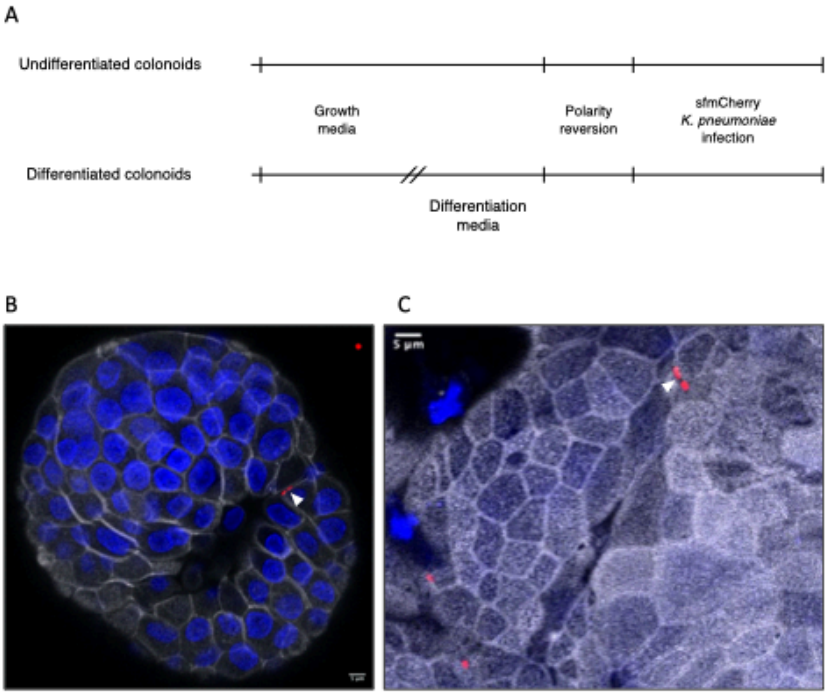

Figure 4. A) Schematic of the experimental workflow. **B)** Undifferentiated organoid, 2 hours upon infection. **C)** Differentiated organoid, 2 hours upon infection. *K. pneumoniae* is depicted in red, nuclei in blue and actin in white.

instead of adhering to those present at the top, colon-derived organoids (colonoids) prior to differentiation (which will be referred to as undifferentiated) as well as five days after differentiation (referred to as differentiated) were employed. Upon 24 hours of polarity reversion, sfmCherry-expressing *K. pneumoniae* was added to the undifferentiated and to the differentiated colonoid cultures to reach a ratio of 1:1 colonoids-to-bacteria (**Figure 4A**). Colonoids were fixed at t0, 2h, and 4h after infection. To first assess presence of bacteria on the colonic surface, organoids were probed with DAPI and phalloidin to stain nuclei and

the actin cytoskeleton, respectively. From 2 hours after infection, *K. pneumoniae* mCherry signal was detected on the surface of both undifferentiated and differentiated colonoids

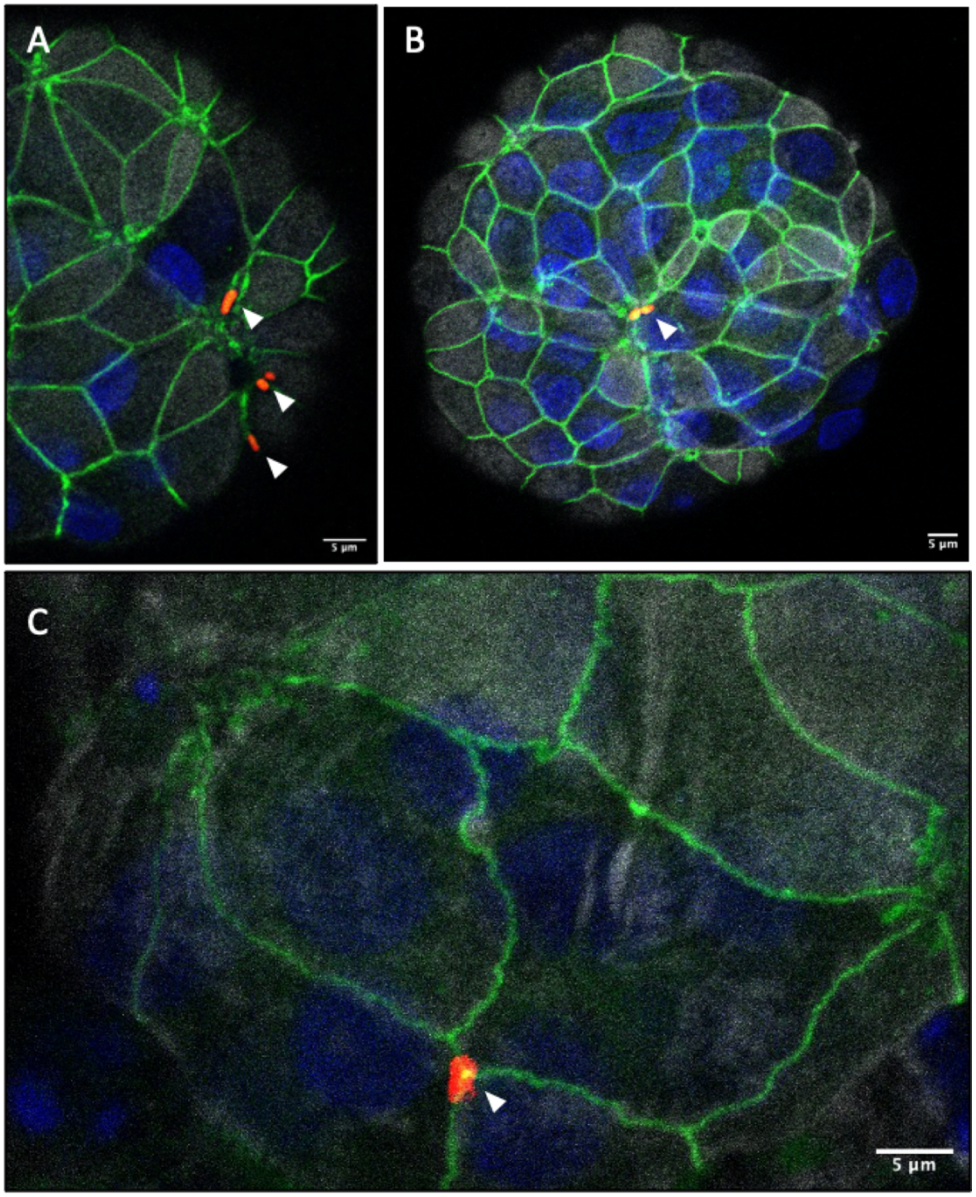

Figure 5. *K. pneumoniae* on tight junctions of colonoids. *K. pneumoniae* mCherry signal, depicted in red, can be found on the tight junction on the surface of undifferentiated **(A, B)** and differentiated **(C)** colonoids. Nuclei are shown in blue, actin in white and ZO-1 in green. Scale bars are 5µm

(**Figure 4B and 4C**). Interestingly, most bacteria were seemingly localizing on the epithelial surface between cells suggesting that, like many other Gram-negative species[195], *K. pneumoniae* may adhere to cell junctions. To test this hypothesis, infected colonoids were probed with antibodies to tight junctions (anti-ZO-1). Indeed, bacterial mCherry signal overlapped with ZO-1 fluorescent signal (**Figure 5**), indicating that *K. pneumoniae* adheres preferentially to the intercellular barrier between epithelial cells. In addition to this, bacterial

adhesion was also observed on shedding cells (**Figure 6**). This phenotype was observed on both undifferentiated (**Figure 6 A and B**) and differentiated (**Figure 6 C and D**) colonoids.

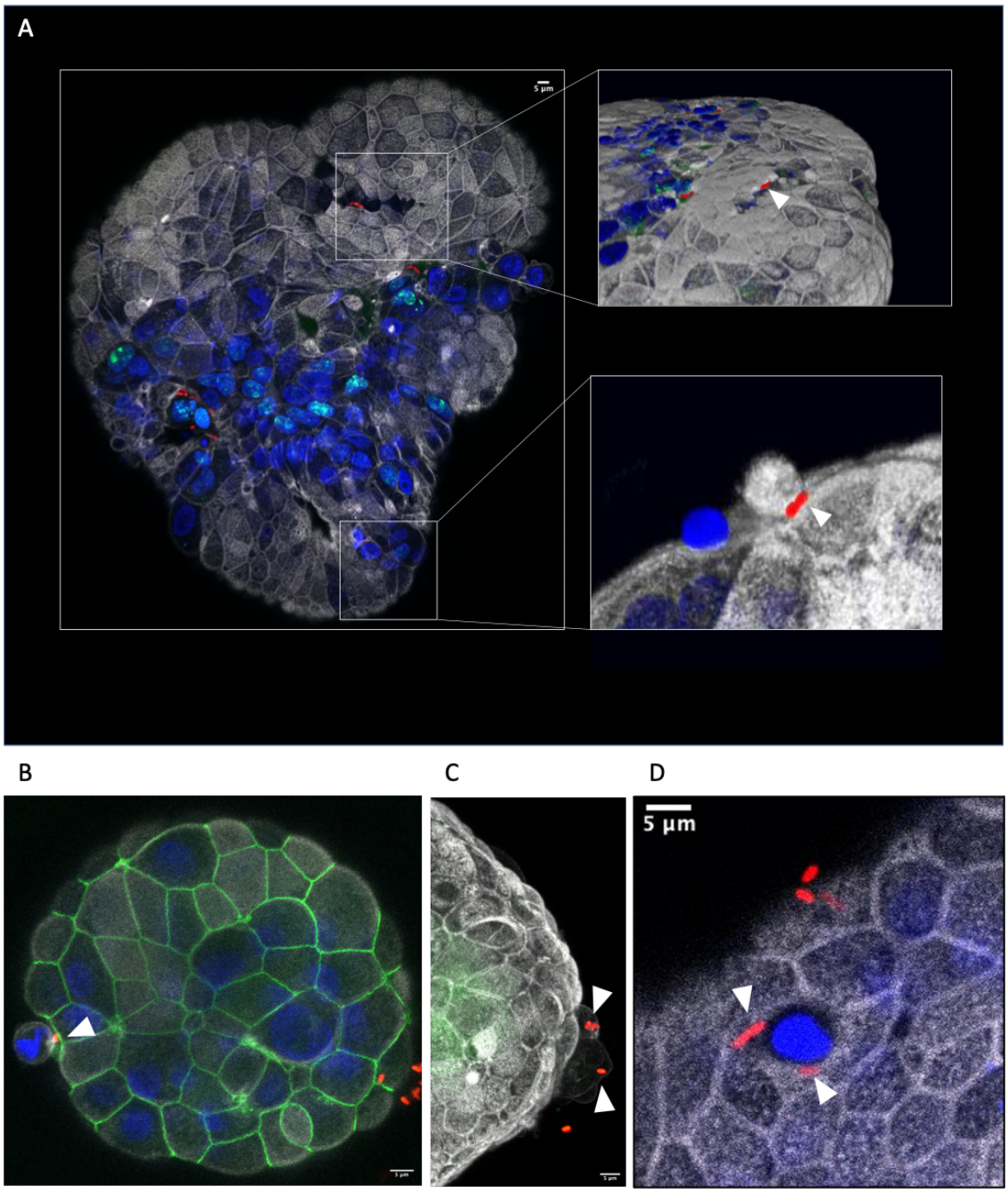

Figure 6. *K. pneumoniae* on extrusion zones on the surface of colonoids. In all images, nuclei are depicted in blue, actin in white, *K. pneumoniae* in red. **A)** Undifferentiated colonoid 4 hours after infection, bacteria can be found on shedding cells and are pointed by white arrows. Ki67 is depicted in green. **B)** Undifferentiated colonoid 2 hours after infection. *K. pneumoniae* indicated by the arrow can be seen in the space between a shedding cell and the surface of the organoid. ZO-1 is depicted in green. **C)** Extrusion zone on a differentiated organoid with bacteria adhering to shedding cells, as indicated by arrows. Muc2 signal is depicted in green. **D)** Bacteria in proximity to shedding cells on the surface of a differentiated organoid 2 hours upon infection. Scale bars are 5µm.

Interestingly, increased levels of shedding cells sites were detected on colonoids in the presence of *K. pneumoniae* in cell culture media when compared to uninfected controls, suggesting that the pathogen may exert a cytotoxic effect on gut epithelia. *K. pneumoniae* may take advantage of cell extrusion sites as a point of adhesion and invasion of gut epithelia, while increased cell shedding, hence higher amounts of damaged cells that will eventually undergo programmed cell death, may be promoted by the pathogen for survival and proliferation.

***2. K. pneumoniae* forms bacterial clusters on apoptotic cells and promotes programmed cell death through an adhesion-independent cytotoxic effect.** High levels of cell death and dismantlement of colonoids were observed in the presence of bacteria (**Figure 7 A and B**). To delve deeper into the role of *K. pneumoniae* on cell extrusion and programmed cell death on gut epithelia, apoptotic pathways were examined. To this end, upon infection with *K. pneumoniae*, undifferentiated and differentiated colonoids were incubated with a fluorogenic substrate of caspases 3 and 7 (Cas3/7) to evaluate the apoptotic state of epithelial cells (**Figure 7C-F**). The majority of bacteria was found on extruding cells as well as on colonoids that were highly damaged by the presence of *K. pneumoniae* (**Figures 7C**). Notably, not only increased levels of fluorescently labeled Cas3/7 apoptotic cells could be detected in the presence of *K. pneumoniae*, but also bacterial clusters were found in conjunction with fluorescently labeled caspase 3/7 cells, highlighting adhesion of *K. pneumoniae* to apoptotic cells (**Figure 7F**).

Indeed, despite keeping a low ratio of bacteria-to-organoids to keep the infection contained, excessive bacterial growth could not be avoided and would eventually lead to extreme cell shedding and apoptosis within 4 hours upon infection. In this regard, bacterial overgrowth was only detected in bacterial cultures grown in the presence of colonoids, while those grown in fresh HBSS in the absence of organoids grew from OD_{600} 0.005 to OD_{600} 0.08 in 24 hours. Altogether, these observations suggest that *K. pneumoniae* may exert a cytotoxic effect to break epithelial barrier integrity and to adapt to shortage of nutrients by acquiring them from damaged host cells.

To further investigate *K. pneumoniae* pathogenicity on gut epithelia and to explore the hypothesis of an adhesion-independent mechanism of cytotoxicity, experiments with 0.1μm membrane transwells were carried out on undifferentiated colonoids and samples were fixed after 4 hours (**Figure 8**). Interestingly, colonoids in the underside of transwells,

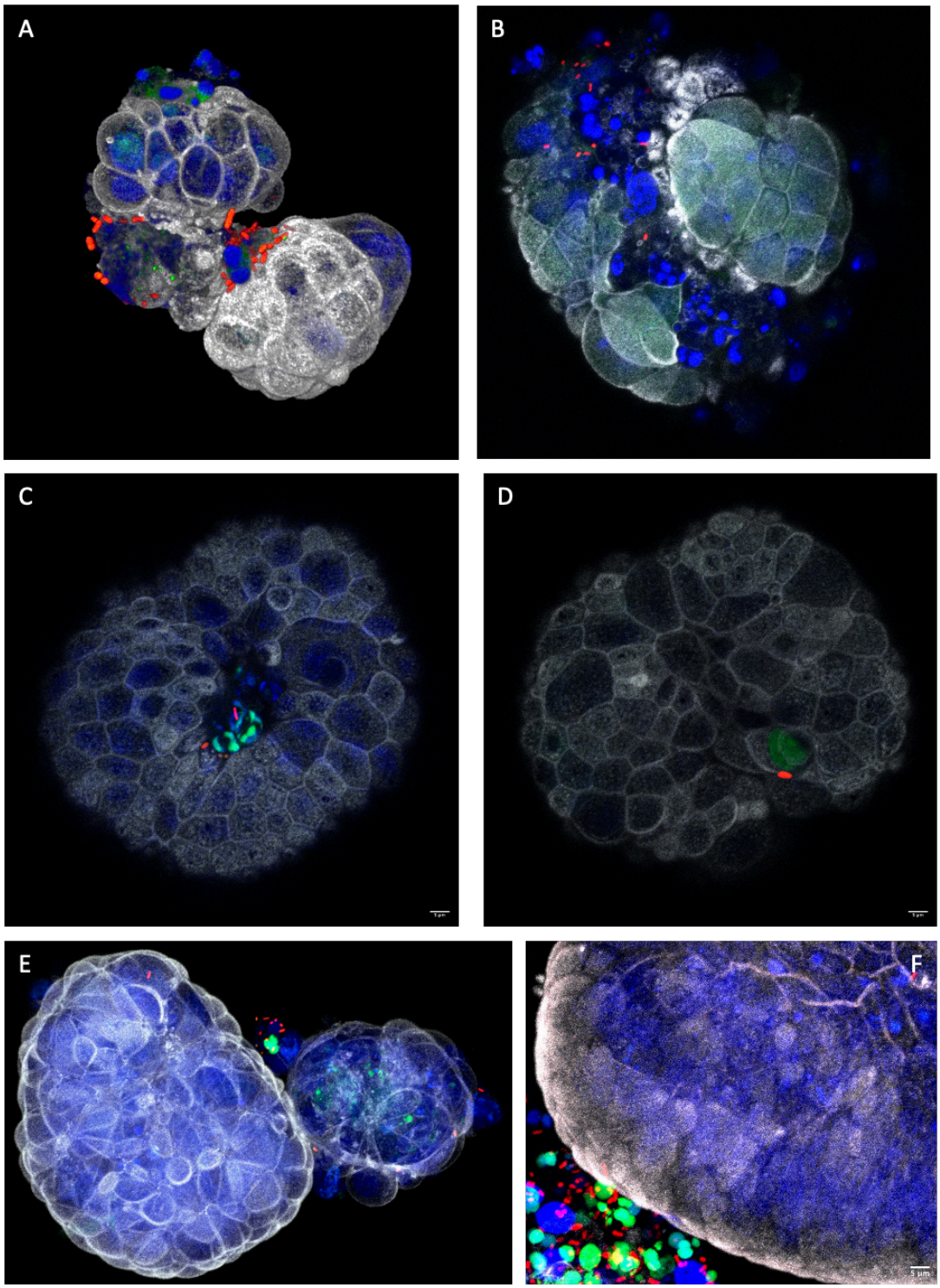

Figure 7. *K. pneumoniae* binding to apoptotic cells on the surface of undifferentiated and differentiated colonoids. In all images nuclei are depicted in blue, actin in white, and *K. pneumoniae* in red. **A)** Undifferentiated colonoid 4 hours after infection. Bacteria form clusters where actin signal is not observed anymore. Ki-67 in green. **B.** Differentiated colonoid disintegrating after 4 hours of infection. *K. pneumoniae* can be found where the actin cytoskeleton has faded. Villin is depicted in green. Undifferentiated **(C and D)** and differentiated **(E and F)** organoids with apoptotic cells highlighted in green. In both cases, *K. pneumoniae* can be found in proximity to Cas3/7 positive cells.

therefore grown in presence of but not in direct contact with *K. pneumoniae*, showed higher levels of apoptotic cells (**Figure 8**, right side) compared to colonoids grown in the absence of bacteria (**Figure 8**, left side). Moreover, in order to evaluate if *K. pneumoniae* could benefit from nutrients released from organoid cultures, bacterial proliferation was evaluated by growing bacteria in fresh HBSS and in HBSS taken from organoids overnight culture (conditioned HBSS). After 4 hours, bacteria were plated to count CFUs. Notably, $6 \bullet 10^6$ CFU/ml were detected in the sample grown in conditioned media, 100-fold higher than the $4 \bullet 10^4$ CFU/mL counted in the sample grown in fresh HBSS. Hence, in parallel with the increased levels of apoptosis observed in colonoids samples, bacterial growth was promoted even in the absence of direct contact between eukaryotic and bacterial cells.

Taken together, these results highlight the aggressiveness of an unknown *K. pneumoniae* mechanism of pathogenesis, which may lead to rupture of the intestinal barrier integrity for bacterial growth. Moreover, the associated extreme bacterial proliferation may facilitate invasion and eventually advance into dissemination to other tissues.

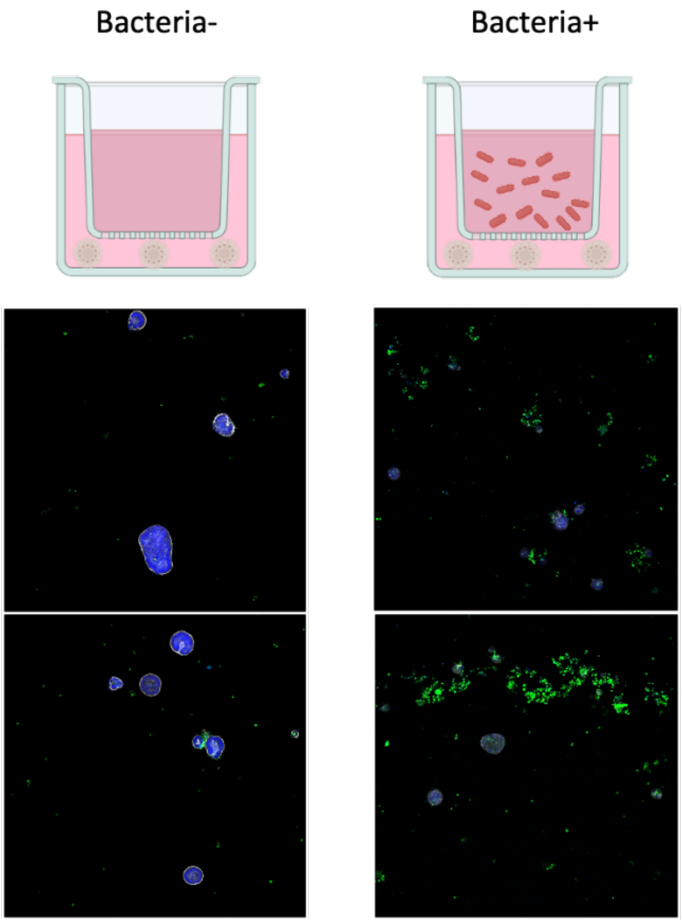

Figure 8. *K. pneumoniae* triggers apoptosis of colonoids through an adhesion-independent mechanism. Schematic of transwells employed for the experiment are found on top of the figure. Left panels show colonoids images from no bacteria control samples. Panels on the right display colonoids images upon 4 hours of co-culture with *K. pneumoniae*. Organoids were grown in the lower side of transwells and were not in contact with bacteria during incubation time. Cas3/7 is depicted in green, nuclei in blue and actin in white.

3. 08O09 promotes colonoids survival by reducing *K. pneumoniae* bacterial adhesion and triggers enchained bacterial growth. Finally, to assess the role of 08O09 on protecting intestinal epithelia from *K. pneumoniae*, 2 μg/mL of mAb were added to the experimental conditions used throughout the study. Colonoids were fixed at t0 and 2 hours after infection and the *K. pneumoniae*-containing supernatant was plated to count CFUs.

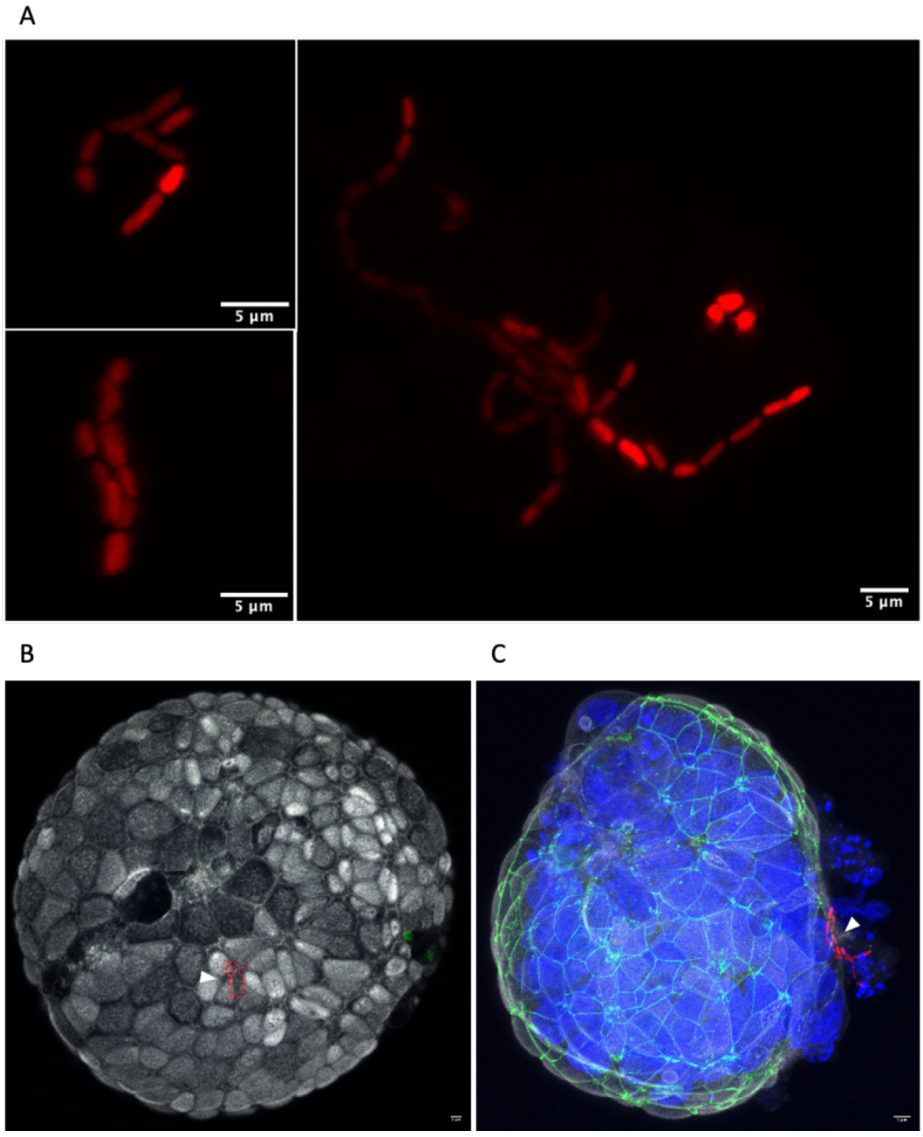

Figure 9. Presence of 08O09 triggers enchained bacterial growth and promotes organoids survival. A) Chains of *K. pneumoniae*, depicted in red, could be found in the presence of 08O09. **B)** Undifferentiated colonoid upon 2 hours of infection. A cluster of enchained bacteria was found on the surface. **C)** Differentiated colonoid 2 hours after infection. Enchained bacteria were found in proximity to the organoids surface, most probably attached to dead cells as pinpointed by the absence of white actin signal around the blue nuclei. ZO-1 is depicted in green.

The presence of 08O09 counteracted *K. pneumoniae* overgrowth, as confirmed by the drop from $1.5 \bullet 10^6$ CFU/mL detected in the absence of mAb to 10^5 CFU/mL in the presence of the antibody. Furthermore, an interesting phenotype of enchained growth was observed

when 08O09 was added (**Figure 9A**). Enchained bacteria were found on the surface of undifferentiated organoids (**Figure 9B**) and in proximity to differentiated organoids on dead cells (**Figure 9C**), as confirmed by the absence of the actin fluorescent signal around some DAPI-stained eukaryotic nuclei.

Overall, reduced bacterial growth correlated with less pronounced levels of cell death on organoids, as healthy colonoids were detected after infection in the presence of the mAb, but almost none could be found in no mAb controls.

Discussion and Conclusions

The need of physiologically relevant models of infection to define new therapeutic options against antimicrobial resistant pathogens is undeniable. In this regard, 3D *ex vivo* cultures are a novel, powerful tool that can overcome not only some of the limitations of *in vitro* approaches but also, and most importantly, the inconsistencies between *in vitro* activity and *in vivo* responses to antimicrobial agents[219,220]. With this study, an improved model of pandrug-resistant *K. pneumoniae* gut infection has been developed with the use of apical-out, human-derived colon organoids. Such model has been interrogated to elucidate the first steps of *K. pneumoniae* pathogenesis, but also to further characterize the mechanisms of protection exerted by the most promising mAb isolated in the MAD-Lab.

During infection of colonoids, *K. pneumoniae* was found on their surface on junction sites, as well as in proximity to shedding cells. Tight junctions may serve as *K. pneumoniae* preferential sites of adhesion on the colonic niche, with mechanisms that could resemble those described for other pathogenic species, such as *Listeria monocytogenes*[221]. Furthermore, the high amount of *K. pneumoniae* found on extrusion zones and shedding cells may be attributed to favorable growth conditions in proximity to apoptotic cells. *K. pneumoniae* may scavenge energy sources and nutrients from the host cells that are undergoing anoikis[222], therefore promoting its own growth. In addition to this, *K. pneumoniae* may exert a cytotoxic effect on the host gut epithelia, leading to increased cell shedding on colonic crypts regardless of the state of cell differentiation. This evidence is sustained by the prevalence of the pathogen on apoptotic cells of both undifferentiated and differentiated colonoids.

Interestingly, a *K. pneumoniae* adhesion-independent mechanism of toxicity has been highlighted, suggesting that not only adherence, but also proximity may play a pivotal role during *K. pneumoniae* infection. This unknown virulence mechanism may enable bacteria to acquire nutrients by inducing apoptosis in host cells, thus facilitating *K. pneumoniae* pathogenicity and persistence in the gut. This may eventually culminate in bacterial proliferation, invasion, and dissemination in other tissues. Moreover, a mAb-dependent *K. pneumoniae* enchained growth phenotype has been observed. Such phenotype may be the result of a host defense mechanism to counteract bacterial overgrowth, as described for other bacterial species[171,172]. In addition to this, some mAbs may promote enchained bacterial growth to eliminate the pathogen more efficiently.

In conclusion, this study lays the foundation for more comprehensive analyses on the molecular mechanisms regulating *K. pneumoniae* host-pathogen interactions and driving invasion of the colonic niche. The use of organoids derived both from the colon and from different segments of the small intestine, as well as the creation of a library of intestinal organoids derived from different adult donors, should be considered as an efficient way to unravel molecular mechanisms of *K. pneumoniae* pathogenesis that are still unclear and to successfully advance in the development of innovative antimicrobial mAbs and novel vaccines.

Materials and Methods

***Klebsiella pneumoniae* strains and culture conditions:** The *K. pneumoniae* clinical isolate used in this study was provided by the University Hospital of Pisa (Tuscany, Italy). The strain originated from a patient affected by bloodstream infection and was identified by whole-genome sequencing as *K. pneumoniae* ST147, K-locus KL64, O-locus O2a. It expresses the NDM-1 plasmid, which confers resistance to beta lactam antibiotics. The strain has been classified as pandrug-resistant. *K. pneumoniae* has been engineered to express the super folder mCherry fluorescent protein, thereby obtaining *K. pneumoniae* sfmCherry, which was used for infecting organoids in this study. *K. pneumoniae* was grown at 37°C on LB Agar plates or in LB broth with the addition of 150 μg/mL hygromycin. Bacteria were grown at 37°C with shaking to OD_{600} 0.5. Cultures were centrifuged at 5000 xg for 10 minutes at room temperature. Upon centrifugation, the supernatant was discarded, and bacteria were resuspended in Hanks' Balanced Salt Solution (HBSS).

Colonic epithelial organoids cultivation and growth: Organoids were generated following the principles described by Toshiro Sato, Hans Clevers, and colleagues[212]. Gastrointestinal epithelial organoids derived from healthy adult patient colon biopsies were generated by the lab of Calvin Kuo at Stanford University and maintained as previously described[217,218]. For maintenance, organoids were seeded within Cultrex Reduced Growth Factor Basement Membrane Matrix, Type II (BME, equivalent to Matrigel) in droplets within a 24-well tissue culture treated plate (40 µL/well). BME was polymerized by incubation for 10 minutes at 37°C, then growth media was overlaid atop BME. Growth media consists of: Advanced Dulbecco's modified Eagle medium/F12, 1 mM HEPES, 1x Glutamax, 1x B27, 1 mM N-Acetyl-cysteine, 10 nM Gastrin, 50 ng/mL EGF, 10 mM Nicotinamide, 500 nM A83-01, 10 µM SB202190, and 50% L-WRN-conditioned media. L-WRN conditioned media was prepared from L-WRN cells as previously described[223]. Growth media was replaced every 1-4 days as needed. To passage, organoids were dissociated to single cells in TrypLE Express for 10-15 min at 37°C, manually disrupted by pipetting, then trypsin was inactivated with FBS. Cells were counted on a Countess II Cell Counter (ThermoFisher) and reseeded in BME at a concentration of 10^4 cells per well. For 2-3 days after initial passage, 10 µM Y27623 and 250 nM CHIR99021 were included in growth media to prevent detachment-mediated cell death. Organoids were passaged every 4-10 days as needed.

Colonoids differentiation: After 4 days of growth, growth media was replaced with differentiation media: Advanced Dulbecco's modified Eagle medium/F12, 1 mM HEPES, 1x Glutamax, 1x B27, 1 mM N-Acetyl-cysteine, 10 nM Gastrin, 50 ng/mL EGF, 10 ng/mL Noggin, 500 nM A83-01, 5 µM γ-Secretase Inhibitor IX (also known as DAPT), and 10 µM Y27623. Media was replaced every 1-3 days as needed.

Colonoids polarity reversal: After 7 days of growth, organoids were removed from BME and induced to revert their polarity in order to expose the apical surface. A previously published procedure[217,218] was followed. In brief, Organoids were incubated in 5 mM EDTA in Phosphate Buffered Saline (PBS) at 4°C for 60 minutes, washed with DMEM, and resuspended in growth or differentiation media depending on the colonoids differentiation state required. Organoids in suspension culture were plated in ultra-low attachment plates or flasks (Corning Costar) and incubated at 37°C for 24 hours to complete polarity reversal prior to experimental use.

Colonoids infection with *K. pneumoniae*: Undifferentiated and differentiated apical-out organoids were gently spun to remove culture media and were resuspended in HBSS. Organoids were counted and then infected with sfmCherry *K. pneumoniae* at a multiplicity of infection (MOI) of 1:1 bacterium per organoid. Infection of cells was allowed to proceed for 4 hours in HBSS at 37°C with 5% CO_2. The infection was interrupted at appropriate time points to evaluate infection rates through microscopy and colony forming units (CFUs).

Confocal microscopy: Organoids were fixed in 2% paraformaldehyde in 100 mM sodium phosphate buffer (pH 7.4) for at least 30 minutes and washed with PBS. Organoids were stained by incubation with antibodies and/or stains in blocking/permeabilization buffer (PBS with 3% bovine serum albumin, 1% saponin, and 0.02% sodium azide) overnight with gentle agitation. Stained organoids were washed 3x in PBS, mounted onto glass slides using Vectashield mounting medium (Vector Laboratories, H-1000), and glass coverslips were affixed using vacuum grease. Organoids were imaged on an LSM 700 confocal microscope (Carl Zeiss) with Zen 2009 software (Carl Zeiss) at 40x with oil immersion and 20x objectives. 3D renderings of organoids were generated using Volocity 3D Image Analysis Software (Perkin Elmer). Organoids were stained with DAPI (4',6-Diamidino-2-Phenylindole,

Dihydrochloride, Life Technologies, D1306) and AlexaFluor 660 phalloidin (Invitrogen, A22285) to visualize nuclei (in blue in following figures) and actin (in grey in following figures). Primary antibodies were diluted as follows: anti-Ki67 (1:100), anti-ZO-1 (1:100), anti-Muc2 (1:100), and anti-Villin (1:100). Secondary antibody (Invitrogen Cross-Absorbed) dilutions were performed at 1:500 dilution. For visualization of caspase 3/7 activity, CellEventTM Caspase 3/7 Green Detection Reagent (Invitrogen, C10723) was added to live organoids at 10 μM 30 minutes before fixation, then organoids were fixed and stained as described above.

Conclusions and future perspectives

For this PhD work, an antigen-unbiased mAb discovery workflow has been designed to efficiently identify extremely potent candidates against ST147$_{NDM-1}$ *Klebsiella pneumoniae*, a pandrug-resistant strain responsible for an ongoing outbreak in the hospitals of the Tuscany region in Italy. In addition to this, selected mAbs have been thoroughly characterized to assess their functional properties and binding efficiency. Moreover, through antigen discovery approaches, mAb targets have been identified, highlighting that anti-capsular, but not anti-LPS, candidates have poly-functional bactericidal features. Anti-capsular mAbs not only show extremely potent *in vitro* bactericidal activity, but also promote opsonophagocytosis and enchained bacterial growth. Interestingly, bacterial enchainment in the presence of top candidate mAb 08O09 has also been observed in the 3D *ex vivo K. pneumoniae* gut infection model that has been developed for this PhD work. Through the same model, an adhesion-independent mechanism of virulence has been described for the first time, suggesting that proximity may be sufficient to *K. pneumoniae* for exerting a cytotoxic effect on gut epithelia. Finally, the anti-capsular top candidate mAb 08O09 exhibited efficacy in protecting and treating a murine model of fulminant septicemia caused by ST147$_{NDM-1}$ *K. pneumoniae*. Considering that to date no vaccines or alternative immunotherapies have been licensed against *K. pneumoniae*, the results obtained in this study hold great value in the fight against this pathogen. Notably, mAb 08O09 is, to date, the only fully human drug that can clear an *in vivo* bloodstream infection caused by KL64-bearing, pandrug-resistant *K. pneumoniae* lineage. Future development of 08O09 includes the design of clinical trials that evaluate safety, pharmacokinetics and prophylactic or therapeutic efficacy of the mAb candidate in humans. In this framework, selection of the most appropriate cohort of patients among those with acute bloodstream infection, urinary tract infection or intestinal carriage will be crucial. Additional exploration of the *in vitro* bactericidal properties of 08O09 against other *K. pneumoniae* sequence types which share the same KL64 locus will shed light on the possibility to propose our candidate antibody for broader application.

In the future, the antigen-unbiased methodology described to select functional mAbs against *K. pneumoniae* could be employed to identify new effective therapeutics against other critical AMR species like those belonging to the Enterobacteriaceae family. Moreover, to boost infection clearance and opsonophagocytosis, combinations of anti-*K. pneumoniae* mAbs and antibiotics should be considered. In alternative, antibody-antibiotic conjugates

that combine the specificity of mAbs with the efficacy of some antibiotics could be investigated as successful therapies against AMR pathogens and limit the toxic effects of antibiotics on the host and its microbiota. In this regard, the potential of *ex vivo* human-derived organotypic cultures should be employed to identify host and bacterial factors that are essential for infection. Importantly, mAbs can be exploited as baits for fishing their cognate antigens and therefore support rational vaccine design within the Reverse Vaccinology 2.0 approach. In this way, basic research on host-pathogen interactions could be translationally applied to the vaccinology field, with the purpose of designing efficacious vaccines to address the global burden of AMR infectious diseases.

Bibliography

1. Walsh, T. R., Gales, A. C., Laxminarayan, R. & Dodd, P. C. Antimicrobial Resistance: Addressing a Global Threat to Humanity. *PLoS Med* **20**, e1004264 (2023).
2. Global action plan on antimicrobial resistance. https://www.who.int/publications-detail-redirect/9789241509763.
3. Murray, C. J. L. *et al.* Global burden of bacterial antimicrobial resistance in 2019: a systematic analysis. *The Lancet* **399**, 629–655 (2022).
4. No time to Wait: Securing the future from drug-resistant infections. https://www.who.int/publications-detail-redirect/no-time-to-wait-securing-the-future-from-drug-resistant-infections.
5. WHO publishes list of bacteria for which new antibiotics are urgently needed. https://www.who.int/news/item/27-02-2017-who-publishes-list-of-bacteria-for-which-new-antibiotics-are-urgently-needed.
6. Rice, L. B. Federal Funding for the Study of Antimicrobial Resistance in Nosocomial Pathogens: No ESKAPE. *The Journal of Infectious Diseases* **197**, 1079–1081 (2008).
7. De Oliveira, D. M. P. *et al.* Antimicrobial Resistance in ESKAPE Pathogens. *Clin Microbiol Rev* **33**, e00181-19 (2020).
8. Arcari, G. & Carattoli, A. Global spread and evolutionary convergence of multidrug-resistant and hypervirulent Klebsiella pneumoniae high-risk clones. *Pathog Glob Health* **117**, 328–341.
9. Friedlaender, C. Ueber die Schizomyceten bei der acuten fibrösen Pneumonie. *Archiv f. pathol. Anat.* **87**, 319–324 (1882).
10. Wang, G., Zhao, G., Chao, X., Xie, L. & Wang, H. The Characteristic of Virulence, Biofilm and Antibiotic Resistance of Klebsiella pneumoniae. *Int J Environ Res Public Health* **17**, 6278 (2020).
11. Cruz-Córdova, A. *et al.* Pathogenic determinants of clinical Klebsiella pneumoniae strains associated with their persistence in the hospital environment. *Bol. Med. Hosp. Infant. Mex. (English version)* **71**, 15–24 (2014).
12. Podschun, R. & Ullmann, U. Klebsiella spp. as Nosocomial Pathogens: Epidemiology, Taxonomy, Typing Methods, and Pathogenicity Factors. *Clin Microbiol Rev* **11**, 589–603 (1998).
13. Martin, R. M. & Bachman, M. A. Colonization, Infection, and the Accessory Genome of Klebsiella pneumoniae. *Front Cell Infect Microbiol* **8**, 4 (2018).

14. Holt, K. E. *et al.* Genomic analysis of diversity, population structure, virulence, and antimicrobial resistance in Klebsiella pneumoniae, an urgent threat to public health. *Proc Natl Acad Sci U S A* **112**, E3574-3581 (2015).

15. Choby, J. E., Howard-Anderson, J. & Weiss, D. S. Hypervirulent Klebsiella pneumoniae - clinical and molecular perspectives. *J Intern Med* **287**, 283–300 (2020).

16. Davies, J. & Davies, D. Origins and Evolution of Antibiotic Resistance. *Microbiol Mol Biol Rev* **74**, 417–433 (2010).

17. Paczosa, M. K. & Mecsas, J. Klebsiella pneumoniae: Going on the Offense with a Strong Defense. *Microbiol Mol Biol Rev* **80**, 629–661 (2016).

18. Ramos, P. I. P. *et al.* Pyrosequencing-based analysis reveals a novel capsular gene cluster in a KPC-producing Klebsiella pneumoniae clinical isolate identified in Brazil. *BMC Microbiology* **12**, 173 (2012).

19. Choi, M. *et al.* The Diversity of Lipopolysaccharide (O) and Capsular Polysaccharide (K) Antigens of Invasive Klebsiella pneumoniae in a Multi-Country Collection. *Frontiers in Microbiology* **11**, (2020).

20. Shankar-Sinha, S. *et al.* The Klebsiella pneumoniae O Antigen Contributes to Bacteremia and Lethality during Murine Pneumonia. *Infect Immun* **72**, 1423–1430 (2004).

21. Murphy, C. N., Mortensen, M. S., Krogfelt, K. A. & Clegg, S. Role of Klebsiella pneumoniae Type 1 and Type 3 Fimbriae in Colonizing Silicone Tubes Implanted into the Bladders of Mice as a Model of Catheter-Associated Urinary Tract Infections. *Infect Immun* **81**, 3009–3017 (2013).

22. Arato, V., Raso, M. M., Gasperini, G., Berlanda Scorza, F. & Micoli, F. Prophylaxis and Treatment against Klebsiella pneumoniae: Current Insights on This Emerging Anti-Microbial Resistant Global Threat. *Int J Mol Sci* **22**, 4042 (2021).

23. Holden, V. I., Breen, P., Houle, S., Dozois, C. M. & Bachman, M. A. Klebsiella pneumoniae Siderophores Induce Inflammation, Bacterial Dissemination, and HIF-1α Stabilization during Pneumonia. *mBio* **7**, e01397-16 (2016).

24. Han, R. *et al.* The effect of siderophore virulence genes entB and ybtS on the virulence of Carbapenem-resistant Klebsiella pneumoniae. *Microbial Pathogenesis* **171**, 105746 (2022).

25. Bengoechea, J. A. & Pessoa, J. S. Klebsiella pneumoniae infection biology: living to counteract host defences. *FEMS Microbiology Reviews* **43**, 123 (2019).

26. Fleeman, R. M., Macias, L. A., Brodbelt, J. S. & Davies, B. W. Defining principles that

influence antimicrobial peptide activity against capsulated Klebsiella pneumoniae. *Proc Natl Acad Sci U S A* **117**, 27620–27626 (2020).

27. Patro, L. P. P., Sudhakar, K. U. & Rathinavelan, T. K-PAM: a unified platform to distinguish Klebsiella species K- and O-antigen types, model antigen structures and identify hypervirulent strains. *Sci Rep* **10**, 16732 (2020).

28. Pan, Y.-J. *et al.* Genetic analysis of capsular polysaccharide synthesis gene clusters in 79 capsular types of Klebsiella spp. *Sci Rep* **5**, 15573 (2015).

29. Whitfield, C. Biosynthesis and assembly of capsular polysaccharides in Escherichia coli. *Annu Rev Biochem* **75**, 39–68 (2006).

30. Wyres, K. L. *et al.* Identification of Klebsiella capsule synthesis loci from whole genome data. *Microb Genom* **2**, e000102 (2016).

31. Patro, L. P. P. & Rathinavelan, T. Targeting the Sugary Armor of Klebsiella Species. *Front Cell Infect Microbiol* **9**, 367 (2019).

32. Follador, R. *et al.* The diversity of Klebsiella pneumoniae surface polysaccharides. *Microb Genom* **2**, e000073 (2016).

33. Fung, C.-P. *et al.* A global emerging disease of Klebsiella pneumoniae liver abscess: is serotype K1 an important factor for complicated endophthalmitis? *Gut* **50**, 420–424 (2002).

34. Struve, C. *et al.* Mapping the Evolution of Hypervirulent Klebsiella pneumoniae. *mBio* **6**, e00630-15 (2015).

35. Marr, C. M. & Russo, T. A. Hypervirulent Klebsiella pneumoniae: a new public health threat. *Expert Rev Anti Infect Ther* **17**, 71–73 (2019).

36. Roger, T. *et al.* Protection from lethal Gram-negative bacterial sepsis by targeting Toll-like receptor 4. *Proc Natl Acad Sci U S A* **106**, 2348–2352 (2009).

37. Trautmann, M. *et al.* O-antigen seroepidemiology of Klebsiella clinical isolates and implications for immunoprophylaxis of Klebsiella infections. *Clin Diagn Lab Immunol* **4**, 550–555 (1997).

38. Hansen, D. S. *et al.* Klebsiella pneumoniae lipopolysaccharide O typing: revision of prototype strains and O-group distribution among clinical isolates from different sources and countries. *J Clin Microbiol* **37**, 56–62 (1999).

39. Kelly, R. F., Perry, M. B., MacLean, L. L. & Whitfield, C. Structures of the O-antigens of Klebsiella serotypes 02 (2a,2e), 02 (2a,2e,2h), and 02 (2a,2f,2g), members of a family of related D-galactan O-antigens in Klebsiella spp. *Journal of Endotoxin Research* **2**, 131–140

(1995).

40. Kelly, R. F. *et al.* Structural variation in the O-specific polysaccharides of *Klebsiella pneumoniae* serotype O1 and O8 lipopolysaccharide: evidence for clonal diversity in *rfb* genes. *Molecular Microbiology* **10**, 615–625 (1993).

41. Hsieh, P.-F. *et al.* D-galactan II is an immunodominant antigen in O1 lipopolysaccharide and affects virulence in Klebsiella pneumoniae: implication in vaccine design. *Front Microbiol* **5**, 608 (2014).

42. Prehm, P., Jann, B. & Jann, K. The O9 antigen of Escherichia coli. Structure of the polysaccharide chain. *Eur J Biochem* **67**, 53–56 (1976).

43. Jansson, P. E. *et al.* Structural studies of the O-antigen polysaccharides of Klebsiella O5 and Escherichia coli O8. *Carbohydr Res* **145**, 59–66 (1985).

44. Vinogradov, E. *et al.* Structures of lipopolysaccharides from Klebsiella pneumoniae. Eluicidation of the structure of the linkage region between core and polysaccharide O chain and identification of the residues at the non-reducing termini of the O chains. *J Biol Chem* **277**, 25070–25081 (2002).

45. Ofek, I. & Doyle, R. J. *Bacterial Adhesion to Cells and Tissues*. (Springer US, Boston, MA, 1994). doi:10.1007/978-1-4684-6435-1.

46. Struve, C., Bojer, M. & Krogfelt, K. A. Identification of a conserved chromosomal region encoding Klebsiella pneumoniae type 1 and type 3 fimbriae and assessment of the role of fimbriae in pathogenicity. *Infect Immun* **77**, 5016–5024 (2009).

47. Rosen, D. A. *et al.* Molecular variations in Klebsiella pneumoniae and Escherichia coli FimH affect function and pathogenesis in the urinary tract. *Infect Immun* **76**, 3346–3356 (2008).

48. Schroll, C., Barken, K. B., Krogfelt, K. A. & Struve, C. Role of type 1 and type 3 fimbriae in Klebsiella pneumoniae biofilm formation. *BMC Microbiol* **10**, 179 (2010).

49. Struve, C., Bojer, M. & Krogfelt, K. A. Characterization of Klebsiella pneumoniae Type 1 Fimbriae by Detection of Phase Variation during Colonization and Infection and Impact on Virulence. *Infect Immun* **76**, 4055–4065 (2008).

50. Di Martino, P., Cafferini, N., Joly, B. & Darfeuille-Michaud, A. Klebsiella pneumoniae type 3 pili facilitate adherence and biofilm formation on abiotic surfaces. *Res Microbiol* **154**, 9–16 (2003).

51. *Virulence Mechanisms of Bacterial Pathogens*. (ASM Press, Washington, DC, 2016).

52. Smith, K. D. Iron metabolism at the host pathogen interface: lipocalin 2 and the

pathogen-associated iroA gene cluster. *Int J Biochem Cell Biol* **39**, 1776–1780 (2007).

53. Holden, V. I. & Bachman, M. A. Diverging roles of bacterial siderophores during infection. *Metallomics* **7**, 986–995 (2015).

54. Bachman, M. A. *et al.* Klebsiella pneumoniae yersiniabactin promotes respiratory tract infection through evasion of lipocalin 2. *Infect Immun* **79**, 3309–3316 (2011).

55. Knothe, H., Shah, P., Krcmery, V., Antal, M. & Mitsuhashi, S. Transferable resistance to cefotaxime, cefoxitin, cefamandole and cefuroxime in clinical isolates of Klebsiella pneumoniae and Serratia marcescens. *Infection* **11**, 315–317 (1983).

56. Quinn, J. P., Miyashiro, D., Sahm, D., Flamm, R. & Bush, K. Novel plasmid-mediated beta-lactamase (TEM-10) conferring selective resistance to ceftazidime and aztreonam in clinical isolates of Klebsiella pneumoniae. *Antimicrob Agents Chemother* **33**, 1451–1456 (1989).

57. Paterson, D. L. Recommendation for treatment of severe infections caused by Enterobacteriaceae producing extended-spectrum beta-lactamases (ESBLs). *Clin Microbiol Infect* **6**, 460–463 (2000).

58. Yigit, H. *et al.* Novel Carbapenem-Hydrolyzing β-Lactamase, KPC-1, from a Carbapenem-Resistant Strain of Klebsiella pneumoniae. *Antimicrob Agents Chemother* **45**, 1151–1161 (2001).

59. Bush, K. & Fisher, J. F. Epidemiological Expansion, Structural Studies, and Clinical Challenges of New β-Lactamases from Gram-Negative Bacteria. *Annual Review of Microbiology* **65**, 455–478 (2011).

60. Logan, L. K. & Weinstein, R. A. The Epidemiology of Carbapenem-Resistant Enterobacteriaceae: The Impact and Evolution of a Global Menace. *J Infect Dis* **215**, S28–S36 (2017).

61. Chang, D., Sharma, L., Dela Cruz, C. S. & Zhang, D. Clinical Epidemiology, Risk Factors, and Control Strategies of Klebsiella pneumoniae Infection. *Frontiers in Microbiology* **12**, (2021).

62. Pitout, J. D. D., Peirano, G., Kock, M. M., Strydom, K.-A. & Matsumura, Y. The Global Ascendency of OXA-48-Type Carbapenemases. *Clin Microbiol Rev* **33**, e00102-19 (2019).

63. Cuzon, G., Ouanich, J., Gondret, R., Naas, T. & Nordmann, P. Outbreak of OXA-48-Positive Carbapenem-Resistant Klebsiella pneumoniae Isolates in France. *Antimicrob Agents Chemother* **55**, 2420–2423 (2011).

64. Suay-García & Pérez-Gracia. Present and Future of Carbapenem-resistant

Enterobacteriaceae (CRE) Infections. *Antibiotics* **8**, 122 (2019).

65. Poirel, L., Hombrouck-Alet, C., Freneaux, C., Bernabeu, S. & Nordmann, P. Global spread of New Delhi metallo-β-lactamase 1. *The Lancet Infectious Diseases* **10**, 832 (2010).

66. Moellering, R. C. NDM-1 — A Cause for Worldwide Concern. *N Engl J Med* **363**, 2377–2379 (2010).

67. Spapen, H., Jacobs, R., Van Gorp, V., Troubleyn, J. & Honoré, P. M. Renal and neurological side effects of colistin in critically ill patients. *Annals of Intensive Care* **1**, 14 (2011).

68. Tigecycline. in *LiverTox: Clinical and Research Information on Drug-Induced Liver Injury* (National Institute of Diabetes and Digestive and Kidney Diseases, Bethesda (MD), 2012).

69. Wei, W.-J., Yang, H.-F., Ye, Y. & Li, J.-B. New Delhi Metallo-β-Lactamase-Mediated Carbapenem Resistance: Origin, Diagnosis, Treatment and Public Health Concern. *Chin Med J (Engl)* **128**, 1969–1976 (2015).

70. Dong, N., Yang, X., Chan, E. W.-C., Zhang, R. & Chen, S. Klebsiella species: Taxonomy, hypervirulence and multidrug resistance. *EBioMedicine* **79**, 103998 (2022).

71. Gonzalez-Ferrer, S. *et al.* Finding Order in the Chaos: Outstanding Questions in Klebsiella pneumoniae Pathogenesis. *Infect Immun* **89**, e00693-20 (2021).

72. Peirano, G., Chen, L., Kreiswirth, B. N. & Pitout, J. D. D. Emerging Antimicrobial-Resistant High-Risk Klebsiella pneumoniae Clones ST307 and ST147. *Antimicrob Agents Chemother* **64**, e01148-20 (2020).

73. Martin, M. J. *et al.* Anatomy of an extensively drug-resistant Klebsiella pneumoniae outbreak in Tuscany, Italy. *Proc Natl Acad Sci U S A* **118**, e2110227118 (2021).

74. Hirai, J., Sakanashi, D., Kinjo, T., Haranaga, S. & Fujita, J. The First Case of Community-Acquired Pneumonia Due to Capsular Genotype K2-ST86 Hypervirulent Klebsiella pneumoniae in Okinawa, Japan: A Case Report and Literature Review. *Infect Drug Resist* **13**, 2237–2243 (2020).

75. Russo, T. A. & Marr, C. M. Hypervirulent Klebsiella pneumoniae. *Clin Microbiol Rev* **32**, e00001-19 (2019).

76. Walker, K. A. *et al.* A Klebsiella pneumoniae Regulatory Mutant Has Reduced Capsule Expression but Retains Hypermucoviscosity. *mBio* **10**, e00089-19 (2019).

77. Lan, P., Jiang, Y., Zhou, J. & Yu, Y. A global perspective on the convergence of hypervirulence and carbapenem resistance in Klebsiella pneumoniae. *Journal of Global*

Antimicrobial Resistance **25**, 26–34 (2021).

78. Tang, M., Kong, X., Hao, J. & Liu, J. Epidemiological Characteristics and Formation Mechanisms of Multidrug-Resistant Hypervirulent Klebsiella pneumoniae. *Front Microbiol* **11**, 581543 (2020).

79. Wyres, K. L. *et al.* Distinct evolutionary dynamics of horizontal gene transfer in drug resistant and virulent clones of Klebsiella pneumoniae. *PLoS Genet* **15**, e1008114 (2019).

80. Pilato, V. D. *et al.* Resistome and virulome accretion in an NDM-1-producing ST147 sublineage of Klebsiella pneumoniae associated with an outbreak in Tuscany, Italy: a genotypic and phenotypic characterisation. *The Lancet Microbe* **3**, e224–e234 (2022).

81. Rapid risk assessment: Regional outbreak of New Delhi metallo-betalactamase-producing carbapenem-resistant Enterobacteriaceae, Italy, 2018–2019. https://www.ecdc.europa.eu/en/publications-data/RRA-new-delhi-metallo-beta-lactamase-producing-CRE (2019).

82. Starkova, P. *et al.* Emergence of Hybrid Resistance and Virulence Plasmids Harboring New Delhi Metallo-β-Lactamase in Klebsiella pneumoniae in Russia. *Antibiotics (Basel)* **10**, 691 (2021).

83. Turton, J. *et al.* Hybrid Resistance and Virulence Plasmids in “High-Risk” Clones of Klebsiella pneumoniae, Including Those Carrying blaNDM-5. *Microorganisms* **7**, 326 (2019).

84. Ahmed, M. A. E.-G. E.-S. *et al.* Emergence of Hypervirulent Carbapenem-Resistant Klebsiella pneumoniae Coharboring a *bla* $_{\text{NDM-1}}$ -Carrying Virulent Plasmid and a *bla* $_{\text{KPC-2}}$ -Carrying Plasmid in an Egyptian Hospital. *mSphere* **6**, e00088-21 (2021).

85. Heiden, S. E. *et al.* A Klebsiella pneumoniae ST307 outbreak clone from Germany demonstrates features of extensive drug resistance, hypermucoviscosity, and enhanced iron acquisition. *Genome Med* **12**, 113 (2020).

86. Martin, M. J. *et al.* Anatomy of an extensively drug-resistant Klebsiella pneumoniae outbreak in Tuscany, Italy. *Proc Natl Acad Sci U S A* **118**, e2110227118 (2021).

87. Martin, M. J. *et al.* A panel of diverse Klebsiella pneumoniae clinical isolates for research and development. *Microb Genom* **9**, mgen000967 (2023).

88. Rodrigues, C., Desai, S., Passet, V., Gajjar, D. & Brisse, S. Genomic evolution of the globally disseminated multidrug-resistant Klebsiella pneumoniae clonal group 147. *Microbial Genomics* **8**, 000737 (2022).

89. Christensen, K., Doblhammer, G., Rau, R. & Vaupel, J. W. Ageing populations: the challenges ahead. *Lancet* **374**, 1196–1208 (2009).

90. Rosini, R., Nicchi, S., Pizza, M. & Rappuoli, R. Vaccines Against Antimicrobial Resistance. *Front. Immunol.* **11**, 1048 (2020).

91. Rappuoli, R., Pizza, M., Del Giudice, G. & De Gregorio, E. Vaccines, new opportunities for a new society. *Proc. Natl. Acad. Sci. U.S.A.* **111**, 12288–12293 (2014).

92. Delany, I., Rappuoli, R. & De Gregorio, E. Vaccines for the 21st century. *EMBO Mol Med* **6**, 708–720 (2014).

93. The discovery of antibiotics – Part 1. *ReAct* https://www.reactgroup.org/antibiotic-resistance/course-antibiotic-resistance-the-silent-tsunami/part-1/the-discovery-of-antibiotics/.

94. Dubourg, G. *et al.* Culturomics and pyrosequencing evidence of the reduction in gut microbiota diversity in patients with broad-spectrum antibiotics. *Int J Antimicrob Agents* **44**, 117–124 (2014).

95. Blaser, M. Antibiotic overuse: Stop the killing of beneficial bacteria. *Nature* **476**, 393–394 (2011).

96. Patangia, D. V., Anthony Ryan, C., Dempsey, E., Paul Ross, R. & Stanton, C. Impact of antibiotics on the human microbiome and consequences for host health. *Microbiologyopen* **11**, e1260 (2022).

97. History of antibiotic development – Antibiotics. *ReAct* https://www.reactgroup.org/toolbox/understand/antibiotics/development-of-antibiotics-as-medicines/.

98. Poudel, A. N. *et al.* The economic burden of antibiotic resistance: A systematic review and meta-analysis. *PLOS ONE* **18**, e0285170 (2023).

99. Ryman, J. T. & Meibohm, B. Pharmacokinetics of Monoclonal Antibodies. *CPT Pharmacometrics Syst Pharmacol* **6**, 576–588 (2017).

100. Chiu, M. L., Goulet, D. R., Teplyakov, A. & Gilliland, G. L. Antibody Structure and Function: The Basis for Engineering Therapeutics. *Antibodies (Basel)* **8**, 55 (2019).

101. Vidarsson, G., Dekkers, G. & Rispens, T. IgG Subclasses and Allotypes: From Structure to Effector Functions. *Front Immunol* **5**, 520 (2014).

102. Brekke, O. H. & Sandlie, I. Therapeutic antibodies for human diseases at the dawn of the twenty-first century. *Nat Rev Drug Discov* **2**, 52–62 (2003).

103. Breedveld, F. C. Therapeutic monoclonal antibodies. *The Lancet* **355**, 735–740 (2000).

104. Castelli, M. S., McGonigle, P. & Hornby, P. J. The pharmacology and therapeutic

applications of monoclonal antibodies. *Pharmacol Res Perspect* **7**, e00535 (2019).

105. Geng, X. *et al.* Research and development of therapeutic mAbs: An analysis based on pipeline projects. *Hum Vaccin Immunother* **11**, 2769–2776 (2015).

106. Chow, S.-K. & Casadevall, A. Monoclonal antibodies and toxins--a perspective on function and isotype. *Toxins (Basel)* **4**, 430–454 (2012).

107. Pizarro-Cerdá, J. & Cossart, P. Bacterial adhesion and entry into host cells. *Cell* **124**, 715–727 (2006).

108. Yougbare, I. *et al.* Anti-FIM and Anti-FHA Antibodies Inhibit Bordetella pertussis Growth and Reduce Epithelial Cell Inflammation Through Bacterial Aggregation. *Front Immunol* **11**, 605273 (2020).

109. Leininger, E., Probst, P. G., Brennan, M. J. & Kenimer, J. G. Inhibition of Bordetella pertussis filamentous hemagglutinin-mediated cell adherence with monoclonal antibodies. *FEMS Microbiol Lett* **106**, 31–38 (1993).

110. Gogesch, P., Dudek, S., van Zandbergen, G., Waibler, Z. & Anzaghe, M. The Role of Fc Receptors on the Effectiveness of Therapeutic Monoclonal Antibodies. *International Journal of Molecular Sciences* **22**, 8947 (2021).

111. Strohl, W. R. Optimization of Fc-mediated effector functions of monoclonal antibodies. *Curr Opin Biotechnol* **20**, 685–691 (2009).

112. Vacca, F., Sala, C. & Rappuoli, R. Monoclonal Antibodies for Bacterial Pathogens: Mechanisms of Action and Engineering Approaches for Enhanced Effector Functions. *Biomedicines* **10**, 2126 (2022).

113. Diago-Navarro, E. *et al.* Antibody-Based Immunotherapy To Treat and Prevent Infection with Hypervirulent Klebsiella pneumoniae. *Clin Vaccine Immunol* **24**, e00456-16 (2017).

114. Nonaka, M. & Kimura, A. Genomic view of the evolution of the complement system. *Immunogenetics* **58**, 701–713 (2006).

115. Sarma, J. V. & Ward, P. A. The complement system. *Cell Tissue Res* **343**, 227–235 (2011).

116. Bordron, A. *et al.* Complement System: a Neglected Pathway in Immunotherapy. *Clin Rev Allergy Immunol* **58**, 155–171 (2020).

117. Diebolder, C. A. *et al.* Complement Is Activated by IgG Hexamers Assembled at the Cell Surface. *Science* **343**, 1260–1263 (2014).

118. Wu, Y. *et al.* A potent broad-spectrum protective human monoclonal antibody

crosslinking two haemagglutinin monomers of influenza A virus. *Nat Commun* **6**, 7708 (2015).

119. Alter, G. *et al.* High-resolution definition of humoral immune response correlates of effective immunity against HIV. *Mol Syst Biol* **14**, e7881 (2018).

120. Rossi, O. *et al.* The essential role of complement in antibody-mediated resistance to Salmonella. *Immunology* **156**, 69–73 (2019).

121. Gulati, S. *et al.* Complement alone drives efficacy of a chimeric antigonococcal monoclonal antibody. *PLoS Biology* **17**, (2019).

122. de Jong, R. N. *et al.* A Novel Platform for the Potentiation of Therapeutic Antibodies Based on Antigen-Dependent Formation of IgG Hexamers at the Cell Surface. *PLoS Biol* **14**, e1002344 (2016).

123. Chakraborti, S. *et al.* Bypassing Phase Variation of Lipooligosaccharide (LOS): Using Heptose 1 Glycan Mutants To Establish Widespread Efficacy of Gonococcal Anti-LOS Monoclonal Antibody 2C7. *Infect Immun* **88**, e00862-19 (2020).

124. Köhler, G. & Milstein, C. Derivation of specific antibody-producing tissue culture and tumor lines by cell fusion. *Eur J Immunol* **6**, 511–519 (1976).

125. Khazaeli, M. B., Conry, R. M. & LoBuglio, A. F. Human Immune Response to Monoclonal Antibodies. *Journal of Immunotherapy* **15**, 42 (1994).

126. Morrison, S. L., Johnson, M. J., Herzenberg, L. A. & Oi, V. T. Chimeric human antibody molecules: mouse antigen-binding domains with human constant region domains. *Proc Natl Acad Sci U S A* **81**, 6851–6855 (1984).

127. Boulianne, G. L., Hozumi, N. & Shulman, M. J. Production of functional chimaeric mouse/human antibody. *Nature* **312**, 643–646 (1984).

128. Yamashita, M., Katakura, Y. & Shirahata, S. Recent advances in the generation of human monoclonal antibody. *Cytotechnology* **55**, 55–60 (2007).

129. Smith, G. P. Filamentous Fusion Phage: Novel Expression Vectors That Display Cloned Antigens on the Virion Surface. *Science* **228**, 1315–1317 (1985).

130. McCafferty, J., Griffiths, A. D., Winter, G. & Chiswell, D. J. Phage antibodies: filamentous phage displaying antibody variable domains. *Nature* **348**, 552–554 (1990).

131. Rappuoli, R., Bottomley, M. J., D'Oro, U., Finco, O. & De Gregorio, E. Reverse vaccinology 2.0: Human immunology instructs vaccine antigen design. *Journal of Experimental Medicine* **213**, 469–481 (2016).

132. Corti, D. *et al.* Heterosubtypic neutralizing antibodies are produced by individuals

immunized with a seasonal influenza vaccine. *J. Clin. Invest.* **120**, 1663–1673 (2010).

133. Andreano, E. *et al.* Extremely potent human monoclonal antibodies from COVID-19 convalescent patients. *Cell* **184**, 1821-1835.e16 (2021).

134. Troisi, M. *et al.* A new dawn for monoclonal antibodies against antimicrobial resistant bacteria. *Front. Microbiol.* **13**, 1080059 (2022).

135. Zurawski, D. V. & McLendon, M. K. Monoclonal Antibodies as an Antibacterial Approach Against Bacterial Pathogens. *Antibiotics (Basel)* **9**, 155 (2020).

136. Mazumdar, S. Raxibacumab. *MAbs* **1**, 531–538 (2009).

137. Tsai, C.-W. & Morris, S. Approval of Raxibacumab for the Treatment of Inhalation Anthrax Under the US Food and Drug Administration 'Animal Rule'. *Front Microbiol* **6**, 1320 (2015).

138. Yamamoto, B. J. *et al.* Obiltoxaximab Prevents Disseminated Bacillus anthracis Infection and Improves Survival during Pre- and Postexposure Prophylaxis in Animal Models of Inhalational Anthrax. *Antimicrob Agents Chemother* **60**, 5796–5805 (2016).

139. Greig, S. L. Obiltoxaximab: First Global Approval. *Drugs* **76**, 823–830 (2016).

140. Markham, A. Bezlotoxumab: First Global Approval. *Drugs* **76**, 1793–1798 (2016).

141. Speziale, P. & Pietrocola, G. Monoclonal Antibodies Targeting Surface-Exposed and Secreted Proteins from Staphylococci. *Vaccines (Basel)* **9**, 459 (2021).

142. Motley, M. P., Banerjee, K. & Fries, B. C. Monoclonal Antibody-Based Therapies for Bacterial Infections. *Curr Opin Infect Dis* **32**, 210–216 (2019).

143. 10 global health issues to track in 2021. https://www.who.int/news-room/spotlight/10-global-health-issues-to-track-in-2021.

144. Papp-Wallace, K. M. The latest advances in β-lactam/β-lactamase inhibitor combinations for the treatment of Gram-negative bacterial infections. *Expert Opinion on Pharmacotherapy* **20**, 2169–2184 (2019).

145. Baker, S., Thomson, N., Weill, F.-X. & Holt, K. E. Genomic insights into the emergence and spread of antimicrobial-resistant bacterial pathogens. *Science* **360**, 733–738 (2018).

146. Shon, A. S., Bajwa, R. P. S. & Russo, T. A. Hypervirulent (hypermucoviscous) Klebsiella pneumoniae: a new and dangerous breed. *Virulence* **4**, 107–118 (2013).

147. Pathogenwatch | Genomes. https://pathogen.watch/genomes/all?genusId=570&mlst=147&speciesId=573.

148. Banerjee, K. *et al.* Patient-Derived Antibody Data Yields Development of Broadly

Cross-Protective Monoclonal Antibody against ST258 Carbapenem-Resistant Klebsiella pneumoniae. *Microbiol Spectr* **10**, e0176022 (2022).

149. Diago-Navarro, E. *et al.* Novel, Broadly Reactive Anticapsular Antibodies against Carbapenem-Resistant Klebsiella pneumoniae Protect from Infection. *mBio* **9**, e00091-18 (2018).

150. Cohen, T. S. *et al.* Anti-LPS antibodies protect against Klebsiella pneumoniae by empowering neutrophil-mediated clearance without neutralizing TLR4. *JCI Insight* **2**, e92774, 92774 (2017).

151. Rollenske, T. *et al.* Cross-specificity of protective human antibodies against Klebsiella pneumoniae LPS O-antigen. *Nat Immunol* **19**, 617–624 (2018).

152. Held, T. K., Jendrike, N. R., Rukavina, T., Podschun, R. & Trautmann, M. Binding to and opsonophagocytic activity of O-antigen-specific monoclonal antibodies against encapsulated and nonencapsulated Klebsiella pneumoniae serotype O1 strains. *Infect Immun* **68**, 2402–2409 (2000).

153. Wang, Q. *et al.* Target-Agnostic Identification of Functional Monoclonal Antibodies Against Klebsiella pneumoniae Multimeric MrkA Fimbrial Subunit. *J Infect Dis* **213**, 1800–1808 (2016).

154. Wang, Q. *et al.* Anti-MrkA Monoclonal Antibodies Reveal Distinct Structural and Antigenic Features of MrkA. *PLoS One* **12**, e0170529 (2017).

155. Falcone, M. *et al.* Extremely drug-resistant NDM-9-producing ST147 Klebsiella pneumoniae causing infections in Italy, May 2020. *Eurosurveillance* **25**, (2020).

156. Merrifield, E. H. & Stephen, A. M. Structural studies on the capsular polysaccharide from Klebsiella serotype K64. *Carbohydr Res* **74**, 241–257 (1979).

157. Kos, V. & Whitfield, C. A Membrane-located Glycosyltransferase Complex Required for Biosynthesis of the d-Galactan I Lipopolysaccharide O Antigen in Klebsiella pneumoniae. *J Biol Chem* **285**, 19668–19687 (2010).

158. Clarke, B. R. *et al.* Molecular basis for the structural diversity in serogroup O2-antigen polysaccharides in Klebsiella pneumoniae. *J Biol Chem* **293**, 4666–4679 (2018).

159. Apicella, M. A. *et al.* Identification, Characterization and Immunogenicity of an O-Antigen Capsular Polysaccharide of Francisella tularensis. *PLoS One* **5**, e11060 (2010).

160. Overdijk, M. B. *et al.* Dual Epitope Targeting and Enhanced Hexamerization by DR5 Antibodies as a Novel Approach to Induce Potent Antitumor Activity Through DR5 Agonism. *Mol Cancer Ther* **19**, 2126–2138 (2020).

161. Broug-Holub, E. *et al.* Alveolar macrophages are required for protective pulmonary defenses in murine Klebsiella pneumonia: elimination of alveolar macrophages increases neutrophil recruitment but decreases bacterial clearance and survival. *Infect Immun* **65**, 1139–1146 (1997).

162. Cheung, D. O., Halsey, K. & Speert, D. P. Role of pulmonary alveolar macrophages in defense of the lung against Pseudomonas aeruginosa. *Infect Immun* **68**, 4585–4592 (2000).

163. Alvarez, D., Merino, S., Tomás, J. M., Benedí, V. J. & Albertí, S. Capsular polysaccharide is a major complement resistance factor in lipopolysaccharide O side chain-deficient Klebsiella pneumoniae clinical isolates. *Infect Immun* **68**, 953–955 (2000).

164. Cortés, G. *et al.* Molecular analysis of the contribution of the capsular polysaccharide and the lipopolysaccharide O side chain to the virulence of Klebsiella pneumoniae in a murine model of pneumonia. *Infect Immun* **70**, 2583–2590 (2002).

165. Regueiro, V., Campos, M. A., Pons, J., Albertí, S. & Bengoechea, J. A. The uptake of a Klebsiella pneumoniae capsule polysaccharide mutant triggers an inflammatory response by human airway epithelial cells. *Microbiology (Reading)* **152**, 555–566 (2006).

166. March, C. *et al.* Role of bacterial surface structures on the interaction of Klebsiella pneumoniae with phagocytes. *PLoS One* **8**, e56847 (2013).

167. Abdelraouf, K., Kim, A., Krause, K. M. & Nicolau, D. P. In Vivo Efficacy of Plazomicin Alone or in Combination with Meropenem or Tigecycline against Enterobacteriaceae Isolates Exhibiting Various Resistance Mechanisms in an Immunocompetent Murine Septicemia Model. *Antimicrob Agents Chemother* **62**, e01074-18 (2018).

168. Tavoschi, L. *et al.* Prolonged outbreak of New Delhi metallo-beta-lactamase-producing carbapenem-resistant Enterobacterales (NDM-CRE), Tuscany, Italy, 2018 to 2019. *Euro Surveill* **25**, 2000085 (2020).

169. Camprubí, S., Merino, S., Benedí, V. J. & Tomás, J. M. The role of the O-antigen lipopolysaccharide and capsule on an experimental Klebsiella pneumoniae infection of the rat urinary tract. *FEMS Microbiol Lett* **111**, 9–13 (1993).

170. Lawlor, M. S., Hsu, J., Rick, P. D. & Miller, V. L. Identification of Klebsiella pneumoniae virulence determinants using an intranasal infection model. *Mol Microbiol* **58**, 1054–1073 (2005).

171. Moor, K. *et al.* High-avidity IgA protects the intestine by enchaining growing bacteria. *Nature* **544**, 498–502 (2017).

172. Bansept, F. *et al.* Enchained growth and cluster dislocation: A possible mechanism for microbiota homeostasis. *PLoS Comput Biol* **15**, e1006986 (2019).

173. Hu, D. *et al.* Hypercapsule is the cornerstone of Klebsiella pneumoniae in inducing pyogenic liver abscess. *Front Cell Infect Microbiol* **13**, 1147855 (2023).

174. Biedrzycka, M. *et al.* Dissemination of Klebsiella pneumoniae ST147 NDM-1 in Poland, 2015-19. *J Antimicrob Chemother* **76**, 2538–2545 (2021).

175. Wyres, K. L., Lam, M. M. C. & Holt, K. E. Population genomics of Klebsiella pneumoniae. *Nat Rev Microbiol* **18**, 344–359 (2020).

176. Lapp, Z. *et al.* Regional Spread of blaNDM-1-Containing Klebsiella pneumoniae ST147 in Post-Acute Care Facilities. *Clin Infect Dis* **73**, 1431–1439 (2021).

177. Zhou, K. *et al.* Novel Subclone of Carbapenem-Resistant Klebsiella pneumoniae Sequence Type 11 with Enhanced Virulence and Transmissibility, China. *Emerg Infect Dis* **26**, 289–297 (2020).

178. Zhao, D. *et al.* The Emergence of Novel Sequence Type Strains Reveals an Evolutionary Process of Intraspecies Clone Shifting in ICU-Spreading Carbapenem-Resistant Klebsiella pneumoniae. *Front Microbiol* **12**, 691406 (2021).

179. Wantuch, P. L. & Rosen, D. A. Klebsiella pneumoniae: adaptive immune landscapes and vaccine horizons. *Trends Immunol* **44**, 826–844 (2023).

180. Riser, E., Noone, P. & Thompson, R. E. M. The Use of a Fluorescence Typing Method in an Epidemiological Study of Klebsiella Infection in a London Hospital. *The Journal of Hygiene* **80**, 43–56 (1978).

181. Micoli, F., Giannelli, C. & Di Benedetto, R. O-Antigen Extraction, Purification, and Chemical Conjugation to a Carrier Protein. *Methods Mol Biol* **2183**, 267–304 (2021).

182. Yurist-Doutsch, S., Arrieta, M.-C., Vogt, S. L. & Finlay, B. B. Gastrointestinal Microbiota–Mediated Control of Enteric Pathogens. *Annu. Rev. Genet.* **48**, 361–382 (2014).

183. Malys, M. K., Campbell, L. & Malys, N. Symbiotic and antibiotic interactions between gut commensal microbiota and host immune system. *Medicina* **51**, 69–75 (2015).

184. Sepich-Poore, G. D. *et al.* The microbiome and human cancer. *Science* **371**, eabc4552 (2021).

185. De Luca, F. & Shoenfeld, Y. The microbiome in autoimmune diseases. *Clin Exp Immunol* **195**, 74–85 (2019).

186. Taebnia, N., Römling, U. & Lauschke, V. M. In vitro and ex vivo modeling of enteric bacterial infections. *Gut Microbes* **15**, 2158034 (2023).

187. Gargiullo, L., Del Chierico, F., D'Argenio, P. & Putignani, L. Gut Microbiota Modulation for Multidrug-Resistant Organism Decolonization: Present and Future Perspectives. *Frontiers in Microbiology* **10**, (2019).

188. Hansson, G. C. Mucins and the Microbiome. *Annu Rev Biochem* **89**, 769–793 (2020).

189. Allaire, J. M. *et al.* The Intestinal Epithelium: Central Coordinator of Mucosal Immunity. *Trends Immunol* **39**, 677–696 (2018).

190. Ulluwishewa, D. *et al.* Regulation of tight junction permeability by intestinal bacteria and dietary components. *J Nutr* **141**, 769–776 (2011).

191. Anderson, J. M. & Van Itallie, C. M. Physiology and Function of the Tight Junction. *Cold Spring Harb Perspect Biol* **1**, a002584 (2009).

192. Ngo, P. A., Neurath, M. F. & López-Posadas, R. Impact of Epithelial Cell Shedding on Intestinal Homeostasis. *Int J Mol Sci* **23**, 4160 (2022).

193. Gehart, H. & Clevers, H. Tales from the crypt: new insights into intestinal stem cells. *Nat Rev Gastroenterol Hepatol* **16**, 19–34 (2019).

194. Guttman, J. A. & Finlay, B. B. Tight junctions as targets of infectious agents. *Biochimica et Biophysica Acta (BBA) - Biomembranes* **1788**, 832–841 (2009).

195. Paradis, T., Bègue, H., Basmaciyan, L., Dalle, F. & Bon, F. Tight Junctions as a Key for Pathogens Invasion in Intestinal Epithelial Cells. *IJMS* **22**, 2506 (2021).

196. Backert, S., Boehm, M., Wessler, S. & Tegtmeyer, N. Transmigration route of Campylobacter jejuni across polarized intestinal epithelial cells: paracellular, transcellular or both? *Cell Commun Signal* **11**, 72 (2013).

197. Shi, D., Mi, G., Wang, M. & Webster, T. J. In vitro and ex vivo systems at the forefront of infection modeling and drug discovery. *Biomaterials* **198**, 228–249 (2019).

198. Aguilar, C. *et al.* Organoids as host models for infection biology – a review of methods. *Exp Mol Med* **53**, 1471–1482 (2021).

199. Walter, J., Armet, A. M., Finlay, B. B. & Shanahan, F. Establishing or Exaggerating Causality for the Gut Microbiome: Lessons from Human Microbiota-Associated Rodents. *Cell* **180**, 221–232 (2020).

200. Wahl, A. *et al.* Precision mouse models with expanded tropism for human pathogens. *Nat Biotechnol* **37**, 1163–1173 (2019).

201. Puschhof, J., Pleguezuelos-Manzano, C. & Clevers, H. Organoids and organs-on-chips: Insights into human gut-microbe interactions. *Cell Host & Microbe* **29**, 867–878 (2021).

202. Kim, J., Koo, B.-K. & Knoblich, J. A. Human organoids: model systems for human biology and medicine. *Nat Rev Mol Cell Biol* **21**, 571–584 (2020).

203. Bein, A. *et al.* Microfluidic Organ-on-a-Chip Models of Human Intestine. *Cellular and Molecular Gastroenterology and Hepatology* **5**, 659–668 (2018).

204. Blokzijl, F. *et al.* Tissue-specific mutation accumulation in human adult stem cells during life. *Nature* **538**, 260–264 (2016).

205. Fujii, M., Matano, M., Nanki, K. & Sato, T. Efficient genetic engineering of human intestinal organoids using electroporation. *Nat Protoc* **10**, 1474–1485 (2015).

206. Jowett, G. M. *et al.* Organoids capture tissue-specific innate lymphoid cell development in mice and humans. *Cell Reports* **40**, 111281 (2022).

207. Yin, Y. *et al.* Modeling rotavirus infection and antiviral therapy using primary intestinal organoids. *Antiviral Research* **123**, 120–131 (2015).

208. Han, X. *et al.* Creating a More Perfect Union: Modeling Intestinal Bacteria-Epithelial Interactions Using Organoids. *Cell Mol Gastroenterol Hepatol* **12**, 769–782 (2021).

209. Stroulios, G. *et al.* Culture Methods to Study Apical-Specific Interactions using Intestinal Organoid Models. *JoVE* 62330 (2021) doi:10.3791/62330.

210. Kim, S. *et al.* Tissue extracellular matrix hydrogels as alternatives to Matrigel for culturing gastrointestinal organoids. *Nat Commun* **13**, 1692 (2022).

211. Blutt, S. E. & Estes, M. K. Organoid Models for Infectious Disease. *Annu. Rev. Med.* **73**, 167–182 (2022).

212. Sato, T. *et al.* Long-term expansion of epithelial organoids from human colon, adenoma, adenocarcinoma, and Barrett's epithelium. *Gastroenterology* **141**, 1762–1772 (2011).

213. Bartfeld, S. & Clevers, H. Organoids as Model for Infectious Diseases: Culture of Human and Murine Stomach Organoids and Microinjection of Helicobacter Pylori. *J Vis Exp* 53359 (2015) doi:10.3791/53359.

214. Lamers, M. M. *et al.* SARS-CoV-2 productively infects human gut enterocytes. *Science* **369**, 50–54 (2020).

215. VanDussen, K. L. *et al.* Development of an enhanced human gastrointestinal epithelial culture system to facilitate patient-based assays. *Gut* **64**, 911–920 (2015).

216. Moon, C., VanDussen, K. L., Miyoshi, H. & Stappenbeck, T. S. Development of a primary mouse intestinal epithelial cell monolayer culture system to evaluate factors that modulate IgA transcytosis. *Mucosal Immunol* **7**, 818–828 (2014).

217. Co, J. Y., Margalef-Català, M., Monack, D. M. & Amieva, M. R. Controlling the polarity of human gastrointestinal organoids to investigate epithelial biology and infectious diseases. *Nat Protoc* **16**, 5171–5192 (2021).

218. Co, J. Y. *et al.* Controlling Epithelial Polarity: A Human Enteroid Model for Host-Pathogen Interactions. *Cell Rep* **26**, 2509-2520.e4 (2019).

219. Washington, J. A. Discrepancies between in vitro activity of and in vivo response to antimicrobial agents. *Diagn Microbiol Infect Dis* **1**, 25–31 (1983).

220. Szijártó, V. *et al.* Endotoxin neutralization by an O-antigen specific monoclonal antibody: A potential novel therapeutic approach against *Klebsiella pneumoniae* ST258. *Virulence* **8**, 1203–1215 (2017).

221. Pentecost, M., Otto, G., Theriot, J. A. & Amieva, M. R. Listeria monocytogenes invades the epithelial junctions at sites of cell extrusion. *PLoS Pathog* **2**, e3 (2006).

222. Malagobadan, S. & Nagoor, N. H. Anoikis. in *Reference Module in Biomedical Sciences* B9780128012383650213 (Elsevier, 2017). doi:10.1016/B978-0-12-801238-3.65021-3.

223. Miyoshi, H. & Stappenbeck, T. S. In vitro expansion and genetic modification of gastrointestinal stem cells in spheroid culture. *Nat Protoc* **8**, 2471–2482 (2013).

Acknowledgements

Un ringraziamento sentito al professor Rino Rappuoli per avermi trasmesso il significato di dedizione e impegno in questi intensi e formativi tre anni di dottorato. Grazie a Claudia per avermi saputo guidare indicandomi la giusta strada e allo stesso tempo facendomi sentire libera di esplorare i miei interessi scientifici. Grazie ad Anna, con cui condivido il “pregio” della testardaggine, per avermi fatto sentire sempre ascoltata e per avermi saputo arginare e contrastare quando necessario. Grazie ad Emanuele per essere stato un mentore più o meno inconsapevole e il mio punto di riferimento dal primo giorno in cui ho messo piede in laboratorio. Grazie a Noemi, Samuele, Eleonora, Giulia, Federica, Valentina, non solo dei meravigliosi compagni di laboratorio, ma soprattutto degli ottimi amici che hanno reso Siena la mia seconda casa.

A heartfelt thank you to Prof. Manuel Amieva for hosting me in his laboratory. I deeply appreciated the warm welcome, the guidance and the invaluable support, both professionally and on a personal level throughout the not always easy six months at Stanford. Thanks to Benedikt, Sophia, and Youlim for making my time of research abroad so special. I learnt a lot from each of you and couldn’t have asked for a better group of people to work side by side with.

Thank you, Kate, for being my home away from home in California.

Grazie a mamma, papà e GB per avermi insegnato che vola solo chi osa farlo. La grandezza e il vigore delle ali dipendono dalla profondità e dalla robustezza delle radici: grazie per avermi sempre fornito entrambe in egual misura, concedendomi il privilegio di costruire il mio percorso sentendomi sempre sostenuta nelle mie (non sempre impeccabili) scelte.

Grazie a Matteo, amico prezioso e insostituibile dentro e fuori dal laboratorio, per aver imparato a capirmi con uno sguardo, per avermi donato una solida spalla su cui appoggiarmi (soprattutto quando non ero in grado di chiederlo) e per avere saputo scuotermi con parole sempre attente e mai indelicate.

Grazie a Vita, anima affine, amicizia senza tempo esplosa forte come un petardo e salda àncora in innumerevoli momenti di tempeste interiori.

Grazie ad Ari e Serena, mie certezze da sempre e per sempre.